NIRS
HIMAC

NIRS-M-87
HIMAC-002

Energy Loss, Range and Fluence Distributions, Total Reaction and Projectile Fragmentation Cross Sections in Proton-Nucleus and Nucleus-Nucleus Interactions

L. Sihver and T.Kanai

July 1992

National Institute of Radiological Sciences
9-1, Anagawa 4-chome, Inageku, Chiba-shi 263 JAPAN

Energy Loss, Range and Fluence Distributions, Total Reaction and Projectile Fragment Production Cross Sections for Proton-Nucleus and Nucleus-Nucleus Interactions

L. Sihver and T. Kanai

National Institute of Radiological Sciences
Division of Accelerator Research
Chiba-shi, Inage-ku, Anagawa 4-9-1
Chiba 263, Japan

ABSTRACT

We have developed a computer code for calculations of energy loss (dE/dx) and range distributions for heavy ions in any media. The results from our calculations are in very good agreement with previous calculations. We have developed semiempirical total reaction cross section formulae for proton-nucleus (with $Z_p \leq 26$) and nucleus-nucleus (with Z_p and $Z_t \leq 26$) reactions. These formulae apply for incident energies above 15 MeV and 100 MeV/nucleon respectively. From the total reaction cross sections, we can calculate the mean free paths and the fluence distributions of protons and heavy ions in any media. We have compared all the calculated reaction cross sections and the mean free paths with experimental data, and the agreement is good.

We have also constructed a procedure for calculating projectile fragment production cross sections, by scaling semiempirical proton-nucleus partial cross section systematics. The scaling is performed using a scaling parameter deduced from our reaction cross sections formulae, and additional enhancements factors. All products with atomic number ranging from that of the projectile (Z_p) down to Z=2 can be calculated. The agreement between the calculated cross sections and the experimental data is better than earlier published results.

TABLE OF CONTENTS

I. INTRODUCTION

The use of heavy ions, as compared to conventional radiation techniques, is expected to result in significant advantages in therapeutic and diagnostic medicine (ex. Heavy Ion CT). The heavy ions are, among other things, expected to be very effective in treating deep tumors located near vital structures. Some of the favorable properties of these heavy ions are [1,2]

1. the reduced straggling and multiple scattering of highly charged heavy ions allow the design of sharply defined beams, i.e., the pattern of the depth–dose distribution is favorable as the well–defined Bragg Peak increases,
2. due to the reduced straggling and multiple scattering one can get a well–defined Bragg Peak, which increases the efficiency of the irradiation of the target volume, and reduces the dose to the surrounding normal tissue,
3. the high Linear Energy Transfer (LET) gives high Relative Biological Effectiveness (RBE),
4. the Oxygen Enhancement Ratio (OER) of these ions is significantly lower than that of X rays,
5. the reduction of cell repair from radiation damage increases the efficiency of the irradiation,
6. there is less variation in sensitivity on the cell cycle, which may simplify the response of cell killing.

The properties of charged–particle beams are affected by their interaction with matter to a grater degree than those of other types of radiation. When using heavy ions for medical treatments it is therefore essential to understand the behavior of these ions in human tissues. To calculate the total depth–dose distributions in a medium, the energy loss (dE/dx) and the range of a specific fragment in the medium must be known. We have developed our own computer codes for calculating these properties. It is also very important to know how the nuclear interactions contribute to the depth–dose distributions. The total reaction cross section has been extensively studied both theoretically and experimentally for more than 45 years. An overview of references is found in Ref. 26. Our goal was to find the best possible total reaction cross section formulae for proton–nucleus and nucleus–nucleus reactions. When we found that the results from the existing formulae were not satisfactory, we developed our own semiempirical formulae. These formulae apply for incident energies above 15 MeV and 100 MeV/nucleon for proton–nucleus (with $Z_t \leq 26$) and nucleus–nucleus (with Z_p and $Z_t \leq 26$) reactions, respectively. From the total reaction cross sections, we can calculate the mean free paths and the fluence distributions of heavy ions and protons in any materials.

Sometimes when a heavy ion beam impinges upon a target, the collision results in nuclear fragmentation. These events are usually characterized as projectile or target fragmentation. The target fragments are large, high Z fragments, which carry little momentum. These fragments might have biological effects, but as they have a small effect on the dose distributions, we assume we can neglect the effect from these fragments. On the other hand, the projectile fragments loose very little momentum and travel nearly in the beam direction with relatively minor deflection. These latter fragments generally have lower charge than the incident beam, i.e. their stopping

power is less than that of the primary beam. Therefore, they lower the average ionization relative to that of the incident beam, and they will make up a "tail" which extends beyond the stopping region of the primary beam (i.e. beyond the Bragg Peak).

To calculate how much these "secondary" fragments contribute to the dose distributions, one must know their partial cross sections. Silberberg and Tsao [3,4] have developed a semiempirical systematics for calculation of these cross sections for proton–nucleus reactions. This model has also been used [1,5] to calculate how much the fragmentation products from nucleus–nucleus interactions contribute to the depth–dose distributions, but the results have not been so successful until now. Silberberg and Tsao have also developed equations for calculating the cross sections for the breakup of nuclides (Z_i, A_i) colliding with (Z_j, A_j) by scaling their semiempirical systematics [37,38,39]. However, the agreement with the experimental data is not quite satisfactory.

Cummings **et al.** [49] have developed a procedure to calculate fragmentation cross sections for hydrogen targets and "heavy" targets, by fitting experimental data. However, there have not been any attempt to make these fits for "light" ($Z \leq 26$) projectile–target combinations yet. We have therefore constructed a procedure for calculating these cross sections, by scaling the semiempirical proton–nucleus partial cross section systematics. All products with proton number ranging from that of the projectile (Z_p) down to Z=2 can be calculated. The scaling is done by a scaling parameter deduced from our reaction cross section formulae. Additional enhancement factors for single–nucleon stripping, large ΔA reactions and the lightest products (Li, Be and B) are also added. The agreement between the calculated cross sections and the experimental data is better than earlier published results.

To be able to accurately calculate the total dose distributions in a medium, the energy and range straggling, the multiple scattering etc., must also be known. However, these phenomena are beyond the scope of this report.

II. ENERGY LOSS AND RANGE DISTRIBUTIONS

We have developed a computer code (in FORTRAN) for calculation of energy loss (dE/dx) and range distributions in any media. In our code dE/dx is calculated as a function of energy, based on the Bethe equation for the total energy loss for heavy particles

$$\frac{dE}{dx} = -4\pi r_o^2 z^2 \frac{mc^2}{\beta^2} NZ \left[\ln\left(\frac{2mc^2}{I}\beta^2\right) - \ln(1-\beta^2) - \beta^2 - \frac{\delta}{2}\right] \quad (1)$$

where the second and third terms in the square brackets are relativistic correction terms, and the last term is the density correction, which is made according to Sternheimer **et al.** [6].

mc^2 = the rest mass of the electron = 0.511 MeV,
β = v/c, where c = $3*10^8$ (the speed of light),
β^2 = $1 - [mc^2/(T + mc^2)]$, where T = the kinetic energy of the incident particle,
N = the number of atoms/m^3 for the material through which the particle moves,
Z = the atomic number of the material,
z = the charge of the incident particle,
I = the mean excitation potential of the target material.

Shell effect correction is neglected. The effective charge correction at low velocities is given by [7]

$$Z_{eff} = Z\left[1 - e^{(-0.95 v_r)}\right] \quad (2)$$

where

Z = the atomic number of the particle,
v_r = the relative velocity given by $v_r = v/(v_o Z^{2/3})$,
v = the particle velocity,
v_o = the average velocity of the electron in the H atom ($v_o = e^2/\hbar$).

The mass stopping power of a compound can be approximated by the weighted sum of the stopping powers of the atomic constituents of the compound. For the mass stopping power, S_{col}/ρ, this additivity rule takes the form [8]

$$\frac{S_{col}}{\sigma} = \sum_j \omega_j \left(\frac{S_{col}}{\sigma}\right)_j \quad (3)$$

where ω_j is the fraction by weight and $(S_{col}/\rho)_j$ is the mass stopping power of the j'th atomic constituent. This additivity rule is equivalent to replacing, in the stopping-power

formula Eq.(2), the quantity Z/A by

$$\left(\frac{Z}{A}\right) = \sum_j \omega_j \left(\frac{Z_j}{A_j}\right) \tag{4}$$

The range distributions are calculated numerically according to

$$R(E) = \int_0^E \frac{dE}{-\frac{dE}{dx}} \tag{5}$$

We have calculated the energy loss (dE/dx) and range distributions of protons and many different ions in different solids. We have compared our calculated values with those calculated by Steward **et al.** [9], Heinrich **et al.** [10], and those calculated by Ziegler **et al.** [11]. The agreement is very good for all systems studied.

As a typical example, we show our calculated results of the energy loss (dE/dx) of ^{12}C in water, together with those calculated with the code developed by Steward **et al.**, those calculated by Heinrich **et al.**, and those calculated by Ziegler **et el.** (TRIM91) in **Figures 1** and **2**. We use I=75 eV (recommended value [8]) in our calculations and in the code developed by Steward **et al.**, while Heinrich **et al.** and Ziegler **et al.** use I=67.5 eV. In **Figure 2** one can see that the largest difference between the four calculations is less than one percent at the specific energy 100 MeV/nucleon, and less than two percent at 800 MeV/nucleon. The dE/dx values from the four calculations shown in **Figure 1** are tabulated in **Table I**. The range distributions for ^{12}C in water are shown in **Figure 3**. The largest difference between the four calculations of the range distributions is less than one percent at both 100 MeV/nucleon and 800 MeV/nucleon. The range distributions shown in **Figure 3** are tabulated in **Table II**. We have also compared calculations performed with our code using both I=67.5 and 75 eV. The difference between the two calculations is around one percent at 800 MeV/nucleon for both dE/dx and the calculated range, i.e. the different results from the four codes seem to be mainly due to different mean excitation potentials of the target material.

III. REACTION CROSS SECTIONS

In a nuclear interaction, the total cross section consists of the reaction cross section and the elastic scattering cross section

$$\sigma_{tot} = \sigma_{abs} + \sigma_{el} = \sigma_{reac} + \sigma_{el} \tag{6}$$

where

σ_{tot} = the total cross section, i.e. the total probability that a reaction or an elastic scattering will take place,
σ_{reac} = the reaction cross section $\equiv$ σ_{abs} = the absorption cross section,
σ_{el} = the elastic scattering cross section.

The first empirical expression of the total nuclear reaction cross section was proposed by Bradt and Peters [12]

$$\sigma_{reac,BP} = \pi r_o^2 (A_p^{1/3} + A_t^{1/3} - b_o)^2 \tag{7}$$

where

A_p = the mass number of the projectile,
A_t = the mass number of the target,
b_o = the overlap, or transparency parameter,
r_o = the constant of proportionality in the expression for the geometrical nuclear radius $r_i = r_o A_i^{1/3}$.

Expressions like Eq. (7) are often used for calculations of the total cross sections, the reaction cross sections, and the inelastic cross sections. Sometimes the total charge changing cross sections, $\sigma_{\Delta Z \geq 1}$, are measured, other times the total mass changing cross sections, $\sigma_{\Delta A \geq 1}$. The total mass changing cross sections more closely correspond to the total reaction cross section than do the total charge changing cross sections. The measured total charge changing cross sections should be a little bit lower than the total reaction cross sections, since all the events which only change the neutron number in the incident nucleus are excluded. On the other hand, it is easier to measure the total charge changing cross sections than the total mass changing cross sections, so the uncertainties are expected to be lower. This situation is somewhat confusing, because some authors compare their measured charge-changing cross sections with their calculated reaction cross sections etc.

Both the total cross sections, and the total reaction cross sections, are expected to be energy dependent up to $\approx$ 1.5 GeV/nucleon, where these cross sections are approaching their high-energy limit.

A. Nucleus–Nucleus Reaction Cross Sections

We were mainly interested in finding a total reaction cross section formula which gives "good agreement" with the measured nucleus–nucleus absorption cross sections in the energy region 100–800 MeV/nucleon. In a first attempt to find out if there is such a formula, we started by studying the following Bradt–Peters like formulae

$$SIGMA1^{13,14}: \quad \sigma_{reac,1} = \pi r_o^2 (A_p^{1/3} + A_t^{1/3} - \Delta)^2 \tag{8}$$

where Δ=1.0–0.028A_{min} for A_{min}<30, Δ=0 for $A_{min}\geq$30 and r_o=1.29 fm

$$SIGMA2^{15}: \quad \sigma_{reac,2} = \pi r_o^2 (A_p^{1/3} + A_t^{1/3} - 0.2 - A_p^{-1} - A_t^{-1})^2 \tag{9}$$

where r_o=1.26 fm

$$SIGMA3^{16}: \quad \sigma_{reac,3} = 450 (A_p^{1/3} + A_t^{1/3} - 2.380) \quad [mb] \tag{10}$$

$$SIGMA4^{17}: \quad \sigma_{reac,4} = \pi r_o^2 \beta(E) [A_p^{1/3} + A_t^{1/3} - \delta(A_p, A_t, E)]^2 \tag{11}$$

where β(E)=1+5E^{-1} and

$$\delta(A_p, A_T, E) = 0.200 + \left(\frac{1}{A_p}\right) + \left(\frac{1}{A_t}\right) - 0.292 e^{-E/792} \cos(0.229 E^{0.453})$$

with r_o=1.26 fm and E is expressed in units of MeV/nucleon.

SIGMA5 [18]: $\sigma_{reac,5}$ is calculated from a quantum mechanical model of heavy–ion reactions, not a Bradt–Peters like formula.

$$SIGMA6^{19,20,47,48}: \quad \sigma_{reac,6} = \pi r_o^2 [A_p^{1/3} + A_t^{1/3} - b_o (A_p^{-1/3} + A_t^{-1/3})]^2 \tag{13}$$

where r_o=1.36 fm.

We wanted to see which, if any, of these formulae give satisfactory agreement with the experimental reaction cross sections. According to Tanihata **et al.** [14], SIGMA1 should, in the relativistic energy region, fit all the projectile–target combinations within 10%. However, their σ_{reac} were measured by charge–changing reactions, i.e. a nucleus was considered as interacting only when changing its Z in a nuclear collision.

One should notice that SIGMA4 is the only one of the six reaction cross section formulae which is energy dependent, and that SIGMA2 is basically equal to SIGMA4 without its energy dependent terms. In SIGMA3, the sum contained in the σ_{reac}

expression is not squared, since according to Ref. 16 the isotopic cross sections for a heavy ion reaction depend on the sum of the target and projectile radii rather than the square of the sum. This is what expected for peripheral reactions [14]. SIGMA5 is a quantum mechanical model and is only shown as a reference.

Other total reaction cross section formulae were also studied, but since the results from them were not satisfactory, they will not be discussed in this report.

In **Tables III–VII** we compare the six formulae to see how large differences there are between them.

In **Figures 4–9**, the calculated reaction cross sections for ^{12}C with H, ^{12}C with ^{16}O,^{16}O with H, ^{16}O with ^{16}O, ^{20}Ne with H, and ^{12}C with ^{16}O, respectively, are plotted as a function of the projectile energy in the laboratory system, even if only SIGMA4 is energy dependent. This only serves to give an impression of the differences between the results from the six formulae.

In all these tables and figures the overlap parameter, b_0, in SIGMA6 was assumed to be 1.3, as proposed by Jain **et al.** [19].

Neither of the formulae SIGMA1 to SIGMA6 are supposed to be used for proton–heavy ion or heavy ion–hydrogen interactions. To confirm this fact, we also tabulate the calculated reaction cross sections for reactions of heavy ions with hydrogen in **Tables III, V** and **VII**. As can be seen in **Tables III–VII** and **Figures 4–9**, the differences between the formulae are not negligible for any target. It can also be seen that SIGMA3 gives significantly higher values than the other formulae for reactions of heavy ions with hydrogen.

To calculate the total reaction cross section for a mixture or a compound, the following relation should be used

$$\sigma_{reac,tot} = \frac{\sum_i n_i \sigma_{reac,i}}{\sum_i n_i} \qquad (15)$$

where

$\sigma_{reac,tot}$ = the total reaction cross section for the reaction of a projectile with the target material in which the charged particle is travelling,

$\sigma_{reac,i}$ = the reaction cross section for the reaction of a projectile with the nucleus i in the target material in which the charged particle is travelling,

n_i = the number of atoms i per molecule of the target material.

In **Tables VIII–XVII**, we compare our calculated reaction cross sections with experimental data. These data include a variety of projectiles (from ^{3}He to ^{58}Ni) and targets (from H to Ag) at energies from ≈ 600 MeV/nucleon to 2.1 GeV/nucleon. The reaction cross sections are not expected to be energy independent until $E_{proj} \geq 1.5$ GeV/nucleon, but for our purposes the energy dependence above 100 MeV/nucleon is considered negligible compared to other uncertainties in the experimental data. Therefore we compare our calculated values with experimental data at all energies

≥ 100 MeV/nucleon to find the reaction cross section formula which gives the best over all agreement with the experimental data available.

As can bee seen from **Tables VII–XVII**, none of the reaction cross section formulae used gives a very good agreement for all systems studied. SIGMA1 gives reaction cross sections which are lower than the experimental data for most of the systems. SIGMA2 gives a rather good, but not satisfactory, agreement with the experimental data for most systems studied. SIGMA3 gives too high values for "light" projectile–target combinations and too low values for the "heavier" systems. SIGMA6, with the overlap parameter b_o=1.3, always gives too low cross sections. This indicates that 1.3 is a too high value for these interactions.

To see if we could get any better agreement between the calculated values and the experimental data, we calculated a new b_o value, using SIGMA6, for every studied interaction. This b_o was calculated to get the best possible agreement with the experimental value. When all new b_o values were calculated, these values were plotted as a function of $(A_p^{-1/3}+ A_t^{-1/3})$, as can be seen in **Figure 10**. b_o was then fitted as a polynomial function of the first order in $(A_p^{-1/3}+ A_t^{-1/3})$, giving

$$b_o = 1.581-0.876\,(A_p^{-1/3}+A_t^{-1/3}) \qquad (16)$$

In **Tables XVIII–XXIV**, we show our new calculated results, using SIGMA6 with b_o=1.581–0.876*$(A_p^{-1/3}+ A_t^{-1/3})$, together with the results from SIGMA1 and the experimental data. We have also calculated the ratios $\sigma_{calc}/\sigma_{exp}$ for all interactions studied, for both SIGMA1 and SIGMA6. In **Figures 11–12** we show $\sigma_{calc}/\sigma_{exp}$ as functions of $(A_p^{1/3}+A_t^{1/3})$, using SIGMA1 and SIGMA6 respectively. In **Figure 12**, we also show the experimental error bars when they are given. From these tables and figures, we can see that SIGMA6 with b_o=1.581–0.876*$(A_p^{-1/3}+ A_t^{-1/3})$ gives a good agreement with the experimental data for most of the systems studied.

B. Proton-Nucleus Reaction Cross Sections

One way of describing proton-nucleus interactions is in terms of the optical model by a multiparameter potential. To determine the parameters of this potential one needs experimental information about the total cross sections, reaction cross sections, differential elastic cross sections and polarizations. The reaction cross sections are particularly important for limiting the range of the imaginary part of the potential.

Several microscopic models have also been developed. In these models, the nuclear reactions are described in terms of a sum of individual nucleon-nucleon scattering processes.

One can also describe the proton-nucleus interactions using semi-classical approximations as Renberg **et al.** [27] have done. They interpret the reaction cross sections as function of energy in an analytical form. This simplified model, given by Eq. 17 was first developed by Bethe [28]

$$\sigma_R = 10\pi\left(R+\frac{\lambda}{2\pi}\right)^2\left[1-\frac{Z_1Z_2e^2}{10\left(R+\frac{\lambda}{2\pi}\right)e_o}\right][1-T] \qquad (17)$$

where

$$T = \frac{1-(1+2KR)\,e^{-2KR}}{2KR^2R^2}$$

and

$$\sigma_R = \pi R^2(1-T)$$

R = the radius of the nuclear potential and is given in fm,
$\lambda/2\pi$ = the wavelength of the incident particle in fm,
K = the absorption coefficient,
E_o = the incident proton energy
T = the transparency of the nucleus.

σ_R is given in mb, K and R are free parameters.

Many accurate calculations of the reaction cross section for various reactions and energies have been performed with this model using different Monte Carlo methods [27]. Since this model includes the free parameters K and R, we wanted to find out if we could use any other simpler semiempirical nucleus-nucleus reactions cross section formula instead. Therefore, we adjusted the overlap parameter b_o in Eq. (13) so the "best agreement" with the experimentally values was found and set A_p=1. We assumed energy independence for incident energies above 200 MeV, i.e. we fitted one b_0 value for all reactions above 200 MeV, for each projectile-target combination. After that, we fitted all the b_o values to a polynomial function of the first order in $(1+A^{-1/3})$. The results of the "best agreement" b_o values for each reaction is shown as functions

of $(1+A^{-1/3})$ in **Figure 13**. In the same figure we also show the calculated b_0 values.

The stopping power of protons is lower than that of heavy ions, i.e. the range that protons with a specific energy travel in matter, is longer than that for heavy ions. Therefore, it is important to know the proton–nucleus reaction cross sections at lower energies. For incident energies below 200 MeV, we can not assume energy independence of the reaction cross sections. To calculate the energy dependence at these energies, we developed some energy dependent functions, which are then multiplied by our energy independent function. Our total reaction cross section formula then becomes

$$\sigma(E,p,N)_{reac} = 0.14e^{(0.0985E)}\sigma(E,p,N)_{reac,1}\sigma(p,N)_{reac} \tag{18}$$

for E_p<20 MeV and $6 \le Zt_t \le 8$,

$$\sigma(E,p,N)_{reac} = \sigma(E,p,N)_{reac,1}\sigma(p,N)_{reac} \tag{19}$$

for $20 \le E_p \le 150$ MeV and $6 \le Z_t \le 8$, or Z_t<6 or Z_t>8 and $E_p \le 150$ MeV,

$$\sigma(E,p,N)_{reac} = \sigma(E,p,N)_{reac,1}\sigma(E,p,N)_{reac,2}\sigma(p,N)_{reac} + \sigma(E,p,N)_{reac,3}\sigma(p,N)_{reac} \tag{20}$$

for $150 \le E_p$<200 MeV, or

$$\sigma(p,N)_{reac} = \pi r_o^2[1 + A_t^{1/3} - b_o(1 + A_t^{-1/3})]^2 \tag{21}$$

for $E_p \ge 200$ MeV.

In all cases,

$$r_o = 1.36fm$$

$$b_o = 2.247-0.915(1+A_t^{-1/3})$$

$$\sigma(E,p,N)_{reac,1} = 1.15+AK1e^{-E/AK2}(1-0.62e^{-E/200})\sin(10.9E^{-0.28})$$

$$\sigma(E,p,N)_{reac,2} = 4.00-0.02E$$

$$\sigma(E,p,N)_{reac,3} = 0.02*(E-3.00))$$

AK1 is 1.4 if $Z_p \leq 8$, else 0.0.

AK2 is 38 if $Z_p=4$, 25 if $Z_p=5$, 10 if $6 \leq Z_p \leq 8$, else 1.0

E is the kinetic energy of the incident proton.

These formulae can also be used to calculate the total reaction cross sections for reactions between heavy ions and hydrogen. In **Figures 14–17**, we show the calculated cross sections, together with the experimental data [29], for protons with Be, B, C, and Al respectively. No attempt to model the resonance features at low energies was made. In **Tables XXV–XXVIII** we tabulate all the cross sections for all the reactions with incident energies ≥100 MeV, shown in **Figures 14–17**. In **Figure 18**, we show σ(calc)/σ(exp) for all reactions with incident energies ≥100 MeV.

IV. FLUENCE DISTRIBUTIONS

The number of primary particles, which have survived from previous interactions, at a distance x in a material (which can be homogeneous or inhomogeneous, i.e. a compound or a mixture) can be calculated from their mean free paths according to

$$N = N_o e^{-\frac{x}{\lambda}} \tag{21}$$

where

N_o = the number of charged particles entering the target material, i.e. at the distance x=0,
N = the number of charged particles at the distance x,
λ = the mean free path of the charged particle.

The mean free path, λ, can be expressed as

$$\lambda = \frac{1}{N\sigma_{reac,tot}} \tag{22}$$

where

N = atoms per cm^3 of the target material.

The total number of atoms per cm^3 of the target material is given by the relation

$$N = \frac{N_{molec} N_A \rho}{M} \tag{23}$$

where

N_{molec} = the total number of atoms per molecule in the target material,
ρ = the density of the target material,
M = the atomic mass of the target material,
N_A = the Avogadro number.

In **Table XXIX** we compare our calculated reaction cross sections, using SIGMA1–SIGMA6, with the experimental values for some different projectiles in water [30,31] and emulsion (Ilford G5) [19]. In **Table XXX** we compare the same experimental values as in **Table XXIX** with our calculated values, using SIGMA1 and our reaction cross section formula. In **Table XXXI** we compare the calculated reaction cross sections, using SIGMA1 and our reaction cross section formula, with the experimental values

for some other projectiles in emulsion (Ilford G5) [20]. Heckman **et al.** [20] measured the interaction mean free paths of ^{4}He, ^{12}C, ^{14}N, and ^{16}O, at 2.1 GeV/nucleon in Ilford G5 emulsions. For all these systems our calculated values are higher than the measured values. The reason for this is not known, but since these experimental cross sections were deduced from mean free path measurements, the uncertainties are probably higher than for the other tabulated cross sections.

In **Figures 19a** and **19b** we show our calculated fluence distributions for ^{20}Ne with water and ^{12}C with Ilford G5 emulsion, respectively, as examples. In the same figures we also show the calculated fluence distributions for the ^{20}Ne with water and ^{12}C with Ilford G5 emulsion, using SIGMA1, and the measured distributions.

The first 400 MeV/N ^{20}Ne beams was delivered by SIS at GSI (Gesellschaft für Schwerionenforschung in Darmstadt, Germany) recently and the first measurements of the fragmentation of this beam in water was done [32]. A stack of four silicon detectors (D1–D4, each 500 μm thick) was used, and the attenuation of the primary ^{20}Ne ions was obtained by gating on the Z=10 peak distribution. The measured mean free path was 163 ± 8 mm.

We have calculated this mean free path, using SIGMA6 with our b_0 functions. Our calculated value is 163 mm, i.e in total agreement with the experimental value. The calculated fluence distribution is shown in **Figure 20**. The distribution is normalized at the distance 0.0 mm, i.e. at the entrance of the water phantom.

V. PROJECTILE FRAGMENTATION CROSS SECTIONS

The partial inelastic cross sections have systematic regularities that permit the formulation of semiempirical equations. Rudstam [33,34,35] noted the systematic regularities among the relative yields of nuclear reactions that depend on the mass difference of the target and product nuclides and on the neutron–to–proton ratio of the product nuclides. In an attempt to use analytical relations, Rudstam has developed a semiempirical cross section formula which is particularly useful for targets heavier than calcium. It should not be applied to light product nuclei, as pointed out by Rudstam himself, particularly at low energies. For example, the calculated cross section for the production of ^{7}Be from Ni at 130 MeV is too small by a factor $\approx 10^{8}$. Rudstam's equation is

$$\sigma = \sigma_0 e^{-P\Delta A}\, e^{(-R|Z-SA+TA^2|^{3/2})} \qquad (24)$$

The factor $(-p\Delta A)$ describes the diminution of cross sections as the difference of target and product mass, ΔA, increases. The factor $\exp(-R\,|\,Z-SA+TA^2\,|^{\nu})$, with $\nu \approx 3/2$, describes the distribution of cross sections for the production of various isotopes of an element of atomic number Z.

The Gaussian–like distribution is related to the statistical nature of the nuclear evaporation process [36]. The width of the cross section distribution is represented by the parameter R. The parameter S describes the location of the peaks of the distribution curves, which go toward greater neutron excess as the atomic number of the product increases. The parameters Rudstam assigned to the equation apply to proton interactions with nuclei heavier than calcium, except when the target–product mass difference is small or large, i.e., it is not applicable for $\Delta A<5$ and $\Delta A>40$. The nuclear reaction systematics of spallation reactions is not applicable to fission and fragmentation reactions, nor to the evaporation of light nuclei. Fragmentation is a nuclear breakup process in which a nucleus is formed that is lighter than a fission product.

Silberberg and Tsao [3,4] have constructed a semiempirical equation resembling Rudstam's with additional parameters, and have defined regions of target and product mass intervals where these parameters apply. Their basic equation for calculating the partial cross sections is

$$\sigma = \sigma_0\, f(A)\, (F)\, e^{-P\Delta A}\, e^{(-R|Z-SA+TA^2|^{\nu})}\, \Omega\eta\xi \qquad (25)$$

It is applicable for calculating cross sections (in units of mb) of targets having mass numbers in the range $9 \le A_t \le 209$ and products with $6 \le A \le 200$, except for peripheral interactions with small values of $\Delta A = A_t - A$. For the latter reactions, Silberberg and Tsao constructed a different equation [3].

In Eq. 25, σ_0 is a normalization factor. The factors f(A) and f(E) apply only to products from heavy targets (with atomic numbers $Z_t>30$), when ΔA is large, as in the case of fission, fragmentation and evaporation of light product nuclei. The factor

$\exp(-p\Delta A)$ and the next exponential factor, $\exp(-R|Z-SA+TA^2|^{\nu})$ due to Rudstam [33,34,35], have been described above. The parameter Ω is related to the nuclear structure and the number of particle-stable levels of a product nuclide. The factor η depends on the pairing of protons and neutrons in the product nucleus; it is largest for even-even nuclei, and smallest for odd-odd nuclei. The parameter ζ is introduced to represent the enhancement of light evaporation products.

There are deviations from complete proportionality between proton-nucleus and nucleus-nucleus reaction. The deviations have been explained by Lindstrom **et al.** [40] in terms of (1) nuclear transparency (the energy deposition is less in p-nucleus interactions; so, as ΔA increases, the relative yields of proton-nucleus reactions diminish progressively), and (2) the giant dipole resonance, as a result of which single-nucleon stripping is enhanced in collisions with heavy nuclei. The (3) lightest products (Li, Be and B) are also enhanced by a factor of 2-3 beyond the scaling factor for heavier targets [41,42].

Silberberg and Tsao have also developed equations for calculating the cross sections for the breakup of nuclides (Z_i, A_i) colliding with (Z_j, A_j) by scaling their semiempirical systematics [37,38,39]. The scaling factor relative to p-nucleus cross sections is

$$S_C = 1.6 + 0.07A_2^{2/3} \tag{26}$$

They have also added correction factors for the lightest products (Li, Be and B), for reactions with a large value of ΔA (for $A<0.5A_1$ and $Z>5$) and single-nucleon stripping, caused by the giant dipole resonance. However, the agreement with the experimental data is not quite satisfactory.

To get better agreement with the experimental data, we have constructed a new scaling procedure. The scaling is performed using a scaling parameter deduced from our total reaction cross section formulae. Our total reaction cross section formulae include the transparency function, so our scaling takes into account that the energy deposition is less in p-nucleus interactions than in nucleus-nucleus interactions. Our equation for calculating the cross sections for the breakup of nuclides (Z_i, A_i) colliding with (Z_j, A_j) is

$$\sigma(Z_1, A_1, Z_j, A_j, E_1) = S_C\, \varepsilon_L \varepsilon_\Delta \varepsilon_1 \sigma(Z_1, A_1, p, E_p) \tag{27}$$

where

$$S_C = \sqrt{\frac{\sigma_{reac}(Z_1, A_1, Z_j, A_j, E_1)}{\sigma_{reac}(Z_1, A_1, p, E_p)}} \tag{28}$$

$\sigma(Z_i, A_i, Z_j, A_j, E_i)$ = the partial cross section of nucleus–nucleus reactions, for the breakup of nuclides (A_i,Z_i, E_i) colliding with (A_j,Z_j),

$\sigma(Z_i, A_i, p, E_p)$ = the partial cross section of proton–nucleus reactions, for the breakup of nuclides (A_i,Z_i) colliding with protons (E_p),

$\sigma_{reac}(Z_i, A_i, Z_j, A_j, E_i)$ = the total nucleus–nucleus reaction cross section, for the reaction of (A_i,Z_i, E_i) colliding with (A_j,Z_j),

$\sigma_{reac}(Z_i, A_i, p, E_p)$ = the total proton–nucleus reaction cross section, for the reaction of (A_i,Z_i) colliding with protons (E_p),

ε_L = the enhancement factor for the lightest products, Li, Be and B,

ε_Δ = the enhancement factor for reactions with a large value of ΔA,

ε_1 = the enhancement factor for single–nucleon stripping, caused = by the giant dipole resonance.

The enhancement factor for the lightest products

A) For $E_i \leq$ 2000 MeV/nucleon

$$\varepsilon_L = [1+0.7 f_B] f_A \tag{29}$$

B) For $E_i >$ 2000 MeV/nucleon

$$\varepsilon_L = [1+(1+[\frac{5-Z_{frag}}{10}])(\frac{1}{2Z_{frag}})] f_B \tag{30}$$

The enhancement factor for reactions with a large value of ΔA

$$\varepsilon_\Delta = 4 f_A e^{[-2.2A_{frag}/A_1]} \tag{31}$$

for $E_i \leq$ 2000 MeV/nucleon, $A_{frag} < A_p/2$ and $Z_{frag} > 5$

where

$$f_A = \frac{[1+(\frac{A_1}{120})(\frac{E_1}{2000})]}{[1+(\frac{A_1}{120})]} \tag{32}$$

and

$$f_B = [1+0.03(\frac{Z_1}{Z_{frag}})^2][1-1.5(\frac{Z_{frag}}{Z_1})] \quad (33)$$

Z_{frag} = the atomic number of the projectile fragment.

The enhancement factor for single-nucleon stripping, caused by the giant dipole resonance

$$\varepsilon_1 = 1+0.0088 Z_1 Z_j^{0.8} \quad for\ Z_1 \geq 8, \quad \Delta A=1 \quad (34)$$

and

$$\varepsilon_1 = 1 \quad for\ Z_1 < 8, \quad \Delta A=1 \quad (35)$$

We also introduced the following correction factors

$\sigma(^8B)$ was multiplied with 2.4,
$\sigma(^9C)$ was multiplied with 2.1,
$\sigma(^{12}C)$ was multiplied with 0.6,
$\sigma(^6Li)$ is multiplied with 1.2 for E > 2000 MeV/N and $Z_p \geq 8$.

The energy dependence scales to nucleus-proton cross sections approximately as the energy-per-nucleus of the nucleus A_j in the rest frame of A [38]. E.g. for ^{16}O at 200 MeV/nucleon incident on ^{12}C, the cross section scales to the A_j-p cross section at 200 x 12 = 2400 MeV.

All products with proton number ranging from that of the projectile (Z_p) down to Z=2 can be calculated. The following interactions were studied.

250 MeV/N ^{12}C + ^{12}C [43]	600 MeV/N ^{40}Ar + ^{12}C [44]	1.05 GeV/N ^{12}C + ^{27}Al [45]
	600 MeV/N ^{56}Fe + ^{12}C [44]	
600 MeV/N ^{12}C + ^{12}C [44]		2.1 GeV/N ^{12}C + ^{9}Be [45]
600 MeV/N ^{14}N + ^{12}C [44]	1.05 GeV/N ^{12}C + ^{9}Be [45]	2.1 GeV/N ^{12}C + ^{12}C [45]
600 MeV/N ^{16}O + ^{12}C [44]	1.05 GeV/N ^{12}C + ^{12}C [45]	2.1 GeV/N ^{12}C + ^{27}Al [45]

In **Tables 1-13**, the partial nucleus-nucleus cross sections are tabulated. In **Figures 21-46**, we show the calculated results from 8 different interactions. To get an impression of the agreement between the calculated results and the experimental data, we assumed 30% errors for the calculated results in the figures, and in all the tables except two (≈600 MeV/nucleon ^{40}Ar + ^{12}C and ≈600 MeV/nucleon ^{56}Fe + ^{12}C). This estimate serves only to "guide the eye" and does not represent the real errors.

The agreement between the calculated cross sections and the experimental data is better than earlier published results [38,39,46].

VI. RESULTS AND DISCUSSION

We have developed a computer code for calculations of energy loss (dE/dx) and range distributions for heavy ions in any media. In our code dE/dx is calculated as a function of energy, based on the Bethe equation for the total energy loss for heavy particles. Effective charge, relativistic and density correction terms are added. The results from our calculations are in very good agreement with previous calculations [9,10,11]. Our code is written in FORTRAN and can be run on any IBM/XT/AT, VAX, or UNIX computer. The speed of the calculations are roughly the same as for TRIM91 [11], which is developed for IBM. The advantage with our code is that it is short and therefore easy to use as a subroutine in any other computer program, e.g., in depth–dose calculations.

We have also developed semiempirical total reaction cross section formulae for proton–nucleus (with $Z_p \leq 26$) and nucleus–nucleus (with Z_p and $Z_t \leq 26$) reactions. These formulae apply for incident energies above 15 MeV and 100 MeV/nucleon respectively. For the nucleus–nucleus total reaction cross sections, we assumed energy independence for incident energies ≥100 MeV/nucleon. The reaction cross sections are not expected to be energy independent until $E_{proj} \geq 1.5$ GeV/nucleon, but for our purposes the energy dependence above 100 MeV/nucleon is considered negligible as compared to other uncertainties in the experimental data. For the proton–nucleus reaction cross sections we assumed energy independence above 200 MeV.

The transparency function, or the overlap parameter, for the nucleus–nucleus reaction cross section formula was fitted as a polynomial function of the first order in $(A_p^{-1/3}+A_t^{-1/3})$ for all projectile–target combinations with Z_p and $Z_t \leq 26$ and incident energies > 100 MeV/nucleon.

The transparency function for the proton–nucleus reaction cross section formula was fitted as a polynomial function of the first order in $(1+A_t^{-1/3})$ for all targets with $Z_t \leq 26$ and incident energies > 100 MeV. To calculate the energy dependence at energies ≤ 100 MeV, we developed some energy dependent functions, which are then multiplied by our energy independent function.

The formulae can probably be improved by fitting different overlap parameters for each projectile–target combination, but that will make the use of the formulae more complicated.

From the total reaction cross sections, we can calculate the mean free paths and the fluence distributions. We have compared all the calculated reaction cross sections and the mean free paths with experimental data, and found the agreement to be good.

We have also constructed a procedure for calculating projectile fragment production cross sections, by scaling the semiempirical proton–nucleus partial cross section systematics. The scaling is performed using a scaling parameter deduced from our reaction cross sections formulae, and additional enhancement factors. One advantage with our scaling procedure (i.e. that we deduce our scaling parameter from our reaction cross sections formulae) is that we take into account the effect of the nuclear transparency. Due to the nuclear transparency, the energy deposition is less in proton–nucleus interactions; so, as ΔA increases, the relative yields of proton–nucleus reactions diminish progressively.

All products from the Z of the projectile down to Z=2 can be calculated with our

procedure. The agreement between the calculated cross sections and the experimental data is better than earlier published results [38,39,46].

To improve the constructed formulae, there is a strong need for more experimental data. We therefore hope there soon will be more experimental data available, especially projectile fragmentation cross sections.

VII ACKNOWLEDGEMENTS

We wish to thank M. Doi for being very helpful in solving our computer problems. Help and support from H. Koyama is also very much acknowledged. We are also very grateful to R. Silberberg and C.H. Tsao for giving us an updated copy of their code for calculating the partial cross sections for proton–nucleus reactions. Their comments and advice are also very much appreciated. One of us (L.S.) gratefully acknowledges the support of the STA Fellowship Program. One of us (L.S.) also want to thank all colleagues and friends at NIRS for their help and hospitality during his stay in Japan.

procedure. The agreement between the calculated cross sections and the experimental data is better than earlier published results [38,39,46].

To improve the constructed formulae, there is a strong need for more experimental data. We therefore hope there soon will be more experimental data available, especially projectile fragmentation cross sections.

VII ACKNOWLEDGEMENTS

We wish to thank M. Doi for being very helpful in solving our computer problems. Help and support from H. Koyama is also very much acknowledged. We are also very grateful to R. Silberberg and C.H. Tsao for giving us an updated copy of their code for calculating the partial cross sections for proton–nucleus reactions. Their comments and advice are also very much appreciated. One of us (L.S.) gratefully acknowledges the support of the STA Fellowship Program. One of us (L.S.) also want to thank all colleagues and friends at NIRS for their help and hospitality during his stay in Japan.

VIII. REFERENCES

1. W. Schimmerling, S.B. Curtis, and K. G. Vosburgh, Radiat. Res. **72**, 1 (1977).
2. F. Soga, **International Workshop on the NIRS Heavy Ion Particle Accelerator**, NIRS, Chiba-shi, Japan, July 4-5, 1991.
3. R. Silberberg and C.H. Tsao, Astrophys. J. Supp. **25**, 315 (1973), R. Silberberg and C.H. Tsao, *ibid.* **25**, 335 (1973).
4. R. Silberberg and C.H. Tsao, Astrophys. J. Supp. **25**, 873 (1985).
5. M.R. Shavers, S.B. Curtis, J. Miller, and W. Schimmerling, Radiat. Res. **124**, 117 (1990).
6. R.M. Sternheimer, S.M. Seltzer, and M.J. Berger, Phys. Rev. **26**, 6067 (1982).
7. M.C. Pirruccello and C.A. Tobias, **Biological and Medical Research with Heavy Ions at the BEVALAC 1977-1980**, LBL-11220, Nov. 1980.
8. **Stopping Power for Electrons and Positrons**, ICRU Report 37, Oct. 1984.
9. P. Steward and R. Wallace, Univ. California report UCRL-17314 (1966).
10. W. Heinrich, B. Wiegel, and G. Kraft, **β, Z_{eff}, dE/dx, Range and Restricted Energy Loss of Heavy Ions in the Region $1 \leq E \leq 1000$ MeV/nucleon**, GSI-91-30 Preprint June 1990.
11. J.F. Ziegler, J.P. Biersack, and U. Littmark, **The Stopping and Range of Ions in Solids**, (Pergamon Press, New York, 1985).
12. H.L. Bradt and B. Peters, Phys. Rev. **77**, 54-70 (1950).
13. M.R. Shavers, S.B. Curtis, J. Miller, and W. Schimmerling, Radiat. Res. **124**, 117-130 (1990).
14. I. Tanihata, Hyperfine Interact. **21**, 251-264 (1985).
15. J.W. Wilson, L. W. Townsend, and F.F. Badavi, Nucl. Instr. Meth. **B18**, 225-131 (1987).
16. K. Sümmerer and D.J. Morrissey, **Proc. First Int'l Conf. on Radioactive Nuclear. Beams**, 16-18 Oct. 1989, Berkeley, California, USA.
17. L.W. Townsend and J.W. Wilson, Radiat. Res. **106**, 283-287 (1986).
18. J.W. Wilson, L.W. Townsend, and H.B. Bidasaria, Health Phys. **46**, 1101-1111 (1984).
19. P.L. Jain, M.M. Aggarwal, K.L. Gomber, and M.S. El-Nagdy, Radiat. Res. **101**, 225-236 (1985).
20. H.H. Heckman, D.E. Greiner, P.J. Lindstrom, and H. Shwe, Phys. Rev. **C17**, 1735 (1978).
21. W.R. Webber, J.C. Kish, and D.A. Schrier, Phys. Rev. **C41**, 520 (1990).
22. P.J. Lindstrom, D.E. Greiner, and H.H. Heckman, Bull. Am. Phys. Soc. **17**, 488 (1972).
23. G.D. Westfall, L.W. Wilson, P.J. Lindstrom, H.J. Crawford, D.E. Greiner, and H.H. Heckman, Phys. Rev. **C19**, 1309 (1979).
24. I. Tanihata **et al.**, Phys. Rev. Lett. **55**, 2676 (1985).
25. I. Tanihata **et al.**, Phys. Lett. **160B**, 380 (1985).
26. Kox **et al.**, Phys. Rev. **C35**, 1678 (1987).
27. P.U. Renberg, D.F. Measday, M. Pepin, P. Schwaller, B. Favier, and C. Richard-Serre, Nucl. Phys. **A183**, 81-104 (1972).
28. H.A. Bethe, Phys. Rev. **57**, 1125 (1940).
29. W. Bauhoff, Atomic Data and Nuclear Data Tables **35**, 429-447 (1986).
30. J. Llacer, C.A. Tobias, W.R. Holley, and T. Kanai, Med. Phys **11(3)**, 266-278, May-June 1984.
31. J. Llacer, J.B. Scmidt, and C.A. Tobias, LBL Report, LBL-26329, Nov. 1988.

32. A. Fukumura, private communication.
33. G. Rudstam, PhD. Thesis, University of Uppsala 1956.
34. G. Rudstam, Zs. f. Naturforschung **21A**, 1027 (1966).
35. G. Rudstam, Nucl. Phys. **A126, 401** (1969).
36. I. Dostrovsky, P. Rabinowitz, and R. Bivins, Phys. Rev. **111**, 1659 (1958).
37. R. Silberberg and C.H. Tsao, 15th ICRC **2**, 84 (1977).
38. R. Silberberg and C.H. Tsao, **Updated Cross Section Calculations for Cosmic Rays** Proc. to the 21st Internat. Cosmic Ray Conf. (Adelaide) 3, 424 (1990).
39. R. Silberberg and C.H. Tsao, Phys. Rep. **191**, 351 (1990).
40. P.J. Lindstrom, G.E. Greiner, H.H Heckman, B. Cork, and F.S. Bieser, Phys. Rev. Lett. **35**, 152 (1975).
41. J.B. Cumming, R.W. Stoenner, and P.E. Haustein, Phys. Rev. **C14**, 1554 (1976).
42. N.T. Porile, G.D. Cole, and C.R. Rudy, Phys. Rev. **C19**, 2288 (1979).
43. J.M. Kidd, P.J. Lindstrom, H.J. Crawford, and G. Woods, Phys. Rev. **C37**. 2613 (1988).
44. W.R. Webber, J.C. Kish, and D.A. Scrier, Phys. Rev. **C41**, 547 (1990).
45. D.L. Olson, B.B. Berman, D.E. Greiner, H.H. Heckman, P.J. Lindstrom, and H.J. Crawford, Phys. Rev. **C28**, 1602 (1983).
46. R. Silberberg and C.H. Tsao, private communication.
47. S. Barshay, C.B. Dover, and J.P. Vary, Phys. Rev. **C11**, 360 (1975).
48. S. Barshay, C.B. Dover, and J.P. Vary, Phys. Lett. **B51**, 5 (1974).
49. J.R. Cummings **et al.**, Phys. Rev. **C42**, 2508 (1990), J.R. Cummings **et al.**, *ibid.* **C35**, 2530, (1990).

Table I. dE/dx as a function of energy for the four calculations shown in Figure 1 and 2.

Energy [MeV/N]	Our Calc. [MeV/g/cm^2]	Energy [MeV/N]	Steward et al. [MeV/g/cm^2]	Energy [MeV/N]	Heinrich et al. [MeV/g/cm^2]	Energy [MeV/N]	Ziegler et al. [MeV/g/cm^2]
.100E+01	.68413E+04	1.	0.63538E4	1.	7.1790E3	1.	0.6677E+04
.200E+01	.50140E+04	2.	0.47936E4	2.	5.3854E3	2.	0.4900E+04
.300E+01	.39510E+04	3.	0.39273E4	3.	4.2703E3	3.	0.3911E+04
.400E+01	.32671E+04	4.	0.3293E4	4.	3.5217E3	4.2	0.3175E+04
.500E+01	.27913E+04	5.	0.2824E4	5.	2.9484E3	5.	0.2802E+04
.600E+01	.24413E+04	7.	0.22059E4	6.	2.5312E3	5.8	0.2509E+04
.700E+01	.21730E+04	10.	0.16616E4	7.	2.2446E3	6.7	0.2273E+04
.800E+01	.19607E+04	20.	0.93919E3	8.	1.9745E3	7.5	0.2079E+04
.900E+01	.17884E+04	30.	0.67251E3	9.	1.7994E3	8.3	0.1916E+04
.100E+02	.16458E+04	40.	0.53217E3	10.	1.6553E3	9.2	0.1778E+04
.200E+02	.94146E+03	50.	0.4451E3	20.	9.4694E2	10.8	0.1557E+04
.300E+02	.67718E+03	60.	0.38559E3	30.	6.8101E2	21.7	0.8958E+03
.400E+02	.53672E+03	70.	0.34223E3	40.	5.3969E2	30.	0.6848E+03
.500E+02	.44899E+03	80.	0.30917E3	50.	4.514E2	37.5	0.5702E+03
.600E+02	.38872E+03	90.	0.28309E3	60.	3.9075E2	45.8	0.4844E+03
.700E+02	.34465E+03	100.	0.26197E3	70.	3.4641E2	54.2	0.4235E+03
.800E+02	.31096E+03	160.	0.18855E3	80.	3.1252E2	66.7	0.3594E+03
.900E+02	.28433E+03	200.	0.16312E3	90.	2.8574E2	83.3	0.3024E+03
.100E+03	.26274E+03	250.	0.14232E3	100.	2.6403E2	100.	0.2636E+03
.150E+03	.19622E+03	300.	0.12819E3	150.	1.9718E2	150.	0.1971E+03
.200E+03	.16187E+03	350.	0.11795E3	200.	1.6267E2	200.	0.1628E+03
.250E+03	.14091E+03	400.	0.11020E3	250.	1.4163E2	250.	0.1419E+03
.300E+03	.12683E+03	450.	0.10413E3	300.	1.275E2	300.	0.1278E+03
.350E+03	.11676E+03	500.	0.99263E2	350.	1.1739E2	375.	0.1137E+03
.400E+03	.10924E+03	550.	0.95276E2	400.	1.0984E2	458.3	0.1034E+03
.450E+03	.10343E+03	600.	0.9196E2	450.	1.0402E2	500.	0.9953E+02
.500E+03	.98822E+02	650.	0.89168E2	500.	9.9402E1	541.7	0.9631E+02
.550E+03	.95128E+02	700.	0.8679E2	550.	9.5676E1	583.3	0.9358E+02
.600E+03	.92095E+02	750.	0.84749E2	600.	9.2619E1	666.7	0.8920E+02
.650E+03	.89562E+02	800.	0.82983E2	650.	9.0078E1	750.	0.8589E+02
.700E+03	.87423E+02			700.	8.7942E1	833.3	0.8333E+02
.750E+03	.85601E+02			750.	8.6131E1		
.800E+03	.84035E+02			800.	8.4582E1		

Table II. Range distributions as a function of energy for the four calculations shown in Fig. 3.

Energy [MeV/N]	Our Calc. [g/cm^2]	Energy [MeV/N]	Heinrich et al. [g/cm^2]	Energy [MeV/N]	Steward et al. [g/cm^2]	Energy [MeV/N]	Ziegler et al. [g/cm^2]
.100E+01	.14108E-02	100.	2.5554E0	100.	0.25651E1	1.	0.16270E-02
.200E+01	.34824E-02	150.	5.2249E0	125.	0.38013E1	2.	0.37510E-02
.300E+01	.61982E-02	200.	8.5994E0	150.	0.52250E1	3.	0.65080E-02
.400E+01	.95541E-02	250.	1.2569E1	175.	0.68192E1	4.2	0.10500E-01
.500E+01	.13541E-01	300.	1.7046E1	200.	0.85698E1	5.	0.13856E-01
.600E+01	.18149E-01	350.	2.1959E1	220.	0.10075E2	5.8	0.17631E-01
.700E+01	.23369E-01	400.	2.7249E1	250.	0.12492E2	6.7	0.21818E-01
.800E+01	.29191E-01	450.	3.2867E1	280.	0.15088E2	7.5	0.26417E-01
.900E+01	.35606E-01	500.	3.8772E1	300.	0.16911E2	8.3	0.31426E-01
.100E+02	.42607E-01	550.	4.4927E1	320.	0.18802E2	9.2	0.36843E-01
.200E+02	.14328E+00	600.	5.1304E1	350.	0.21760E2	10.8	0.48767E-01
.300E+02	.29595E+00	650.	5.7874E1	380.	0.24854E2	21.7	0.16300E+00
.400E+02	.49659E+00	700.	6.4617E1	400.	0.26987E2	30.	0.29200E+00
.500E+02	.74222E+00	750.	7.1512E1	420.	0.29174E2	37.5	0.43600E+00
.600E+02	.10304E+01	800.	7.8543E1	450.	0.32549E2	45.8	0.62700E+00
.700E+02	.13590E+01			480.	0.36031E2	54.2	0.84800E+00
.800E+02	.17261E+01			500.	0.38408E2	66.7	0.12340E+01
.900E+02	.21302E+01			520.	0.40828E2	83.3	0.12340E+01
.100E+03	.25697E+01			550.	0.44533E2	100.	0.25530E+01
.150E+03	.52524E+01			580.	0.48323E2	150.	0.52240E+01
.200E+03	.86437E+01			600.	0.50895E2	200.	0.85940E+01
.250E+03	.12676E+02			620.	0.53501E2	250.	0.12556E+02
.300E+03	.17207E+02			650.	0.57471E2	275.	0.14729E+02
.350E+03	.22167E+02			680.	0.61510E2	300.	0.17019E+02
.400E+03	.27500E+02			700.	0.64239E2	375.	0.24507E+02
.450E+03	.33157E+02			720.	0.66996E2	458.3	0.33752E+02
.500E+03	.39099E+02			750.	0.71181E2	500.	0.38680E+02
.550E+03	.45292E+02			780.	0.75423E2	541.7	0.43786E+02
.600E+03	.51705E+02			800.	0.78281E2	666.7	0.59998E+02
.650E+03	.58314E+02					750.	0.71423E+02
.700E+03	.65097E+02					833.3	0.83242E+02
.750E+03	.72034E+02						
.800E+03	.79110E+02						

Table III Calculated total reaction cross sections in mb for the interactions of ^{12}C with targets ranging from mass number A=1 to A=20.

Reaction cross Section Formula	Target Mass Number 1	2	4	6	12	16	20
SIGMA1:	280.8	354.9	467.0	560.6	801.2	898.3	984.6
SIGMA2:	200.7	382.6	557.6	666.9	884.9	993.6	1088.0
SIGMA3:	409.2	526.2	673.6	777.0	989.5	1093.2	1180.7
SIGMA6:	117.4	220.9	360.3	463.9	688.9	806.5	909.9

SIGMA4

Energy [MeV/N]	Target Mass Number 1	2	4	6	12	16	20
100.0	172.50	347.20	520.40	628.90	846.74	955.86	1050.77
200.0	162.34	330.32	497.45	602.31	813.09	918.77	1010.72
300.0	177.25	350.61	521.52	628.31	842.32	949.37	1042.41
400.0	196.20	376.64	552.77	662.33	881.15	990.34	1085.12
500.0	211.50	397.46	577.69	689.43	912.08	1022.97	1119.14
600.0	220.79	409.99	592.61	705.63	930.50	1042.37	1139.35
700.0	224.43	414.81	598.28	711.74	937.38	1049.59	1146.83
800.0	223.83	413.90	597.09	710.40	935.73	1047.79	1144.91
900.0	220.61	409.44	591.67	704.43	928.80	1040.42	1137.17
1000.0	216.13	403.27	584.19	696.25	919.32	1030.36	1126.63
1100.0	211.38	396.73	576.27	687.57	909.29	1019.71	1115.47
1200.0	206.99	390.66	568.91	679.51	899.98	1009.82	1105.11
1300.0	203.28	385.52	562.68	672.68	892.08	1001.43	1096.32
1400.0	200.39	381.51	557.80	667.33	885.88	994.85	1089.42
1500.0	198.31	378.62	554.28	663.46	881.40	990.09	1084.42
1600.0	196.97	376.74	552.00	660.95	878.48	986.98	1081.16
1700.0	196.26	375.73	550.75	659.58	876.88	985.28	1079.37
1800.0	196.03	375.41	550.34	659.12	876.33	984.69	1078.74
1900.0	196.18	375.59	550.55	659.34	876.57	984.93	1078.99
2000.0	196.57	376.13	551.19	660.03	877.35	985.75	1079.84
2100.0	197.13	376.88	552.09	661.01	878.46	986.92	1081.06
2200.0	197.76	377.75	553.13	662.14	879.75	988.28	1082.48
2300.0	198.42	378.64	554.20	663.31	881.08	989.69	1083.95
2400.0	199.05	379.50	555.23	664.43	882.37	991.05	1085.37
2500.0	199.63	380.29	556.18	665.46	883.55	992.30	1086.66

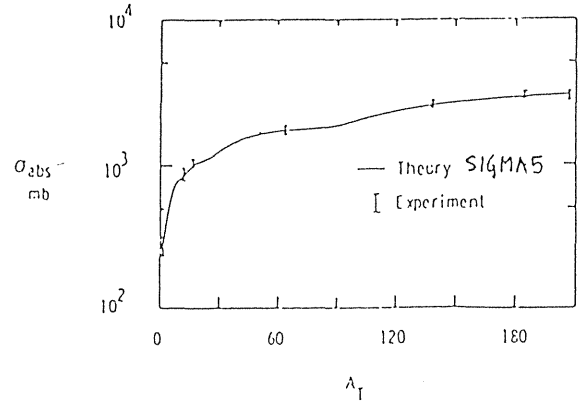

Absorption cross sections for carbon projectiles at 2.1 GeV/amu onto various targets.

Absorption cross sections for ^{12}C projectiles colliding with various target nuclei

Target Mass Number	Theoretical Absorption Cross Sections in mb a	b	Experimental Absorption Cross Sections in mb
0.87 GeV/Nucleon			
12	819	763	[c] 939 ± 49
2.1 GeV/Nucleon			
1	237	246	[c] 269 ± 14 [d] 258 ± 21
12	839	781	[c] 888 ± 50 [d] 826 ± 23
16	990	820	[d] 1022 ± 25
64	1727	1656	[d] 1730 ± 36
138	2519	2447	[e] 2600 ± 100
184	2924		[c] 3000 ± 100
208	3047	2969	[d] 2960 ± 65

a and b are not equal to SIGMA5.

Table IV Calculated total reaction cross sections in mb for the interactions of ^{12}C with targets ranging from mass number A=64 to A=208.

Reaction cross Section Formula	Target Mass Number 64	184	208
SIGMA1:	1654.4	2796.0	2980.4
SIGMA2:	1789.8	2948.2	3133.5
SIGMA3:	1759.2	2518.7	2625.5
SIGMA6:	1692.3	2996.2	3205.4

SIGMA4

Energy [MeV/N]	Target Mass Number 64	184	208
100.0	1761.29	2943.61	3133.38
200.0	1699.87	2848.33	3032.77
300.0	1737.70	2891.90	3076.96
400.0	1791.09	2957.96	3144.70
500.0	1833.73	3011.05	3199.20
600.0	1858.90	3042.19	3231.13
700.0	1867.98	3053.01	3242.17
800.0	1865.16	3048.83	3237.77
900.0	1855.00	3035.37	3223.84
1000.0	1841.31	3017.48	3205.35
1100.0	1826.86	2998.68	3185.93
1200.0	1813.44	2981.23	3167.91
1300.0	1802.05	2966.41	3152.60
1400.0	1793.09	2954.74	3140.54
1500.0	1786.58	2946.23	3131.75
1600.0	1782.32	2940.61	3125.94
1700.0	1779.94	2937.44	3122.65
1800.0	1779.07	2936.22	3121.37
1900.0	1779.33	2936.46	3121.60
2000.0	1780.37	2937.71	3122.88
2100.0	1781.90	2939.59	3124.81
2200.0	1783.68	2941.81	3127.09
2300.0	1785.52	2944.12	3129.46
2400.0	1787.31	2946.35	3131.75
2500.0	1788.94	2948.39	3133.84

Table V Calculated total reaction cross sections in mb for the interactions of ^{16}O with targets ranging from mass number A=1 to A=20.

Reaction cross Section Formula	Target Mass Number 1	2	4	6	12	16	20
SIGMA1:	339.4	420.4	541.8	642.2	898.3	1052.9	1146.2
SIGMA2:	254.2	454.1	644.5	761.6	993.6	1108.6	1208.2
SIGMA3:	512.9	629.9	777.3	880.6	1093.2	1196.9	1284.4
SIGMA6:	168.7	289.5	446.6	560.4	806.5	993.4	1044.3

SIGMA4

Energy [MeV/N]	Target Mass Number 1	2	4	6	12	16	20
100.0	223.57	418.26	606.66	723.40	955.86	1071.60	1171.95
200.0	211.34	398.84	580.81	693.71	918.77	1030.90	1128.17
300.0	228.08	420.81	606.44	721.20	949.37	1062.82	1161.14
400.0	249.40	449.13	639.91	757.41	990.34	1105.90	1205.94
500.0	266.54	471.74	666.59	786.25	1022.97	1140.22	1241.64
600.0	276.92	485.32	682.53	803.46	1042.37	1160.60	1262.81
700.0	280.95	490.52	688.56	809.93	1049.59	1168.14	1270.61
800.0	280.26	489.49	687.25	808.45	1047.79	1166.19	1268.53
900.0	276.63	484.61	681.3.	802.05	1040.42	1158.37	1260.34
1000.0	271.60	477.88	673.34	793.28	1030.36	1147.72	1249.20
1100.0	266.26	470.73	664.81	783.99	1019.71	1136.45	1237.43
1200.0	261.31	464.11	656.89	775.37	1009.82	1125.99	1226.49
1300.0	257.14	458.50	650.18	768.06	1001.43	1117.11	1217.21
1400.0	253.87	454.11	644.93	762.32	994.85	1110.15	1209.92
1500.0	251.53	450.94	641.13	758.18	990.09	1105.10	1204.64
1600.0	250.02	448.89	638.66	755.48	986.98	1101.80	1201.19
1700.0	249.20	447.78	637.32	754.01	985.28	1099.99	1199.29
1800.0	248.95	447.42	636.87	753.51	984.69	1099.36	1198.62
1900.0	249.10	447.61	637.08	753.74	984.93	1099.60	1198.87
2000.0	249.55	448.19	637.76	754.47	985.75	1100.46	1199.75
2100.0	250.17	449.01	638.73	755.51	986.92	1101.70	1201.04
2200.0	250.88	449.95	639.84	756.71	988.28	1103.13	1202.53
2300.0	251.61	450.92	640.99	757.96	989.69	1104.61	1204.07
2400.0	252.32	451.86	642.10	759.16	991.05	1106.04	1205.56
2500.0	252.97	452.72	643.11	760.25	992.30	1107.35	1206.92

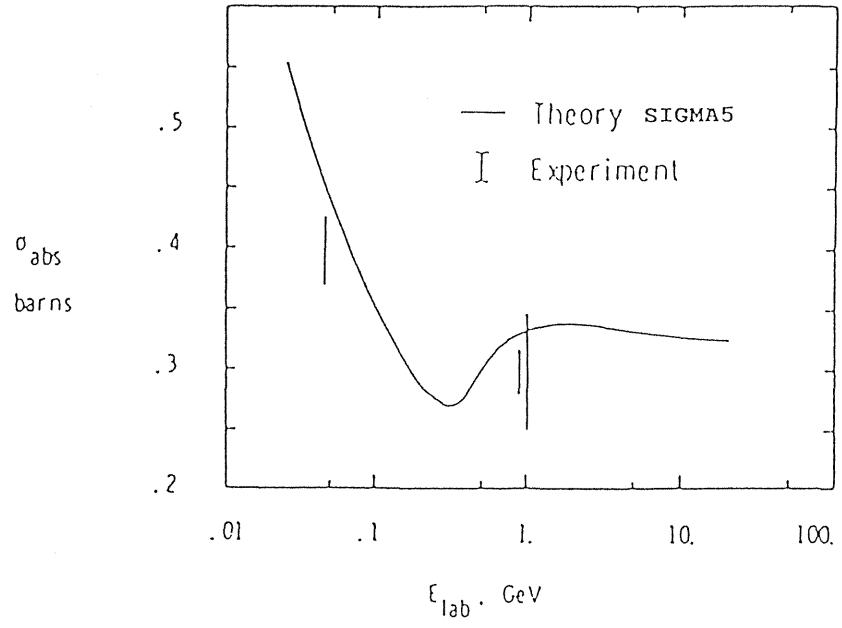

Absorption nuclear cross sections for nucleons on oxygen targets.

Table VI Calculated total reaction cross sections in mb for the interactions of ^{16}O with targets ranging from mass number A=40 to A=140.

Reaction cross Section Formula	Target Mass Number 40	60	80	100	120	140
SIGMA1:	1517.6	1809.2	2059.6	2283.8	2489.2	2680.4
SIGMA2:	1593.5	1889.8	2142.3	2367.0	2572.2	2762.8
SIGMA3:	1601.9	1824.6	2001.9	2151.6	2282.5	2399.6
SIGMA6:	1478.2	1813.6	2099.6	2354.4	2587.3	2803.5

SIGMA4

Energy [MeV/N]	Target Mass Number 40	60	80	100	120	140
100.0	1561.86	1862.98	2120.02	2349.30	2558.98	2753.83
200.0	1506.34	1798.59	2048.17	2270.86	2474.56	2663.90
300.0	1542.73	1837.08	2088.17	2312.02	2516.67	2706.79
400.0	1593.45	1891.75	2145.89	2372.27	2579.07	2771.09
500.0	1633.92	1935.44	2192.08	2420.53	2629.12	2822.71
600.0	1657.85	1961.22	2219.28	2448.92	2658.52	2853.02
700.0	1666.54	1970.48	2228.98	2458.96	2668.86	2863.61
800.0	1663.97	1967.54	2225.74	2455.45	2665.11	2859.64
900.0	1654.44	1957.07	2214.51	2443.57	2652.66	2846.67
1000.0	1641.56	1942.97	2199.44	2427.68	2636.04	2829.40
1100.0	1627.96	1928.10	2183.56	2410.94	2618.55	2811.23
1200.0	1615.33	1914.30	2168.81	2395.41	2602.32	2794.38
1300.0	1604.61	1902.58	2156.30	2382.21	2588.53	2780.06
1400.0	1596.19	1893.36	2146.45	2371.83	2577.68	2768.78
1500.0	1590.07	1886.66	2139.29	2364.27	2569.77	2760.57
1600.0	1586.07	1882.27	2134.57	2359.29	2564.56	2755.15
1700.0	1583.84	1879.82	2131.94	2356.50	2561.64	2752.10
1800.0	1583.04	1878.91	2130.96	2355.46	2560.53	2750.93
1900.0	1583.30	1879.17	2131.22	2355.71	2560.77	2751.17
2000.0	1584.29	1880.24	2132.33	2356.86	2561.97	2752.39
2100.0	1585.74	1881.80	2133.98	2358.59	2563.75	2754.23
2200.0	1587.43	1883.62	2135.91	2360.60	2565.83	2756.38
2300.0	1589.18	1885.51	2137.91	2362.69	2568.01	2758.62
2400.0	1590.87	1887.34	2139.84	2364.72	2570.11	2760.79
2500.0	1592.42	1889.02	2141.62	2366.57	2572.03	2762.78

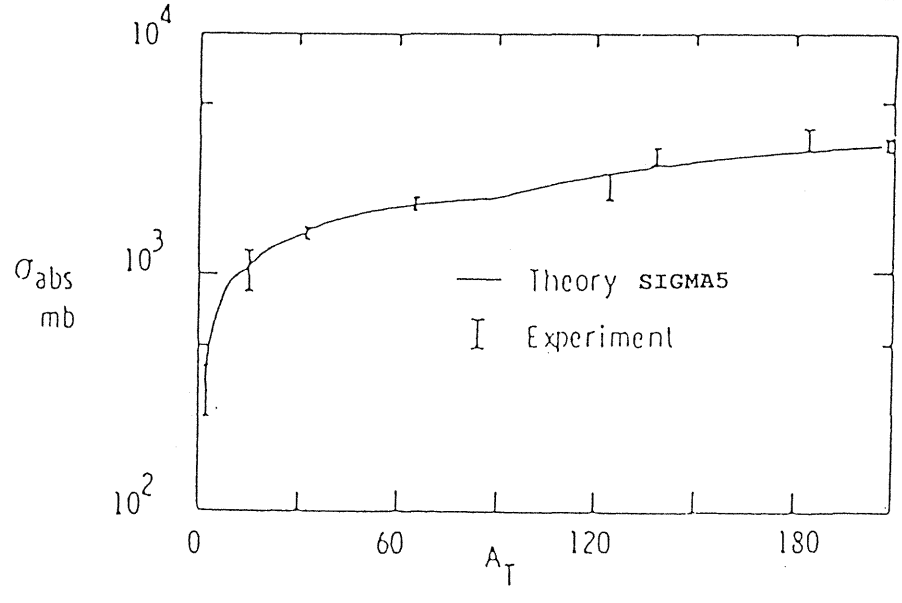

Absorption cross sections for oxygen projectiles at 2.1 GeV/amu onto various targets.

Table VII Calculated total reaction cross sections in mb for the interactions of ^{20}Ne with H and ^{16}O.

Reaction cross Section Formula	Target Mass Number 1	16
SIGMA1:	393.2	1146.2
SIGMA2:	302.9	1208.2
SIGMA3:	600.5	1284.4
SIGMA6:	217.7	1044.3

SIGMA4

Energy [MeV/N]	Target Mass Number 1	16
100.0	270.63	1171.95
200.0	256.58	1128.17
300.0	274.80	1161.14
400.0	298.05	1205.94
500.0	316.69	1241.64
600.0	327.95	1262.81
700.0	332.31	1270.61
800.0	331.53	1268.53
900.0	327.56	1260.34
1000.0	322.07	1249.20
1100.0	316.24	1237.43
1200.0	310.84	1226.49
1300.0	306.27	1217.21
1400.0	302.71	1209.92
1500.0	300.14	1204.64
1600.0	298.48	1201.19
1700.0	297.59	1199.29
1800.0	297.30	1198.62
1900.0	297.47	1198.87
2000.0	297.95	1199.75
2100.0	298.63	1201.04
2200.0	299.40	1202.53
2300.0	300.20	1204.07
2400.0	300.97	1205.56
2500.0	301.68	1206.92
2600.0	302.30	1208.11
2700.0	302.82	1209.11
2800.0	303.25	1209.92
2900.0	303.57	1210.54
3000.0	303.81	1210.98
3100.0	303.98	1211.28
3200.0	304.08	1211.45
3300.0	304.13	1211.51
3400.0	304.13	1211.50
3500.0	304.10	1211.41
3600.0	304.05	1211.29
3700.0	303.98	1211.13
3800.0	303.90	1210.95
3900.0	303.82	1210.77
4000.0	303.74	1210.58

Table VIII. Calculated reaction cross sections (using SIGMA1-SIGMA6) for the interactions of projectiles with A=12 to A=56 on He targets, together with the experimentally determined mass changing cross sections, $\sigma_{\Delta A \geq 1}$, [21] at ≈ 600 MeV/nucleon.

Projectile	Theoretical Reaction Cross Sections in mb				Experimental $\sigma_{\Delta A \geq 1}$ in mb
	SIGMA1	SIGMA2	SIGMA3	SIGMA6 (b_o=1.3)	
^{12}C	467.2	557.7	673.7	360.4	453
^{14}N	505.6	602.8	728.1	404.9	468
^{16}O	541.9	644.7	777.4	446.8	554
^{27}Al	715.6	838.8	993.5	646.5	805
^{56}Fe	1070.8	1220.1	1365.1	1052.1	1136

Table IX. Calculated reaction cross sections (using SIGMA1-SIGMA6) for the interactions of projectiles with A=12 to A=58 on C targets, together with the experimentally determined mass changing cross sections, $\sigma_{\Delta A \geq 1}$, [21] at ≈ 600 MeV/nucleon.

Projectile	Theoretical Reaction Cross Sections in mb				Experimental $\sigma_{\Delta A \geq 1}$ in mb
	SIGMA1	SIGMA2	SIGMA3	SIGMA6 (b_o=1.3)	
^{12}C	801.5	885.2	989.8	689.2	757
^{14}N	851.8	941.9	1044.1	750.2	802
^{16}O	898.8	994.0	1093.5	806.9	891
^{20}Ne	985.1	1088.3	1181.1	910.3	1056
^{24}Mg	1063.8	1173.1	1257.6	1003.8	1218
^{27}Al	1119.0	1231.9	1309.6	1069.0	1232
^{28}Si	1136.8	1250.8	1326.0	1089.9	1271
^{32}S	1205.1	1323.1	1388.2	1170.3	1338
^{40}Ar	1331.3	1455.4	1498.5	1317.8	1595
^{40}Ca	1331.3	1455.4	1498.5	1317.8	1457
^{56}Fe	1554.1	1686.4	1681.2	1576.4	1826
^{58}Ni	1579.9	1713.0	1701.4	1606.2	1949

Table X. Calculated reaction cross sections (using SIGMA1-SIGMA6) for the interactions of projectiles with A=12 to A=56 on He targets, together with the experimentally determined charge changing cross sections, $\sigma_{\Delta Z \geq 1}$, [21] at 1.5 GeV/nucleon.

Projectile	Theoretical Reaction Cross Sections in mb				Experimental $\sigma_{\Delta Z \geq 1}$ in mb
	SIGMA1	SIGMA2	SIGMA3	SIGMA6 (b_o=1.3)	
^{12}C	467.2	557.7	673.7	360.4	431 ± 7
^{14}N	505.6	602.8	728.1	404.9	482 ± 8
^{16}O	541.9	644.7	777.4	446.8	512 ± 9
^{27}Al	715.6	838.8	993.5	646.5	796 ± 12
^{56}Fe	1070.8	1220.1	1365.1	1052.1	1196 ± 21

Table XI. Calculated reaction cross sections (using SIGMA1-SIGMA6) for the interactions of projectiles with A=12 to A=58 on C targets, together with the experimentally determined charge changing cross sections, $\sigma_{\Delta Z \geq 1}$, [21] at 1.5 GeV/nucleon.

Projectile	Theoretical Reaction Cross Sections in mb				Experimental $\sigma_{\Delta Z \geq 1}$ in mb
	SIGMA1	SIGMA2	SIGMA3	SIGMA6 (b_o=1.3)	
^{12}C	801.5	885.2	989.8	689.2	725 ± 9
^{14}N	851.8	941.9	1044.1	750.2	796 ± 10
^{16}O	898.8	994.0	1093.5	806.9	850 ± 10
^{20}Ne	985.1	1088.3	1181.1	910.3	992 ± 12
^{24}Mg	1063.8	1173.1	1257.6	1003.8	1140 ± 14
^{27}Al	1119.0	1231.9	1309.6	1069.0	1188 ± 16
^{28}Si	1136.8	1250.8	1326.0	1089.9	1216 ± 16
^{32}S	1205.1	1323.1	1388.2	1170.3	1270 ± 17
^{40}Ar	1331.3	1455.4	1498.5	1317.8	1390 ± 19
^{40}Ca	1331.3	1455.4	1498.5	1317.8	1390 ± 19
^{56}Fe	1554.1	1686.4	1681.2	1576.4	1615 ± 20
^{58}Ni	1579.9	1713.0	1701.4	1606.2	1745 ± 25

Table XII. Calculated reaction cross sections (using SIGMA1-SIGMA6), together with experimental valus [18,22], for the interactions of 2.1 GeV/nucleon ^{12}C with different targets.

Target	Theoretical Reaction Cross Sections in mb				Experimental σ_{reac} in mb
	SIGMA1	SIGMA2	SIGMA3	SIGMA6 (b_o=1.3)	
H	281.4	202.8	410.4	118.4	258 ± 21
C	801.5	885.2	989.8	689.2	826 ± 23
S	1205.6	1323.7	1388.8	1171.0	1250 ± 51
Cu	1648.8	1784.1	1755.0	1685.8	1730 ± 36

Table XIII. Calculated reaction cross sections (using SIGMA1-SIGMA6), together with experimental valus [18,22], for the interactions of 2.1 GeV/nucleon ^{16}O with different targets.

Target	Theoretical Reaction Cross Sections in mb				Experimental σ_{reac} in mb
	SIGMA1	SIGMA2	SIGMA3	SIGMA6 (b_o=1.3)	
H	340.1	256.5	514.1	169.9	361 ± 24
C	801.9	885.6	990.1	689.6	1022 ± 25
S	1383.7	1456.0	1492.5	1322.9	1420 ± 51
Cu	1856.0	1937.2	1858.7	1867.2	1950 ± 41

Table XIV. Calculated reaction cross sections (using SIGMA1-SIGMA6), together with experimental mass changing cross sections, $\sigma_{\Delta A \geq 1}$, for the interactions of ^{56}Fe with different targets [23] at 1.88 GeV/nucleon.

Target	Theoretical Reaction Cross Sections in mb				Experimental σ_{reac} in mb
	SIGMA1	SIGMA2	SIGMA3	SIGMA6 (b_o=1.3)	
H	777.6	653.0	1101.8	592.1	750 ± 50
Li	1269.5	1439.1	1509.0	1290.2	1430 ± 40
Be	1391.6	1551.9	1587.1	1419.4	1670 ± 50
C	1554.1	1686.4	1681.2	1576.4	1660 ± 60
S	2563.6	2274.9	2080.2	2272.4	2220 ± 90
Cu	3194.0	2867.8	2446.4	2971.2	2940 ± 100
Ag	3854.1	3485.0	2792.8	3694.0	3710 ± 140

Table XV. Calculated reaction cross sections (using SIGMA1-SIGMA6), together with experimental charge changing cross sections, $\sigma_{\Delta Z \geq 1}$, for the interactions of ^{56}Fe with different targets [23] at 1.88 GeV/nucleon.

Target	Theoretical Reaction Cross Sections in mb				Experimental σ_{reac} in mb
	SIGMA1	SIGMA2	SIGMA3	SIGMA6 (b_o=1.3)	
H	777.6	653.0	1101.8	592.1	680 ± 40
Li	1269.5	1439.1	1509.0	1290.2	1340 ± 30
Be	1391.6	1551.9	1587.1	1419.4	1570 ± 30
C	1554.1	1686.4	1681.2	1576.4	1560 ± 50
S	2563.6	2274.9	2080.2	2272.4	2070 ± 80
Cu	3194.0	2867.8	2446.4	2971.2	2710 ± 70
Ag	3854.1	3485.0	2792.8	3694.0	3340 ± 80

Table XVI. Calculated reaction cross sections (using SIGMA1-SIGMA6), together with experimental interaction cross sections, for the interactions of Li and Be with different targets at 790 MeV/nucleon [24].

Interaction	Theoretical Reaction Cross Sections in mb				Experimental σ_{reac} in mb
	SIGMA1	SIGMA2	SIGMA3	SIGMA6 (b_o=1.3)	
^{6}Li + Be	491.5	583.5	683.2	380.2	651 ± 6
^{6}Li + C	560.8	667.1	777.3	463.5	688 ± 10
^{6}Li + Al	830.0	971.2	1096.4	781.6	1010 ± 11
^{7}Li + Be	532.0	625.2	726.3	420.4	686 ± 4
^{7}Li + C	604.0	711.5	820.4	507.7	736 ± 6
^{7}Li + Al	882.4	1024.6	1139.5	838.7	1071 ± 7
^{8}Li + Be	571.1	662.7	765.5	457.6	727 ± 8
^{8}Li + C	645.6	751.6	859.6	548.5	768 ± 9
^{8}Li + Al	932.5	1072.5	1178.7	891.0	1147 ± 14
^{9}Li + Be	609.0	697.3	801.5	492.5	739 ± 5
^{9}Li + C	685.9	788.4	895.6	586.7	796 ± 6
^{9}Li + Al	980.8	1116.4	1214.7	939.5	1135 ± 7
^{11}Li + Be	661.6	759.8	866.2	556.9	
^{11}Li + C	763.7	854.8	960.4	656.8	1040 ± 60
^{11}Li + Al	1073.4	1195.2	1279.5	1027.6	
^{7}Be + Be	532.0	625.1	726.3	420.4	682 ± 6
^{7}Be + C	604.0	711.5	820.4	507.7	738 ± 9
^{7}Be + Al	882.4	1024.6	1139.5	839.7	1050 ± 17
^{9}Be + Be	609.0	697.3	801.5	492.5	755 ± 6
^{9}Be + C	685.9	788.4	895.6	586.7	806 ± 9
^{9}Be + Al	980.8	1116.4	1214.7	939.5	1174 ± 11
^{10}Be + Be	636.0	729.5	835.0	525.5	755 ± 7
^{10}Be + C	725.2	822.7	929.1	622.7	813 ± 10
^{10}Be + Al	1027.7	1157.2	1248.2	984.8	1153 ± 16

Table XVII. Calculated reaction cross sections (using SIGmA1-SIGMA6), together with experimental interaction cross sections, for the interactions of different He isotopes with diffferent targets at 790 MeV/nucleon [25].

Interaction	Theoretical Reaction Cross Sections in mb				Experimental σ_{reac} in mb
	SIGMA1	SIGMA2	SIGMA3	SIGMA6 (b_o=1.3)	
^{3}He + Be	355.4	413.4	514.5	231.8	498 ± 4
^{3}He + C	414.7	484.2	608.6	297.7	550 ± 5
^{3}He + Al	649.8	747.4	927.7	560.8	850 ± 9
^{4}He + Be	404.2	481.6	579.8	287.6	485 ± 4
^{4}He + C	467.2	557.8	673.9	360.5	503 ± 5
					527 ± 26
^{4}He + Al	715.2	838.3	993.0	646.0	780 ± 13
^{4}He + ^{4}He	273.4	305.5	357.7	137.2	262 ± 19
^{6}He + Be	491.5	583.5	683.2	380.2	672 ± 7
^{6}He + C	560.8	667.1	777.3	463.5	722 ± 6
^{6}He + Al	830.0	971.2	1096.4	781.6	1063 ± 8
^{8}He + Be	571.1	662.7	765.5	457.6	757 ± 4
^{8}He + C	645.6	751.6	859.6	548.5	817 ± 6
^{8}He + Al	932.5	1072.5	1178.7	891.0	1197 ± 9

Table XVIII. Calculated reaction cross sections for the interactions of projectiles with A=12 to A=56 on He targets. SIGMA1 is compared with SIGMA6 (with $b_0=1.581-0.876*(A_p^{-1/3}+A_t^{-1/3})$) and the experimentally determined mass changing cross sections at ≈ 600 MeV/nucleon [21].

Projectile	Theoretical Reaction Cross Sections in mb				
	SIGMA1	SIGMA6	Experimental $\sigma_{\Delta z \geq 1}$ in mb	$\frac{\sigma_{SIGMA1}(calc)}{\sigma_{SIGMA1}(exp)}$	$\frac{\sigma_{SIGMA6}(calc)}{\sigma_{SIGMA6}(exp)}$
^{12}C	467	590	453	1.03	1.30
^{14}N	506	634	468	1.08	1.35
^{16}O	542	675	554	0.98	1.22
^{27}Al	716	874	805	0.89	1.09
^{56}Fe	1071	1284	1136	0.94	1.13

Table XIX. Calculated reaction cross sections for the interactions of projectiles with A=12 to A=56 on C targets. SIGMA1 is compared with SIGMA6 (with $b_0=1.581-0.876*(A_p^{-1/3}+A_t^{-1/3})$) and the experimentally determined mass changing cross sections at ≈ 600 MeV/nucleon [21].

Projectile	Theoretical Reaction Cross Sections in mb				
	SIGMA1	SIGMA6	Experimental $\sigma_{\Delta z \geq 1}$ in mb	$\frac{\sigma_{SIGMA1}(calc)}{\sigma_{SIGMA1}(exp)}$	$\frac{\sigma_{SIGMA6}(calc)}{\sigma_{SIGMA6}(exp)}$
^{12}C	802	869	757	1.06	1.15
^{14}N	852	925	802	1.06	1.15
^{16}O	899	977	891	1.01	1.10
^{20}Ne	985	1074	1056	0.93	1.02
^{24}Mg	1064	1163	1218	0.87	0.96
^{27}Al	1119	1225	1232	0.91	1.00
^{28}Si	1137	1246	1271	0.89	0.98
^{32}S	1205	1323	1338	0.90	0.99
^{40}Ar	1331	1466	1595	0.84	0.92
^{40}Ca	1331	1466	1457	0.91	1.01
^{56}Fe	1554	1719	1826	0.85	0.94

Table XX. Calculated reaction cross sections for the interactions of 2.1 GeV/nucleon ^{12}C with different targets. SIGMA1 is compared with SIGMA6 (with $b_0=1.581-0.876*(A_p^{-1/3}+A_t^{-1/3})$) and the experimentally determined reaction cross sections [18,22].

Target	Theoretical Reaction Cross Sections in mb				
	SIGMA1	SIGMA6	Experimental $\sigma_{\Delta z\geq 1}$ in mb	$\frac{\sigma_{SIGMA1}(calc)}{\sigma_{SIGMA1}(exp)}$	$\frac{\sigma_{SIGMA6}(calc)}{\sigma_{SIGMA6}(exp)}$
C	802	869	826 ± 23	0.97	1.05
S	1206	1324	1250 ± 51	0.96	1.06
Cu	1649	1827	1730 ± 36	0.95	1.06

Table XXI. Calculated reaction cross sections for the interactions of 2.1 GeV/nucleon ^{16}O with different targets. SIGMA1 is compared with SIGMA6 (with $b_0=1.581-0.876*(A_p^{-1/3}+A_t^{-1/3})$) and the experimentally determined reaction cross sections [18,22].

Target	Theoretical Reaction Cross Sections in mb				
	SIGMA1	SIGMA6	Experimental $\sigma_{\Delta z\geq 1}$ in mb	$\frac{\sigma_{SIGMA1}(calc)}{\sigma_{SIGMA1}(exp)}$	$\frac{\sigma_{SIGMA6}(calc)}{\sigma_{SIGMA6}(exp)}$
C	802	977	1022 ± 25	0.94	0.96
S	1384	1462	1420 ± 51	0.97	1.03
Cu	1856	1991	1950 ± 41	0.95	1.02

Table XXII. Calculated reaction cross sections for the interactions of ^{56}Fe with different targets. SIGMA1 is compared with SIGMA6 (with $b_0=1.581-0.876*(A_p^{-1/3}+A_t^{-1/3})$) and the experimentally determined reaction cross sections at 1.88 GeV/nucleon [23].

Target	Theoretical Reaction Cross Sections in mb				
	SIGMA1	SIGMA6	Experimental $\sigma_{\Delta z\geq 1}$ in mb	$\frac{\sigma_{SIGMA1}(calc)}{\sigma_{SIGMA1}(exp)}$	$\frac{\sigma_{SIGMA6}(calc)}{\sigma_{SIGMA6}(exp)}$
Li	1270	1471	1430 ± 40	0.89	1.03
Be	1392	1581	1670 ± 50	0.83	0.95
C	1554	1719	1660 ± 60	0.94	1.04
S	2564	2367	2220 ± 90	1.16	1.07
Cu	3194	3043	2940 ± 100	1.08	1.04
Ag	3854	3752	3710 ± 140	1.04	1.04

Table XXIII. Calculated reaction cross sections for the interactions of He, Li and Be with different targets at 790 MeV/nucleon. SIGMA1 is compared with SIGMA6 (with $b_0=1.581-0.876*(A_p^{-1/3}+A_t^{-1/3})$) and the experimentally determined reaction cross sections[24,25].

Projectile	Theoretical Reaction Cross Sections in mb		Experimental $\sigma_{\Delta Z \geq 1}$ in mb	$\frac{\sigma_{SIGMA1}(calc)}{\sigma_{SIGMA1}(exp)}$	$\frac{\sigma_{SIGMA6}(calc)}{\sigma_{SIGMA6}(exp)}$
	SIGMA1	SIGMA6			
^{3}He + Be	355	480	498 ± 4	0.71	0.96
^{3}He + C	415	546	550 ± 5	0.75	0.99
^{3}He + Al	650	814	850 ± 9	0.76	0.98
^{4}He + Be	404	520	485 ± 4	0.83	1.07
^{4}He + C	467	590	503 ± 5	0.93	1.17
			527 ± 26	0.89	1.12
^{4}He + Al	715	873	780 ± 13	0.92	1.12
^{6}He + Be	492	595	672 ± 7	0.73	0.89
^{6}He + C	561	672	722 ± 6	0.78	0.93
^{6}He + Al	830	978	1063 ± 8	0.78	0.92
^{8}He + Be	571	661	757 ± 4	0.75	0.87
^{8}He + C	646	744	817 ± 6	0.79	0.91
^{8}He + Al	932	1070	1197 ± 9	0.78	0.89
^{6}Li + Be	491	595	651 ± 6	0.76	0.91
^{6}Li + C	561	672	688 ± 10	0.82	0.98
^{6}Li + Al	830	978	1010 ± 11	0.82	0.97
^{7}Li + Be	532	629	686 ± 4	0.78	0.92
^{7}Li + C	604	709	736 ± 6	0.82	0.96
^{7}Li + Al	882	1025	1071 ± 7	0.82	0.96
^{8}Li + Be	571	661	727 ± 8	0.79	0.91
^{8}Li + C	646	744	768 ± 9	0.84	0.97
^{8}Li + Al	932	1070	1147 ± 14	0.81	0.93
^{9}Li + Be	609	692	739 ± 5	0.82	0.94
^{9}Li + C	686	777	796 ± 6	0.86	0.98
^{9}Li + Al	981	1111	1135 ± 7	0.86	0.98
^{7}Be + Be	532	629	682 ± 6	0.78	0.92
^{7}Be + C	604	709	738 ± 9	0.82	0.96
^{7}Be + Al	882	1025	1050 ± 17	0.84	0.98
^{9}Be + Be	609	692	755 ± 6	0.81	0.92
^{9}Be + C	686	771	806 ± 9	0.85	0.96
^{9}Be + Al	981	1111	1174 ± 11	0.84	0.95
^{10}Be + Be	636	722	755 ± 7	0.84	0.96
^{10}Be + C	725	809	813 ± 10	0.89	1.00
^{10}Be + Al	1028	1151	1153 ± 16	0.89	1.00

Table XXIV. Calculated reaction cross sections for different interactions at 100-300 MeV/nucleon. SIGMA1 is compared with SIGMA6 (with $b_0 = 1.581 - 0.876 * (A_{p26}^{-1/3} + A_t^{-1/3})$) and the experimentally determined reaction cross sections[39].

Reaction	Theoretical Reaction Cross Sections in mb		Experimental $\sigma_{\Delta z \geq 1}$ in mb	$\frac{\sigma_{SIGMA1}(calc)}{\sigma_{SIGMA1}(exp)}$	$\frac{\sigma_{SIGMA6}(calc)}{\sigma_{SIGMA6}(exp)}$
	SIGMA1	SIGMA6			
200 MeV/N ^{12}C + ^{12}C	801	869	864 ± 45	0.93	1.01 ± 0.05
200 MeV/N ^{27}Al + ^{12}C	1118	1225	1270 ± 70	0.88	0.96 ± 0.05
200 MeV/N ^{nat}Fe + ^{12}C	1552	1716	1648 ± 110	0.94	1.04 ± 0.07
250 MeV/N ^{12}C + ^{12}C	801	869	873 ± 60	0.92	1.00 ± 0.07
250 MeV/N ^{27}Al + ^{12}C	1118	1225	1173 ± 90	0.95	1.04 ± 0.08
250 MeV/N ^{nat}Fe + ^{12}C	1552	1716	1595 ± 120	0.97	1.08 ± 0.08
300 MeV/N ^{12}C + ^{12}C	801	869	858 ± 60	0.93	1.01 ± 0.07
300 MeV/N ^{27}Al + ^{12}C	1118	1225	1220 ± 85	0.92	1.00 ± 0.07
300 MeV/N ^{nat}Fe + ^{12}C	1552	1716	1575 ± 110	0.99	1.09 ± 0.07
100 MeV/N ^{12}C + ^{20}Ne	985	1074	1161 ± 80	0.85	0.93 ± 0.07
100 MeV/N ^{27}Al + ^{20}Ne	1454	1474	1446 ± 120	1.01	1.02 ± 0.08
200 MeV/N ^{12}C + ^{20}Ne	985	1074	1123 ± 80	0.88	0.96 ± 0.07
300 MeV/N ^{12}C + ^{20}Ne	985	1074	1168 ± 100	0.84	0.92 ± 0.09
300 MeV/N ^{27}Al + ^{20}Ne	1454	1474	1328 ± 120	1.09	1.11 ± 0.09

Table XXV

Calculated proton-nucleus reaction cross sections, together with the measured values [29]

Nucleus	Energy [MeV]	Calculated σ_R [mb]	Experimental σ_R [mb]	$\frac{\sigma(calc)}{\sigma(exp)}$
^{9}Be	16.2	575	571 ± 18	1.01 ± 0.03
^{9}Be	17.0	572	599 ± 17	0.95 ± 0.03
^{9}Be	18.5	555	565 ± 15	0.98 ± 0.03
^{9}Be	20.0	555	542 ± 15	1.02 ± 0.03
^{9}Be	20.1	554	547 ± 19	1.01 ± 0.03
^{9}Be	21.9	540	530 ± 16	1.02 ± 0.03
^{9}Be	22.1	539	523 ± 18	1.03 ± 0.03
^{9}Be	24.2	521	519 ± 17	1.00 ± 0.03
^{9}Be	24.5	518	497 ± 14	1.04 ± 0.03
^{9}Be	25.1	513	489 ± 16	1.05 ± 0.03
^{9}Be	26.6	500	484 ± 17	1.03 ± 0.03
^{9}Be	27.3	494	474 ± 14	1.04 ± 0.03
^{9}Be	28.0	488	474 ± 13	1.03 ± 0.03
^{9}Be	30.2	469	454 ± 13	1.03 ± 0.03
^{9}Be	32.2	453	442 ± 13	1.02 ± 0.03
^{9}Be	34.2	437	421 ± 13	1.04 ± 0.03
^{9}Be	36.8	417	410 ± 12	1.02 ± 0.03
^{9}Be	39.7	379	398 ± 12	0.95 ± 0.03
^{9}Be	43.1	376	375 ± 12	1.00 ± 0.03
^{9}Be	46.2	358	367 ± 12	0.98 ± 0.03
^{9}Be	99.3	214	231 ± 6	1.04 ± 0.03
^{9}Be	180.0	180	186 ± 5	0.97 ± 0.03
^{9}Be	185.0	180	172 ± 17	1.05 ± 0.09
^{9}Be	232.0	180	189 ± 7	0.95 ± 0.04
^{9}Be	232.0	180	191 ± 7	0.94 ± 0.04
^{9}Be	240.0	180	169 ± 17	1.06 ± 0.09
^{9}Be	305.0	180	151 ± 15	1.19 ± 0.08
^{9}Be	346.0	180	188 ± 6	0.96 ± 0.03
^{9}Be	346.0	180	186 ± 6	0.97 ± 0.03
^{9}Be	464.0	180	195 ± 6	0.92 ± 0.03
^{9}Be	464.0	180	189 ± 6	0.95 ± 0.03
^{9}Be	553.0	180	195 ± 6	0.92 ± 0.03
^{9}Be	553.0	180	190 ± 6	0.95 ± 0.03
^{9}Be	860.0	180	169 ± 15	1.06 ± 0.08
B	19.2	576	576 ± 23	1.00 ± 0.04
B	22.2	548	535 ± 19	1.02 ± 0.03
B	24.8	522	509 ± 18	1.03 ± 0.03
B	29.8	474	458 ± 16	1.03 ± 0.03
B	34.8	431	424 ± 13	1.02 ± 0.03
B	39.8	395	388 ± 13	1.02 ± 0.03
B	44.8	365	356 ± 13	1.03 ± 0.04
B	44.8	351	346 ± 13	1.01 ± 0.04
B	235.0	205	197 ± 7	1.04 ± 0.03
B	345.0	205	198 ± 7	1.03 ± 0.03
B	410.0	205	206 ± 6	0.99 ± 0.03
B	497.0	205	210 ± 6	0.98 ± 0.03
B	565.0	205	213 ± 6	0.96 ± 0.03

Nucleus	Energy [MeV]	Calculated σ_R [mb]	Experimental σ_R [mb]	$\frac{\sigma(calc)}{\sigma(exp)}$
C	16.2	337	430 ± 16	0.78 ± 0.05
C	16.4	343	368 ± 30	0.93 ± 0.09
C	17.3	378	431 ± 17	0.88 ± 0.04
C	18.6	413	417 ± 17	0.99 ± 0.04
C	19.9	460	438 ± 17	1.05 ± 0.04
C	21.1	454	448 ± 17	1.01 ± 0.04
C	21.8	454	441 ± 21	1.03 ± 0.05
C	22.0	447	420 ± 42	1.06 ± 0.09
C	23.8	434	435 ± 18	1.00 ± 0.04
C	25.0	426	376 ± 40	1.13 ± 0.09
C	25.3	424	416 ± 19	1.02 ± 0.04
C	26.4	417	378 ± 18	1.10 ± 0.04
C	28.0	407	396 ± 13	1.03 ± 0.03
C	29.0	401	418 ± 18	0.96 ± 0.04
C	34.0	375	445 ± 20	0.84 ± 0.05
C	42.0	341	405 ± 35	0.84 ± 0.10
C	54.0	306	355 ± 50	0.86 ± 0.16
C	61.0	290	200 ± 13	1.45 ± 0.04
C	77.0	264	219 ± 8	1.21 ± 0.03
C	95.0	245	232 ± 7	1.06 ± 0.03
C	133.0	221	222 ± 6	0.99 ± 0.03
C	134.0	221	220 ± 24	1.01 ± 0.11
C	180.0	221	212 ± 5	1.04 ± 0.02
C	185.0	221	204 ± 20	1.08 ± 0.09
C	231.0	221	218 ± 5	1.01 ± 0.02
C	231.0	221	215 ± 5	1.02 ± 0.02
C	240.0	221	202 ± 20	1.09 ± 0.09
C	290.0	221	199 ± 20	1.11 ± 0.09
C	305.0	221	187 ± 19	1.18 ± 0.09
C	345.0	221	220 ± 5	1.01 ± 0.02
C	345.0	221	219 ± 5	1.01 ± 0.02
C	464.0	221	232 ± 5	0.95 ± 0.02
C	464.0	221	229 ± 5	0.97 ± 0.02
C	553.0	221	233 ± 5	0.95 ± 0.02
C	553.0	221	229 ± 5	0.97 ± 0.02
C	860.0	221	209 ± 22	1.06 ± 0.10
^{12}C	19.5	445	401 ± 24	1.11 ± 0.05
^{12}C	23.2	439	452 ± 13	0.97 ± 0.03
^{12}C	24.7	428	432 ± 12	0.99 ± 0.03
^{12}C	26.1	419	432 ± 11	0.97 ± 0.03
^{12}C	27.9	407	405 ± 11	1.00 ± 0.03
^{12}C	29.8	396	413 ± 11	0.96 ± 0.03
^{12}C	30.0	395	447 ± 20	0.88 ± 0.05
^{12}C	31.0	390	399 ± 11	0.98 ± 0.03
^{12}C	33.0	379	381 ± 9	0.99 ± 0.02
^{12}C	34.4	372	378 ± 9	0.98 ± 0.02
^{12}C	35.2	369	365 ± 12	1.01 ± 0.03
^{12}C	39.5	350	361 ± 8	0.97 ± 0.02
^{12}C	40.0	348	371 ± 11	0.94 ± 0.03
^{12}C	43.0	338	356 ± 9	0.95 ± 0.03
^{12}C	44.6	332	351 ± 8	0.95 ± 0.02
^{12}C	46.1	327	344 ± 8	0.95 ± 0.02

Nucleus	Energy [MeV]	Calculated σ_R [mb]	Experimental σ_R [mb]	$\frac{\sigma(calc)}{\sigma(exp)}$
^{12}C	47.7	322	341 ± 7	0.94 ± 0.02
^{12}C	49.5	317	345 ± 13	0.92 ± 0.04
^{12}C	60.8	290	310 ± 13	0.94 ± 0.04
^{27}Al	16.4	717	701 ± 34	1.02 ± 0.05
^{27}Al	24.8	706	733 ± 20	0.96 ± 0.03
^{27}Al	27.4	693	731 ± 19	0.95 ± 0.03
^{27}Al	29.0	684	775 ± 37	0.88 ± 0.05
^{27}Al	30.4	676	709 ± 18	0.95 ± 0.03
^{27}Al	33.7	657	668 ± 17	0.98 ± 0.03
^{27}Al	34.0	655	600 ± 42	1.09 ± 0.06
^{27}Al	36.9	638	651 ± 16	0.98 ± 0.03
^{27}Al	39.8	622	633 ± 16	0.98 ± 0.03
^{27}Al	40.0	620	645 ± 35	0.96 ± 0.06
^{27}Al	43.2	603	615 ± 16	0.98 ± 0.03
^{27}Al	46.3	588	600 ± 17	0.98 ± 0.03
^{27}Al	60.8	527	499 ± 27	1.06 ± 0.05
^{27}Al	77.0	480	444 ± 14	1.08 ± 0.03
^{27}Al	95.0	445	415 ± 13	1.07 ± 0.03
^{27}Al	99.7	434	430 ± 12	1.01 ± 0.03
^{27}Al	113.0	402	408 ± 13	0.99 ± 0.03
^{27}Al	133.0	402	424 ± 13	0.95 ± 0.03
^{27}Al	134.0	402	373 ± 37	1.08 ± 0.09
^{27}Al	180.0	402	390 ± 10	1.03 ± 0.02
^{27}Al	185.0	402	408 ± 41	0.99 ± 0.10
^{27}Al	234.0	402	400 ± 7	1.01 ± 0.02
^{27}Al	234.0	402	401 ± 7	1.00 ± 0.02
^{27}Al	240.0	402	383 ± 38	1.05 ± 0.09
^{27}Al	290.0	402	416 ± 42	0.97 ± 0.10
^{27}Al	305.0	402	334 ± 33	1.20 ± 0.08
^{27}Al	348.0 *	402	402 ± 7	1.00 ± 0.02
^{27}Al	348.0 **	402	402 ± 7	1.00 ± 0.02
^{27}Al	466.0	402	424 ± 7	0.95 ± 0.02
^{27}Al	466.0	402	421 ± 8	0.96 ± 0.02
^{27}Al	554.0	402	433 ± 8	0.93 ± 0.02
^{27}Al	554.0	402	425 ± 8	0.95 ± 0.02
^{27}Al	860.0	402	394 ± 10	1.02 ± 0.02

* and ** are two different measurements.

Table XXVI. Calculated reaction cross sections (using SIGMA1-SIGMA6), together with the experimental values for some different projectiles in water [30,31] and emulsion (Ilford G5) [19].

Nuclear Reaction	Theoretical Reaction Cross Sections in mb				Experimental Data	
	SIGMA1	SIGMA2	SIGMA3	SIGMA6 (b_o=1.3)	Cross Section [mb]	Mean free Path [mm]
$^{28}Si + H_2O$	764	722	974	620	643 [19]	155
$^{20}Ne + H_2O$	645	606	829	494	647 [31] 502 [30]	154 198
C + emulsion	911	——	——	832	850 [19]	118
^{28}Si + emuls.	1337	1290	1367	1220	1161 [19]	109±3
^{20}Ne + emuls.	1140	——	——	1046	1021 [19]	98
^{40}Ar + emuls.	1582	——	——	1441	1406 [19]	71

Table XXVII. Calculated reaction cross sections (using SIGMA1-SIGMA6), together with the experimental values for some different projectiles in water [30,31] and emulsion (Ilford G5) [19]. SIGMA1 is compared with SIGMA6 (with $b_0=1.581-0.876*(A_p^{-1/3}+A_t^{-1/3})$ and the experimentally determined reaction cross sections [19].

Projectile	Theoretical Reaction Cross Sections in mb		Experimental $\sigma_{\Delta z\geq 1}$ in mb	$\frac{\sigma_{SIGMA1}(calc)}{\sigma_{SIGMA1}(exp)}$	$\frac{\sigma_{SIGMA6}(calc)}{\sigma_{SIGMA6}(exp)}$
	SIGMA1	SIGMA6			
$^{28}Si + H_2O$	764	735	643	1.19	1.14
$^{20}Ne + H_2O$	645	613	647 502	1.00 1.28	0.95 1.22
C + emulsion	911	968	850	1.07	1.14
^{28}Si + emuls.	1137	1343	1161	1.15	1.16
^{20}Ne + emuls.	1140	1168	1021	1.12	1.14
^{40}Ar + emuls.	1582	1548	1406	1.13	1.10

Table XXVIII. Calculated reaction cross sections for the interactions of different projectiles in Ilford G5 emulsion. SIGMA1 is compared with SIGMA6 with $b_0 = 1.581 - 0.876 * (A_p^{-1/3} + A_t^{-1/3})$ and the experimentally determined reaction cross sections at 2.1 GeV/nucleon [20].

Projectile	Theoretical Reaction Cross Sections in mb		Experimental $\sigma_{\Delta Z \geq 1}$ in mb	$\frac{\sigma_{SIGMA1}(calc)}{\sigma_{SIGMA1}(exp)}$	$\frac{\sigma_{SIGMA6}(calc)}{\sigma_{SIGMA6}(exp)}$
	SIGMA1	SIGMA6			
^{4}He	594	694	580 ± 18	1.02	1.20
^{12}C	910	968	917 ± 25	0.99	1.06
^{14}N	974	1022	924 ± 21	1.05	1.05
^{16}O	1033	1073	974 ± 25	1.06	1.10

Table 1.

250 MeV/N ^{12}C + ^{12}C

Fragment Z,A	Exp. Cross Section [3] [mb] (error)	Calc. Cross Section [mb]
6,11	55.97 ± 4.06	53.3 ± 16.0
6,10	5.33 ± 0.81	2.3 ± 0.7
5,12	0.49 ± 1.00	0.0 ± 0.0
5,11	65.61 ± 2.55	62.5 ± 18.7
5,10	47.50 ± 2.42	34.4 ± 10.3
5,8	3.21 ± 1.20	1.5 ± 0.4
4,11	0.36 ± 0.26	0.0 ± 0.0
4,10	5.88 ± 9.70	4.6 ± 1.4
4,9	10.44 ± 0.85	6.8 ± 2.0
4,7	22.64 ± 1.49	15.4 ± 4.6
3,8	1.33 ± 1.00	1.5 ± 0.4
3,7	17.19 ± 3.00	18.0 ± 5.4
3,6	26.35 ± 2.10	20.0 ± 6.0

Table 2.

≈600 MeV/N ^{12}C + ^{12}C

Fragment Z,A	Exp. Cross Section [1] [mb] (error)	Calc. Cross Section [mb]
6,11	53.6 (A)	53.3 ± 16.0
6,10	2.1 (C)	2.3 ± 0.7
5,11	70.7 (A)	62.5 ± 18.7
5,10	38.6 (A)	34.4 ± 10.3
4,10	5.6 (C)	5.7 ± 1.7
4,9	9.6 (B)	8.4 ± 2.5
4,7	15.5 (B)	19.2 ± 5.8

Errors: A=±1.5%, B=±3%, C=±5%, and D=±10%

Table 3.

≈600 MeV/N ^{14}N + ^{12}C

Fragment Z,A	Exp. Cross Section [1] [mb] (error)	Calc. Cross Section [mb]
7,13	13.3 (B)	20.6 ± 6.2
7,12	2.0 (D)	1.5 ± 0.4
6,13	21.3 (A)	20.3 ± 6.1
6,12	117.2 (A)	73.6 ± 22.1
6,11	27.5 (A)	23.9 ± 7.2
6,10	2.1 (D)	1.2 ± 0.3
5,11	39.8 (A)	29.1 ± 8.7
5,10	23.9 (A)	31.0 ± 9.3
4,10	3.5 (D)	3.7 ± 1.1
4,9	4.1 (D)	8.2 ± 2.5
4,7	21.6 (B)	18.7 ± 5.6

Errors: A=±1.5%, B=±3%, C=±5%, and D=±10%

Table 4.

≈600 MeV/N ^{16}O + ^{12}C

Fragment Z,A	Exp. Cross Section [1] [mb] (error)	Calc. Cross Section [mb]
8,15	84.0 (A)	68.2 ± 20.5
8,14	2.6 (D)	3.2 ± 1.0
7,15	73.2 (A)	77.2 ± 23.2
7,14	66.8 (A)	49.8 ± 14.9
7,13	12.6 (B)	6.9 ± 2.1
7,12	0.6 (D)	0.7 ± 0.2
6,14	3.3 (C)	4.3 ± 1.3
6,13	41.0 (A)	27.2 ± 8.2
6,12	79.2 (A)	61.8 ± 18.6
6,11	26.5 (A)	20.1 ± 6.0
6,10	3.2 (D)	1.0 ± 0.3
5,12	2.4 (D)	6.9 ± 2.1
5,11	36.0 (A)	41.6 ± 12.5
5,10	24.8 (A)	24.7 ± 7.4

Errors: A=±1.5%, B=±3%, C=±5%, and D=±10%

Table 5.

≈600 MeV/N ^{40}Ar + ^{12}C

Fragment Z,A	Exp. Cross Section [1] [mb] (error)	Calc. Cross Section [mb]
18,39	146.4 (A)	118.4
18,38	72.3 (A)	19.2
18,37	8.4 (C)	2.5
17,39	39.1 (A)	41.3
17,38	34.9 (A)	25.1
17,37	59.3 (A)	28.0
17,36	38.0 (A)	33.7
17,35	12.3 (C)	19.7
16,38	0.8 (D)	0.7
16,37	5.1 (C)	3.6
16,36	19.3 (B)	20.0
16,35	32.6 (A)	30.1
16,34	51.0 (A)	45.8
16,33	15.3 (B)	18.9
16,32	1.1 (D)	7.8
15,35	1.2 (D)	2.3
15,34	6.3 (C)	9.1
15,33	23.8 (A)	25.9
15,32	35.9 (A)	27.9
15,31	24.0 (A)	21.6
15,30	2.2 (D)	6.2
14,32	4.1 (C)	8.7
14,31	17.6 (B)	17.6
14,30	40.1 (A)	35.5
14,29	27.6 (A)	19.2
14,28	9.2 (C)	10.3
13,30	1.2 (D)	3.8
13,29	11.8 (B)	14.5
13,28	20.5 (A)	20.4
13,27	33.1 (A)	20.5
13,26	4.2 (D)	7.6

12,27	4.1 (C)	9.5
12,26	23.0 (A)	24.8
12,25	23.1 (A)	17.3
12,24	12.7 (B)	11.8
12,23	1.0 (D)	2.1

Errors: A=±1.5%, B=±3%, C=±5%, and D=±10%

Table 6

≈600 MeV/N ^{56}Fe + ^{12}C

Fragment Z,A	Exp. Cross Section [mb] (error)	Calc. Cross Section [mb]
26,55	164,3 (A)	159.9
26.54	28.2 (B)	23.7
26,53	3.0 (D)	5.2
25,55	53.7 (A)	123.2
25,54	66.9 (A)	71.6
25,53	64.0 (A)	42.6
25,52	21.6 (B)	10.2
25,51	3.9 (D)	2.5
24,54	4.7 (C)	4.7
24,53	16.0 (B)	14.9
24,52	63.6 (A)	47.5
24,51	60.7 (A)	32.3
24,50	30.5 (A)	17.1
24,49	5.1 (C)	2.8
23,52	1.1 (D)	1.2
23,51	8.3 (C)	5.5
23,50	33.1 (A)	16.7
23,49	43.0 (A)	29.5
23,48	24.7 (A)	11.8
23,47	4.9 (D)	3.8
22,50	1.6 (D)	2.9
22,49	8.4 (C)	6.6
22,48	30.5 (A)	26.2
22,47	40.6 (A)	31.0
22,46	23.3 (A)	20.3
22,45	4.0 (D)	4.1
22,44	0.6 (D)	0.8
21,48	0.3 (D)	1.2
21,47	2.7 (D)	4.8
21,46	12.8 (B)	13.0
21,45	28.3 (A)	30.7
21,44	21.5 (A)	15.0
21,43	6.9 (C)	5.2
20,45	2.7 (D)	2.9
20,44	10.6 (B)	13.7
20,43	22.6 (A)	22.8
20,42	22.0 (A)	23.6
20,41	10.9 (C)	5.4
20,40	1.3 (D)	1.3
19,44	0.7 (D)	0.5
19,43	2.8 (D)	2.1
19,42	8.1 (C)	6.5
19,41	16.6 (B)	20.2
19,40	14.6 (B)	16.7
19,39	7.3 (C)	6.8
19,38	1.0 (D)	1.2
18,41	1.7 (D)	1.3
18,40	8.0 (C)	6.6
18,39	17.9 (B)	14.1
18,38	19.1 (B)	25.2
18,37	6.1 (C)	7.0
18,36	1.1 (D)	2.3
17,39	0.9 (D)	0.9
17,38	3.4 (D)	2.9
17,37	12.5 (B)	10.9
17,36	13.5 (B)	15.2
17,35	9.6 (C)	7.8
17,34	0.9 (D)	1.7
16,37	0.6 (D)	0.6
16,36	2.2 (D)	3.3
16,35	8.0 (C)	8.3
16,34	14.6 (B)	22.9
16,33	11.1 (B)	8.5
16,32	5.6 (C)	3.5
16,31	1.6 (D)	0.4

Errors: A=±1.5%, B=±3%, C=±5%, and C=±10%.

Table 7.

1.05 GeV/N ^{12}C + ^{9}Be

Fragment Z,A	Exp. Cross Section [mb] (error)	Calc. Cross Section [mb]
7,12	0.02 ± 0.01	0.05 ± 0.02
6,11	44.7 ± 2.6	50.4 ± 15.1
6,10	4.02 ± 0.23	2.2 ± 0.7
6,9	0.42 ± 0.05	0.6 ± 0.2
5,12	0.09 ± 0.02	0.0 ± 0.0
5,11	50.7 ± 3.2	59.1 ± 17.7
5,10	28.8 ± 2.3	32.5 ± 9.8
5,8	1.55 ± 0.08	1.4 ± 0.4
4,11	0.02 ± 0.01	0.0 ± 0.0
4,10	5.08 ± 0.30	5.4 ± 1.6
4,9	11.60 ± 0.76	8.0 ± 2.4
4,7	17.80 ± 0.90	18.2 ± 5.5
3,9	0.75 ± 0.08	0.7 ± 0.2
3,8	2.36 ± 0.14	1.7 ± 0.5
3,7	23.4 ± 1.2	21.3 ± 6.4
3,6	24.8 ± 2.0	23.6 ± 7.1

Table 8.

1.05 GeV/N ^{12}C + ^{12}C

Fragment Z,A	Exp. Cross Section [mb] (error)	Calc. Cross Section [mb]
7,12	0.05 ± ?	0.05 ± 0.02
6,11	44.7 ± 2.8	53.3 ± 16.0
6,10	4.44 ± 0.24	2.3 ± 0.7
6,9	0.48 ± 0.06	0.6 ± 0.2
5,12	0.10 ± 0.01	0.0 ± 0.0
5,11	48.6 ± 2.4	62.5 ± 18.7
5,10	27.9 ± 2.2	34.4 ± 10.3
5,8	1.43 ± 0.10	1.5 ± 0.4
4,10	5.34 ± 0.29	5.7 ± 1.7
4,9	10.70 ± 0.50	8.4 ± 2.5
4,7	18.60 ± 0.90	19.2 ± 5.8
3,9	0.87 ± 0.01	0.7 ± 0.2
3,8	2.40 ± 0.18	1.8 ± 0.5
3,7	21.5 ± 1.1	22.6 ± 6.8
3,6	27.1 ± 2.2	25.0 ± 7.5
2,6	1.83 ± 0.19	1.5 ± 0.5

Table 9.

1.05 GeV/N ^{12}C + ^{27}Al

Fragment Z,A	Exp. Cross Section [mb] (error)	Calc. Cross Section [mb]
7,12	6.49 ± 0.48	0.06 ± 0.02
6,11	57.8 ± 3.9	63.3 ± 19.0
6,10	5.06 ± 0.37	2.8 ± 0.8
6,9	0.60 ± 0.10	0.7 ± 0.2
5,12	0.18 ± 0.05	0.0 ± 0.0
5,11	64.5 ± 5.3	74.2 ± 22.3
5,10	30.4 ± 3.5	40.8 ± 12.3
5,8	1.73 ± 0.16	1.8 ± 0.5
4,10	6.49 ± 0.48	6.8 ± 2.0
4,9	13.90 ± 0.90	10.0 ± 3.0
4,7	19.9 ± 1.1	22.8 ± 6.8
3,9	0.82 ± 0.16	0.8 ± 0.2
3,8	2.87 ± 0.27	2.2 ± 0.7
3,7	28.5 ± 1.4	26.8 ± 8.0
3,6	24.9 ± 2.9	29.7 ± 8.9
2,6	2.00 ± 0.29	1.8 ± 0.5

Table 10.

2.1 GeV/N ^{12}C + ^{9}Be

Fragment Z,A	Exp. Cross Section [mb] (error)	Calc. Cross Section [mb]
7,12	0.06 ± 0.01	0.05 ± 0.02
6,11	46.7 ± 2.3	50.4 ± 15.1
6,10	4.20 ± 0.21	2.2 ± 0.7
6,9	0.54 ± 0.06	0.6 ± 0.2
5,12	0.14 ± 0.02	0.0 ± 0.0
5,11	53.2 ± 2.9	59.1 ± 17.7
5,10	31.1 ± 2.6	32.5 ± 9.8
5,8	1.48 ± 0.09	1.4 ± 0.4
4,11	0.02 ± 0.01	0.0 ± 0.0
4,10	5.97 ± 0.31	5.4 ± 1.6
4,9	10.98 ± 0.55	8.0 ± 2.4
4,7	18.91 ± 0.95	18.2 ± 5.5
3,9	0.92 ± 0.08	0.7 ± 0.2
3,8	2.52 ± 0.16	1.7 ± 0.5
3,7	22.8 ± 1.1	21.3 ± 6.4
3,6	33.1 ± 2.7	28.3 ± 8.5
2,6	2.54 ± 0.25	1.5 ± 0.4

Table 11.

2.1 GeV/N ^{12}C + ^{12}C

Fragment Z,A	Exp. Cross Section [mb] (error)	Calc. Cross Section [mb]
7,12	0.08 ± 0.01	0.05 ± 0.02
6,11	46.5 ± 2.3	53.3 ± 16.0
6,10	4.11 ± 0.22	2.3 ± 0.7
6,9	0.54 ± 0.07	0.6 ± 0.2
5,12	0.10 ± 0.01	0.0 ± 0.0
5,11	53.8 ± 2.7	62.5 ± 18.7
5,10	35.1 ± 3.4	34.4 ± 10.3
5,8	1.72 ± 0.13	1.5 ± 0.4
4,10	5.81 ± 0.29	5.7 ± 1.7
4,9	10.63 ± 0.53	8.4 ± 2.5
4,7	18.61 ± 0.93	19.2 ± 5.8
3,9	0.85 ± 0.08	0.7 ± 0.2
3,8	2.18 ± 0.15	1.8 ± 0.5
3,7	21.5 ± 1.1	22.6 ± 6.8
3,6	30.0 ± 2.4	30.0 ± 10.0
2,6	2.21 ± 0.22	1.5 ± 0.5

Table 12.

2.1 GeV/N ^{12}C + ^{27}Al

Fragment Z,A	Exp. Cross Section [mb] (error)	Calc. Cross Section [mb]
6,11	59.5 ± 3.1	63.3 ± 19.0
6,10	4.99 ± 0.34	2.8 ± 0.8
6,9	0.50 ± 0.09	0.7 ± 0.2
5,12	0.14 ± 0.03	0.0 ± 0.0
5,11	65.2 ± 4.8	74.2 ± 22.3
5,10	36.4 ± 4.8	40.8 ± 12.3
5,8	1.76 ± 0.14	1.8 ± 0.5
4,10	7.02 ± 0.40	6.8 ± 2.0
4,9	12.74 ± 0.71	10.0 ± 3.0
4,7	25.8 ± 1.3	22.8 ± 6.8
3,9	0.88 ± 0.12	0.8 ± 0.2
3,8	2.79 ± 0.23	2.2 ± 0.7
3,7	27.3 ± 1.4	26.8 ± 8.0
3,6	36.3 ± 2.9	35.6 ± 10.7
2,6	2.82 ± 0.27	1.8 ± 0.5

Table 13.

2.1 GeV/N ^{16}O + ^{12}C

Fragment Z,A	Exp. Cross Section [mb] (error)	Calc. Cross Section [mb]
8,15	42.9 ± 2.3	52.7 ± 15.8
8,14	1.67 ± 0.12	3.2 ± 1.0
8,13	0.22 ± 0.03	0.2 ± 0.1
7,15	54.2 ± 2.9	59.6 ± 17.9
7,14	41.8 ± 3.3	49.8 ± 14.9
7,13	8.06 ± 0.42	6.9 ± 2.1
7,12	0.73 ± 0.07	0.7 ± 0.2
6,15	0.04 ± 0.01	0.0 ± 0.0
6,14	4.71 ± 0.31	4.3 ± 1.3
6,13	27.7 ± 1.4	27.2 ± 8.2
6,12	65.1 ± 5.2	61.8 ± 18.6
6,11	18.46 ± 0.92	20.1 ± 6.0
6,10	2.51 ± 0.16	1.0 ± 0.3
6,9	0.41 ± 0.09	0.4 ± 0.1
5,13	0.44 ± 0.05	0.4 ± 0.1
5,12	2.44 ± 2.15	4.5 ± 1.4
5,11	26.0 ± 1.3	27.2 ± 8.1
5,10	20.3 ± 1.6	16.1 ± 4.8
5,8	1.38 ± 0.13	1.3 ± 0.4
4,12	0.03 ± 0.02	0.01 ± 0.003
4,11	0.19 ± 0.03	0.3 ± 0.1
4,10	3.98 ± 0.30	4.1 ± 1.2
4,9	9.06 ± 0.51	9.0 ± 2.7
4,7	22.3 ± 1.1	20.5 ± 6.2
3,9	0.51 ± 0.07	0.7 ± 0.2
3,8	2.50 ± 0.18	2.0 ± 0.6
3,7	26.3 ± 1.3	24.1 ± 7.2
3,6	35.9 ± 2.9	32.1 ± 9.6
2,6	2.00 ± 0.21	1.8 ± 0.5

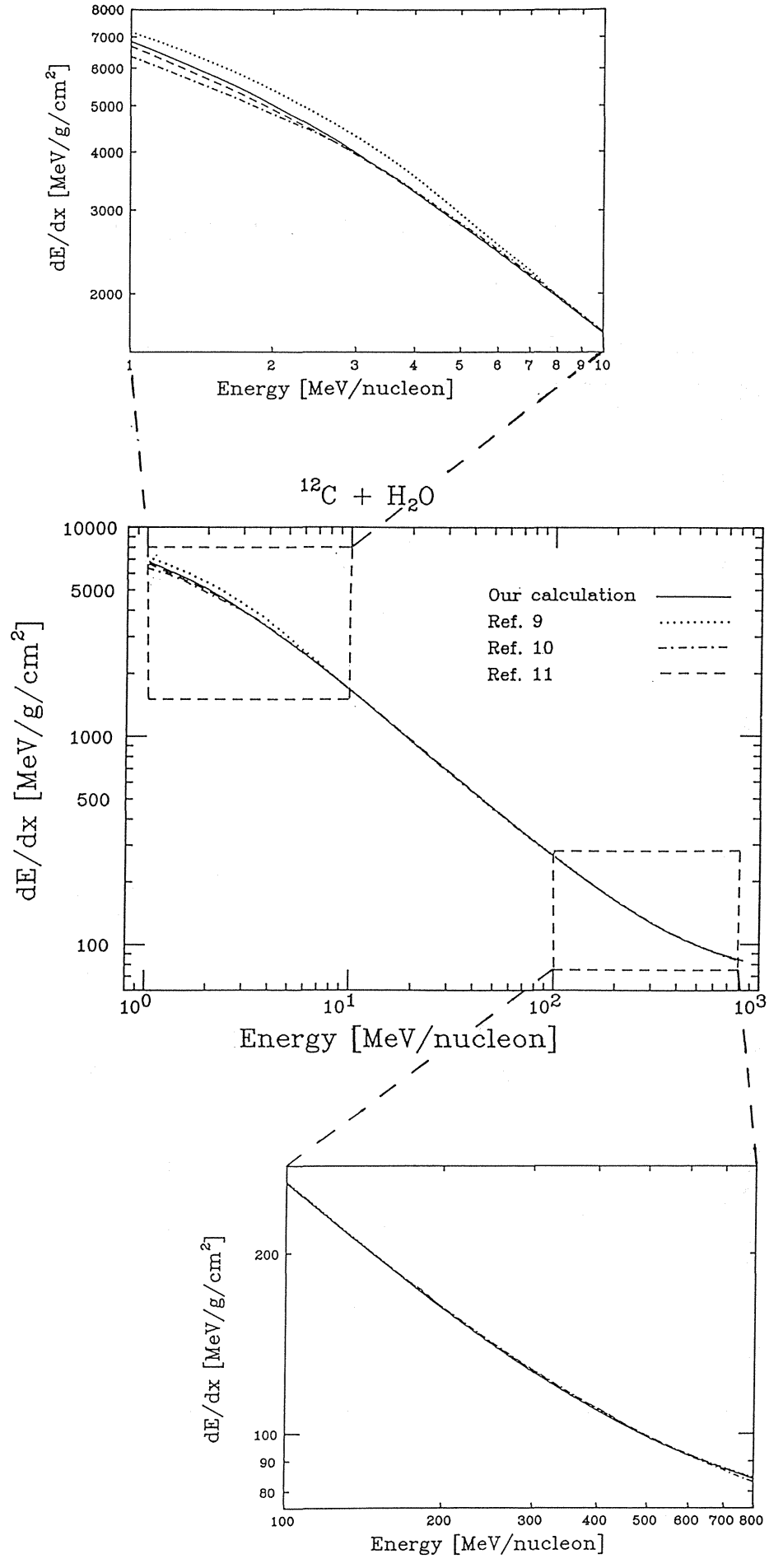

Fig. 1 Energy loss (dE/dx) of ^{12}C ions in water as a function of the specific energy.

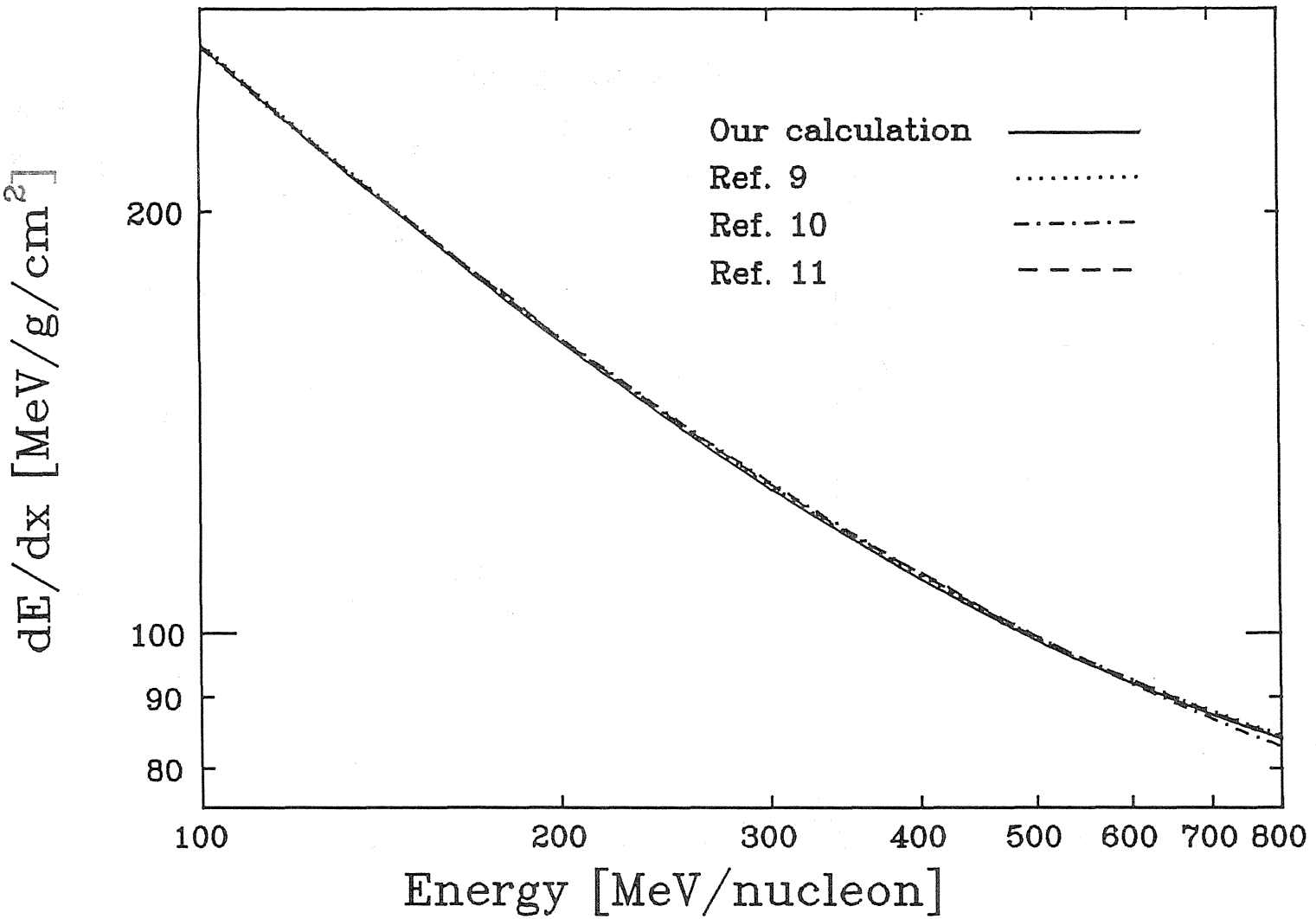

Fig. 2 Energy loss (dE/dx) of ^{12}C ions in water as a function of the specific energy, in the energy region 100-800 MeV/nucleon.

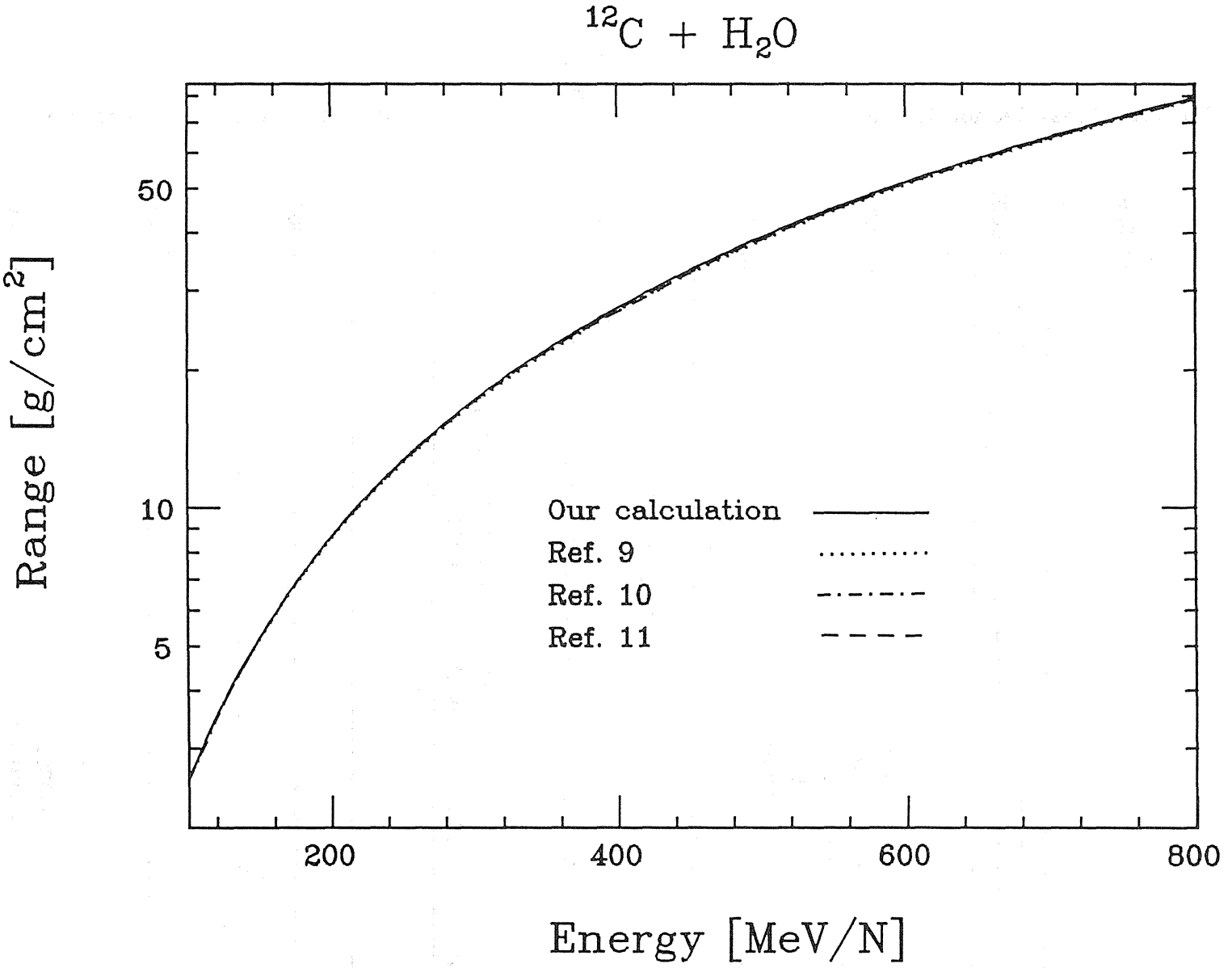

Fig. 3 Range distributions of ^{12}C ions in water as a function of the specific energy.

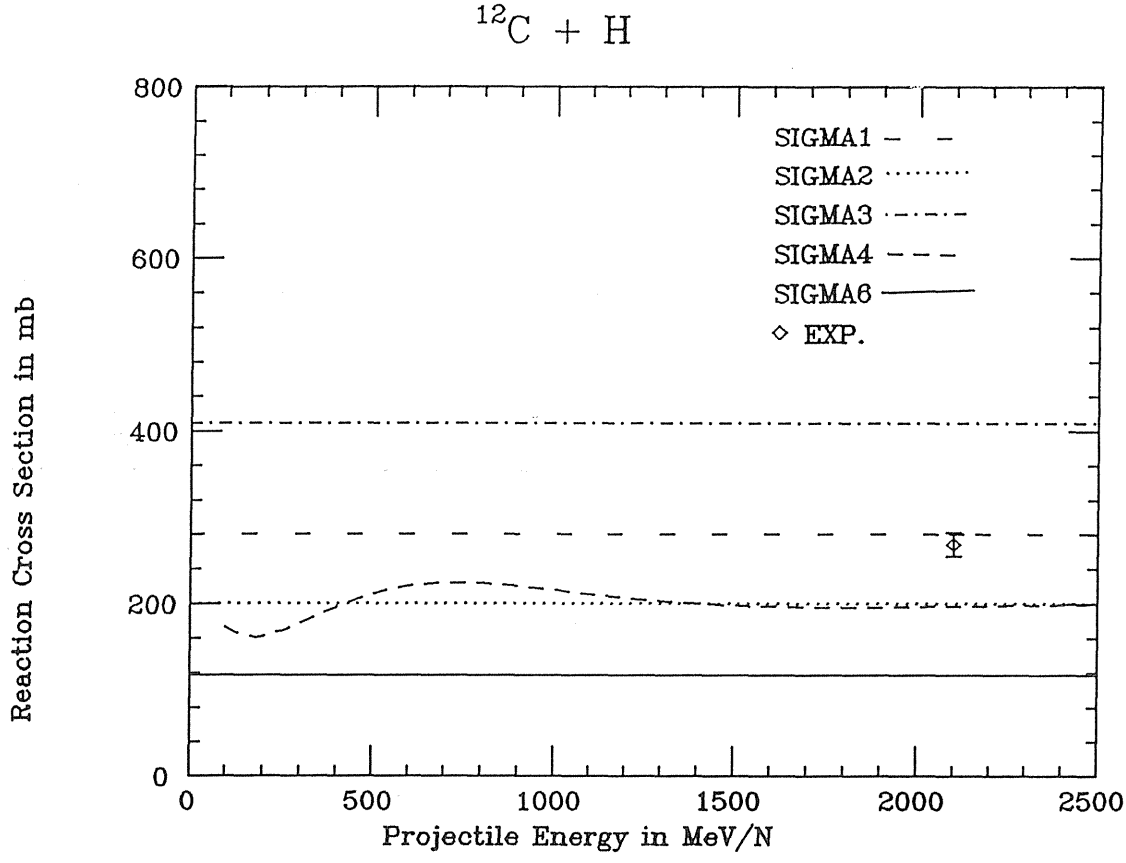

Fig. 4 The reaction cross sections for the interactions of ^{12}C with H.

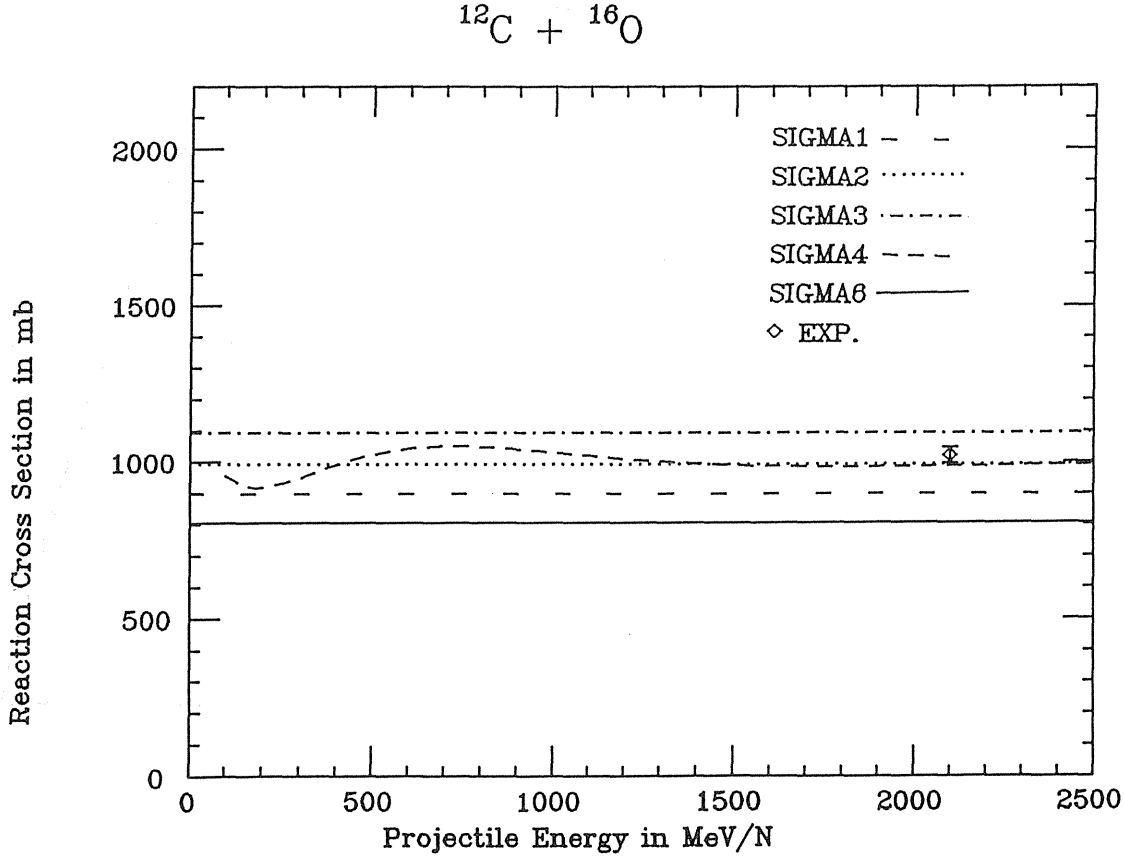

Fig. 5 The reaction cross sections for the interactions of ^{12}C with ^{16}O.

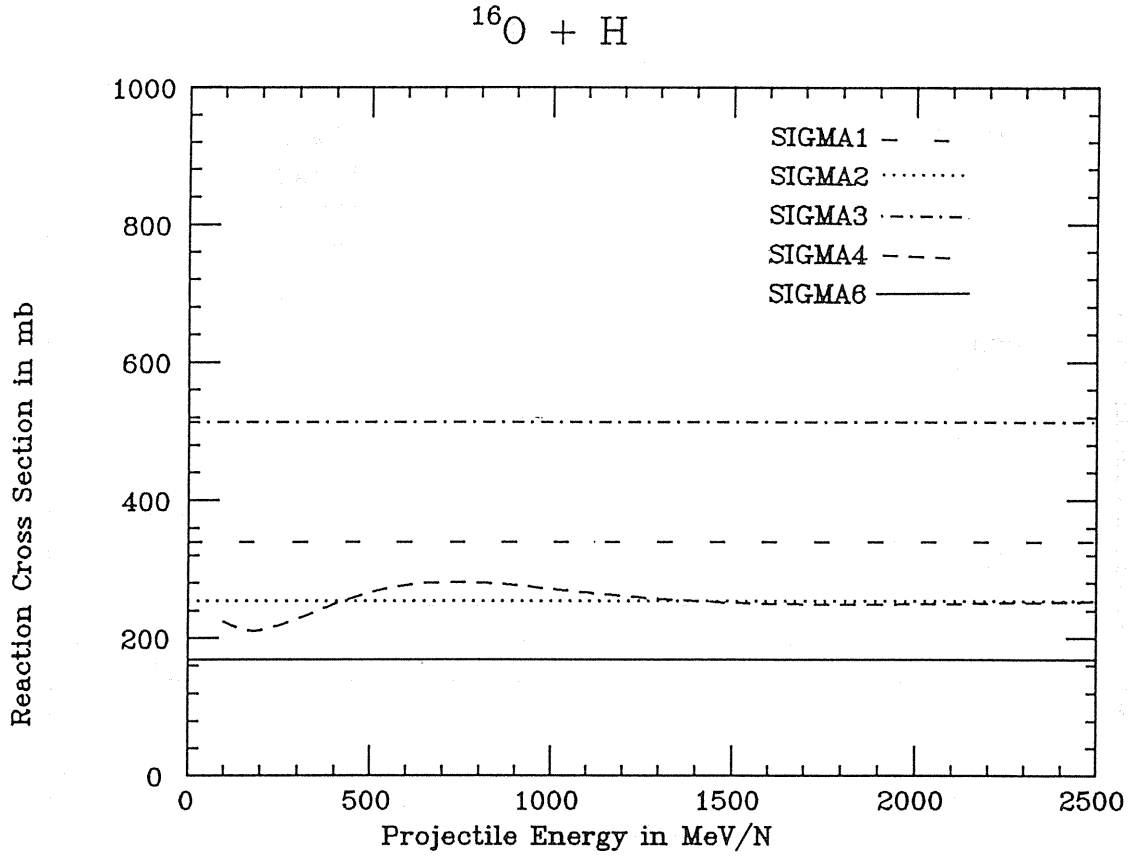

Fig. 6 The reaction cross sections for the interactions of ^{16}O with H.

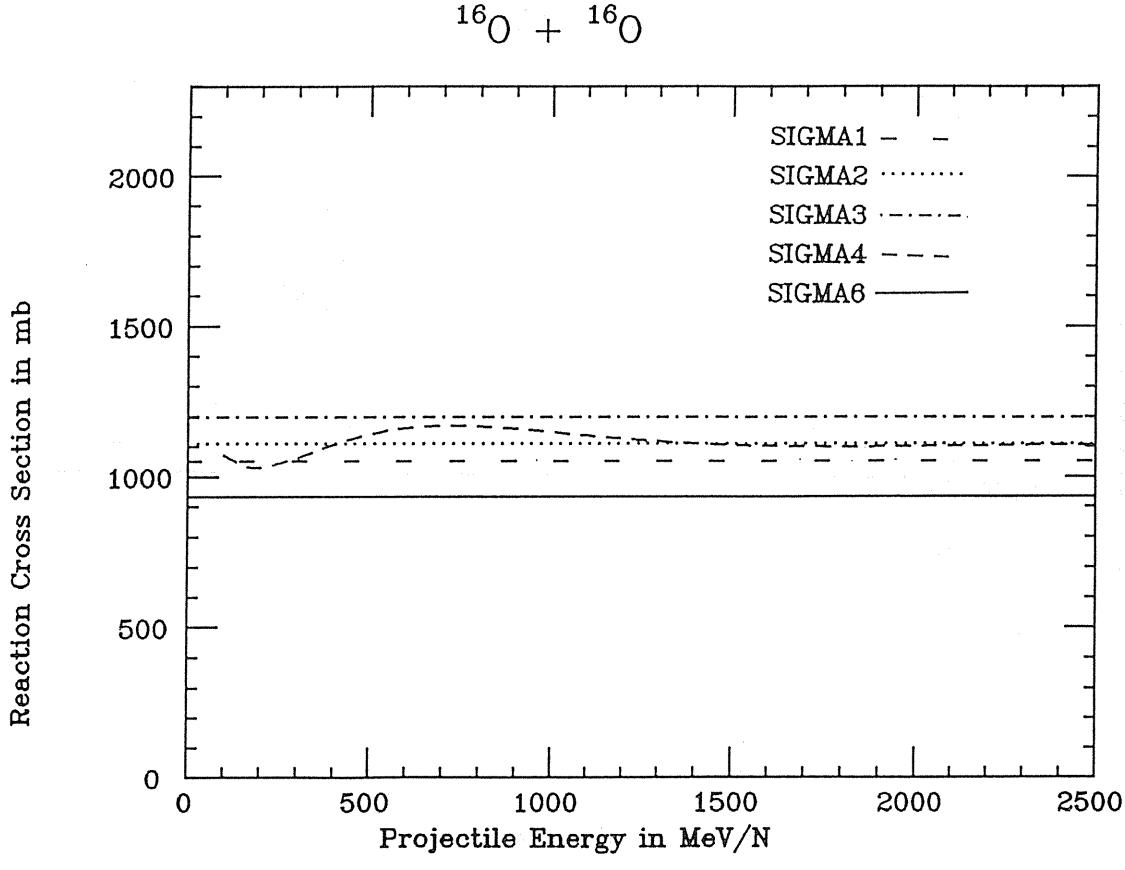

Fig. 7 The reaction cross sections for the interactions of ^{16}O with ^{16}O.

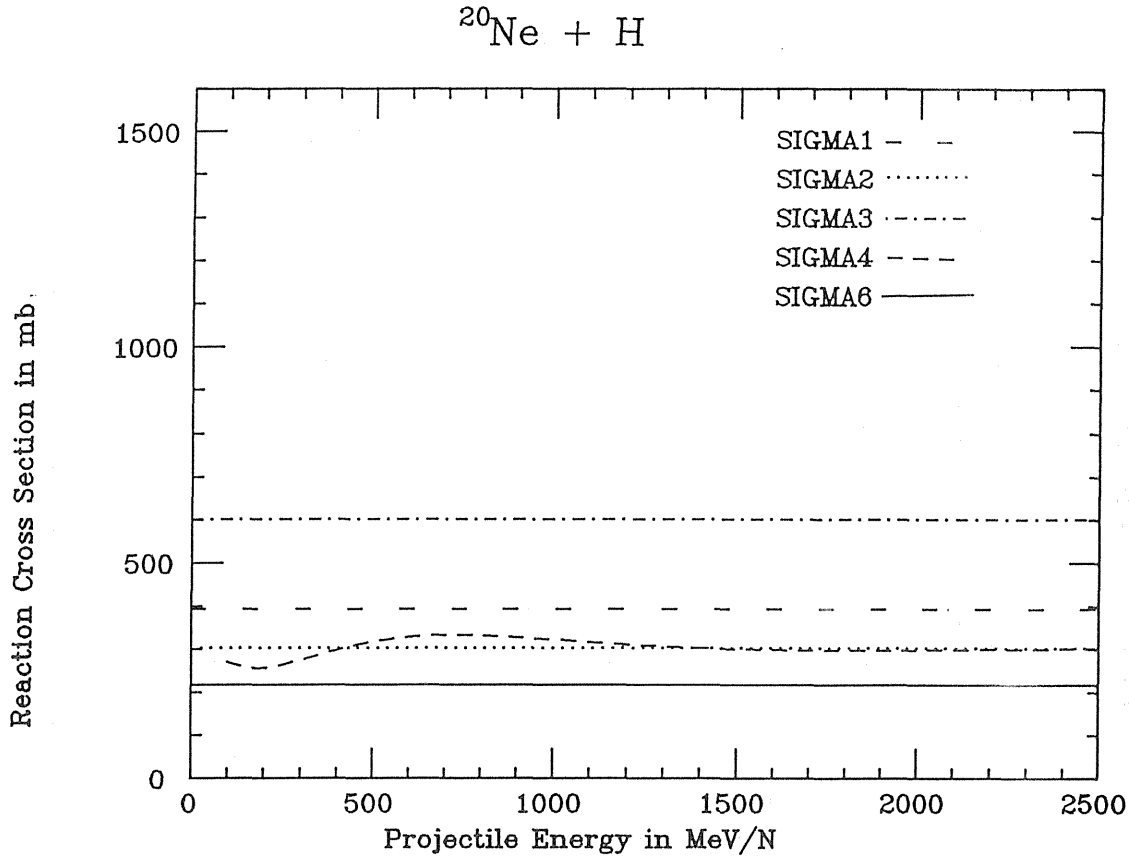

Fig. 8 The reaction cross sections for the interactions of ^{20}Ne with H.

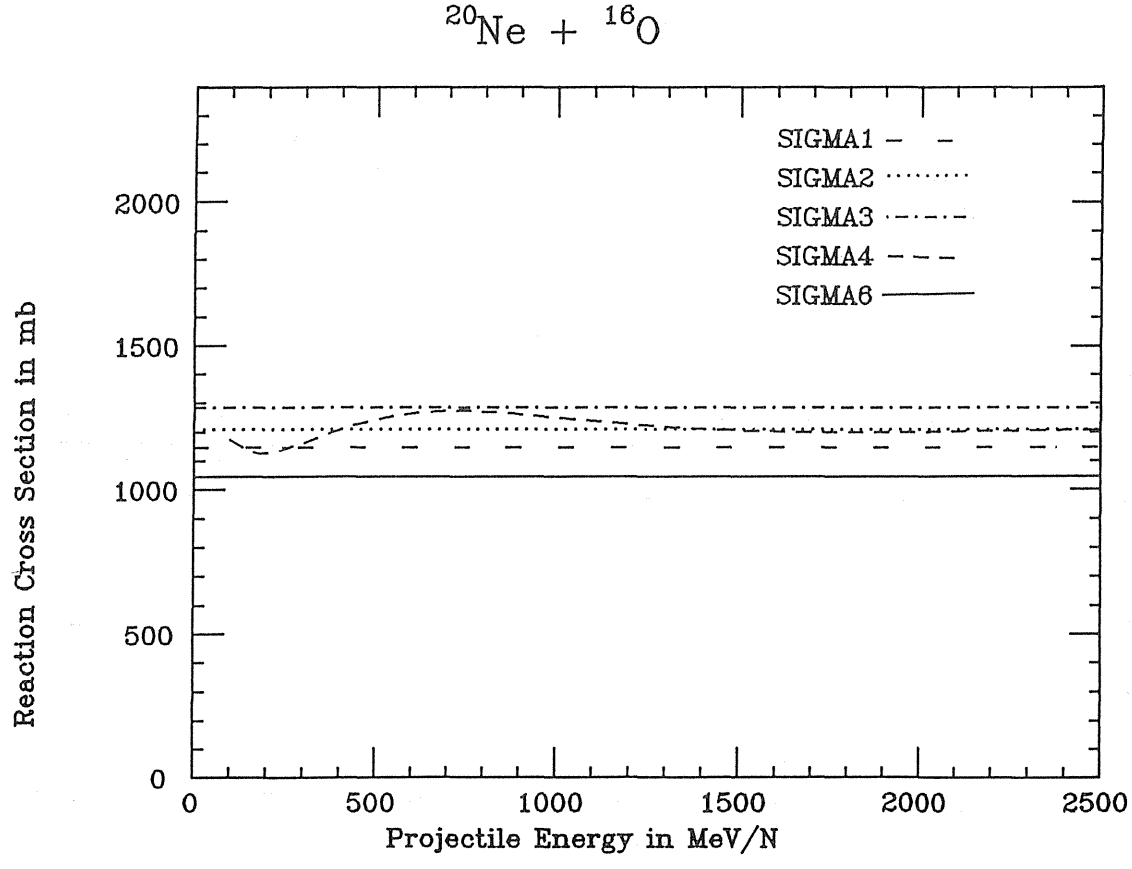

Fig. 9 The reaction cross sections for the interactions of ^{20}Ne with ^{16}O.

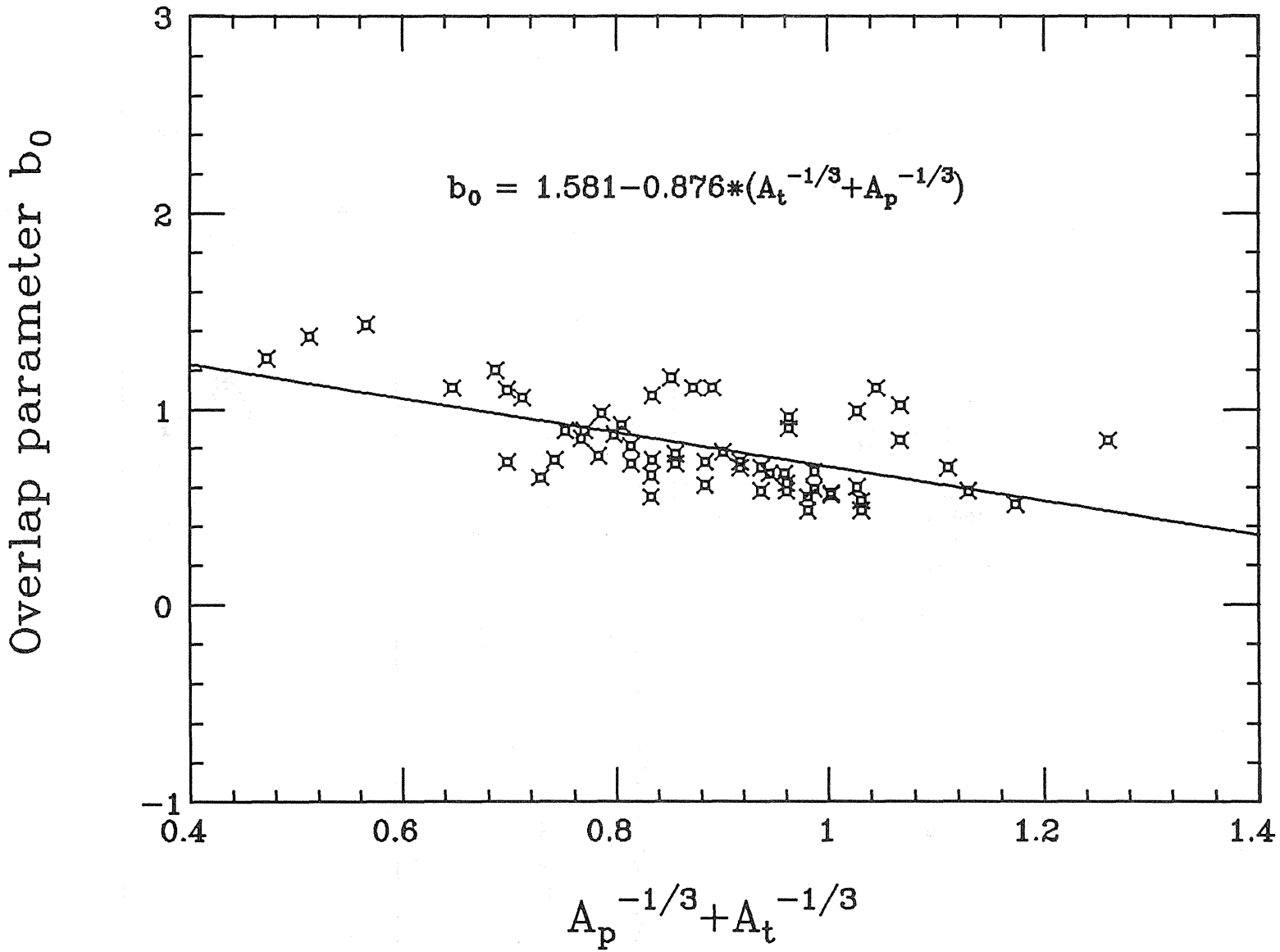

Figure 10 b_o as a function of $(A_p^{-1/3}+A_t^{-1/3})$, together with the calculated values, for all studied projectile-target combinations.

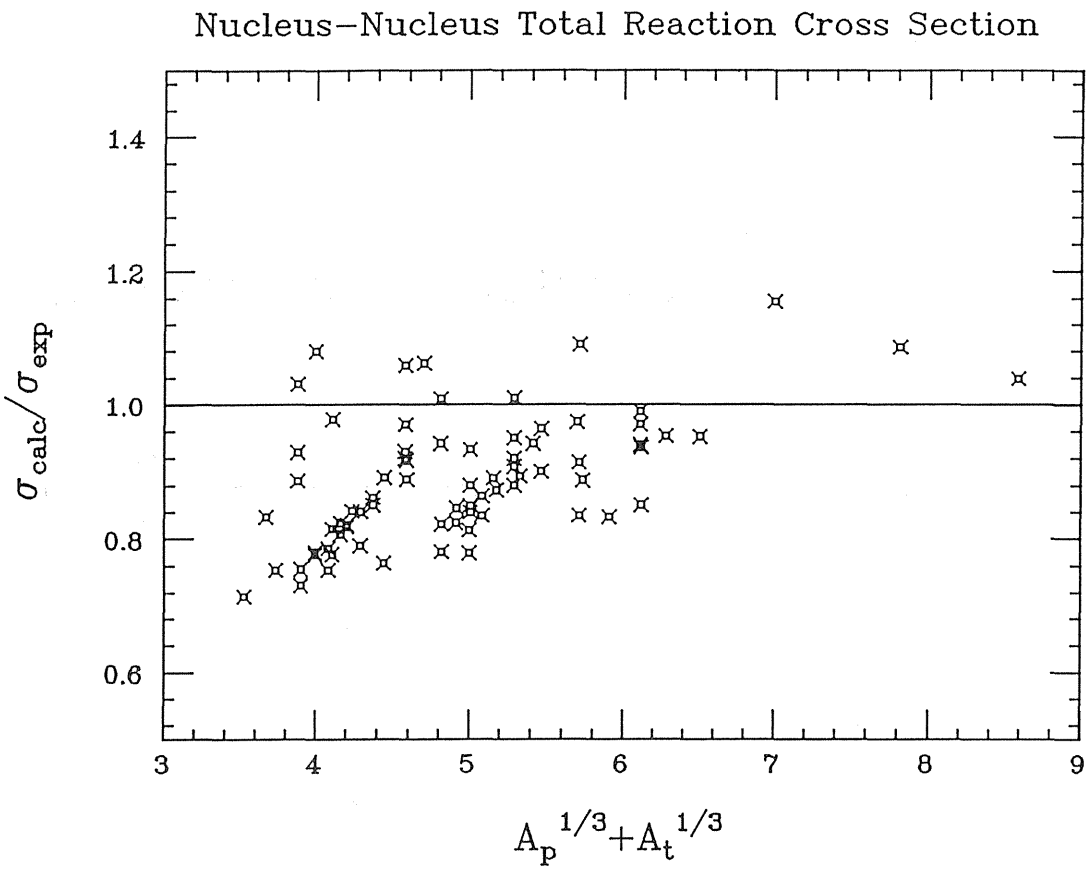

Figure 11 $\sigma_{calc}/\sigma_{exp}$, using SIGMA1, for the projectile target combinations tabulated in **Table XVIII-XXIV.**

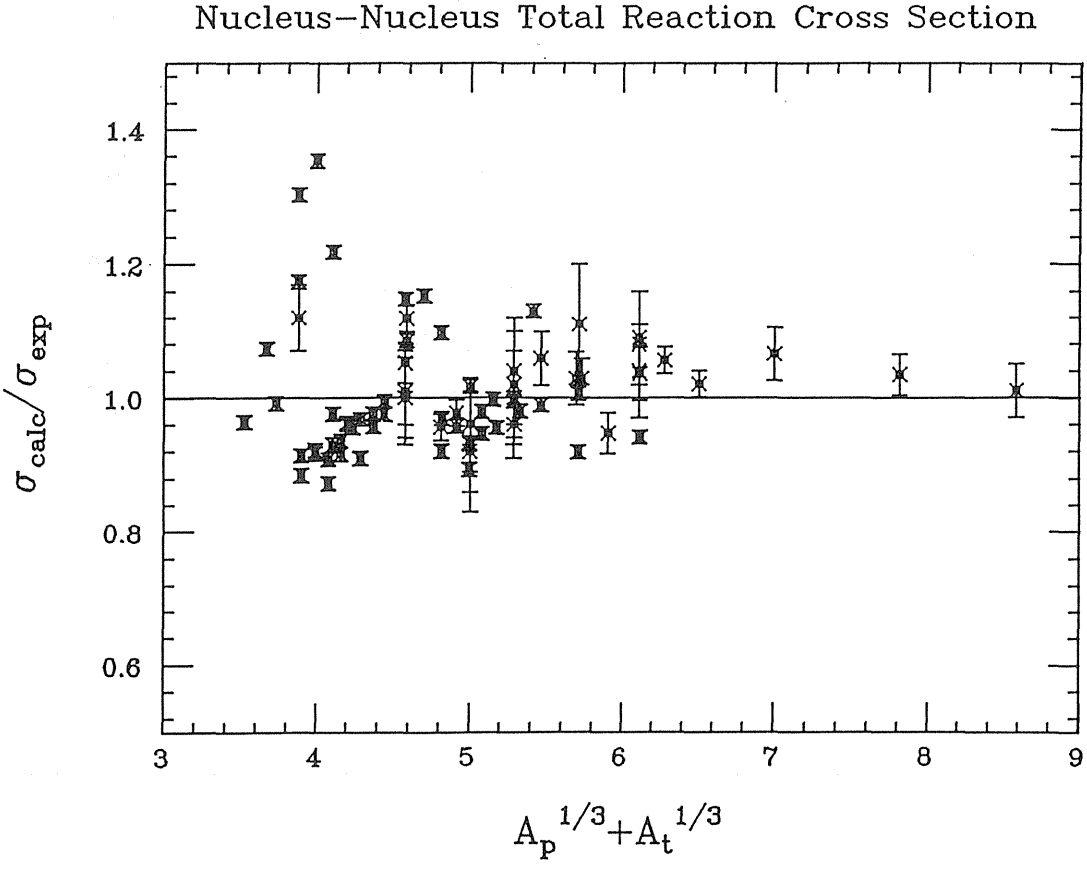

Figure 12 $\sigma_{calc}/\sigma_{exp}$, using SIGMA6, for all the projectile target combinations tabulated in **Table XVIII-XXIV.** Experimental error bars are shown if they are available.

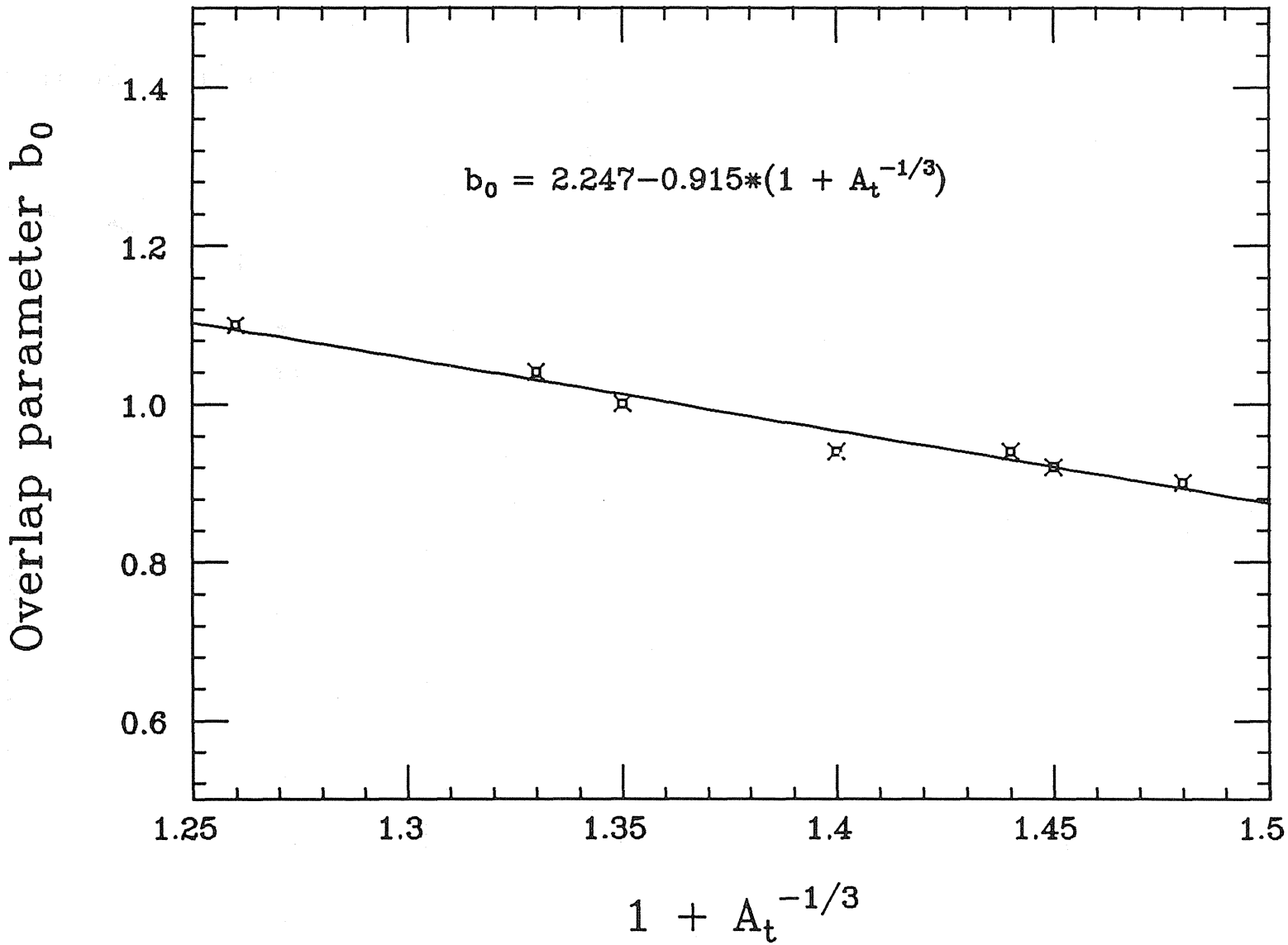

Figure 13 The "best agreement" b_o value for each reaction as a function of $(1+A_t^{-1/3})$, together with the calculated values.

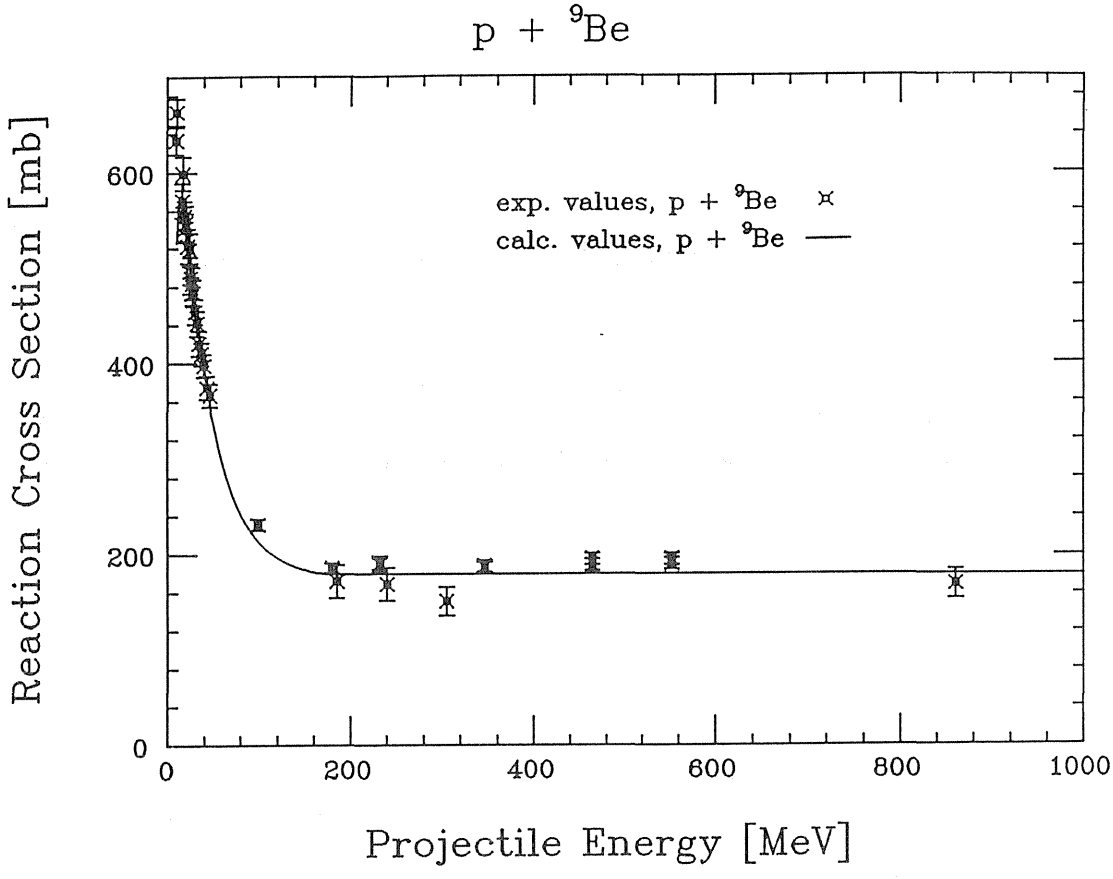

Figure 14a Calculated σ_{reac}, together with experimental data [29], for the interactions of protons with ^{9}Be.

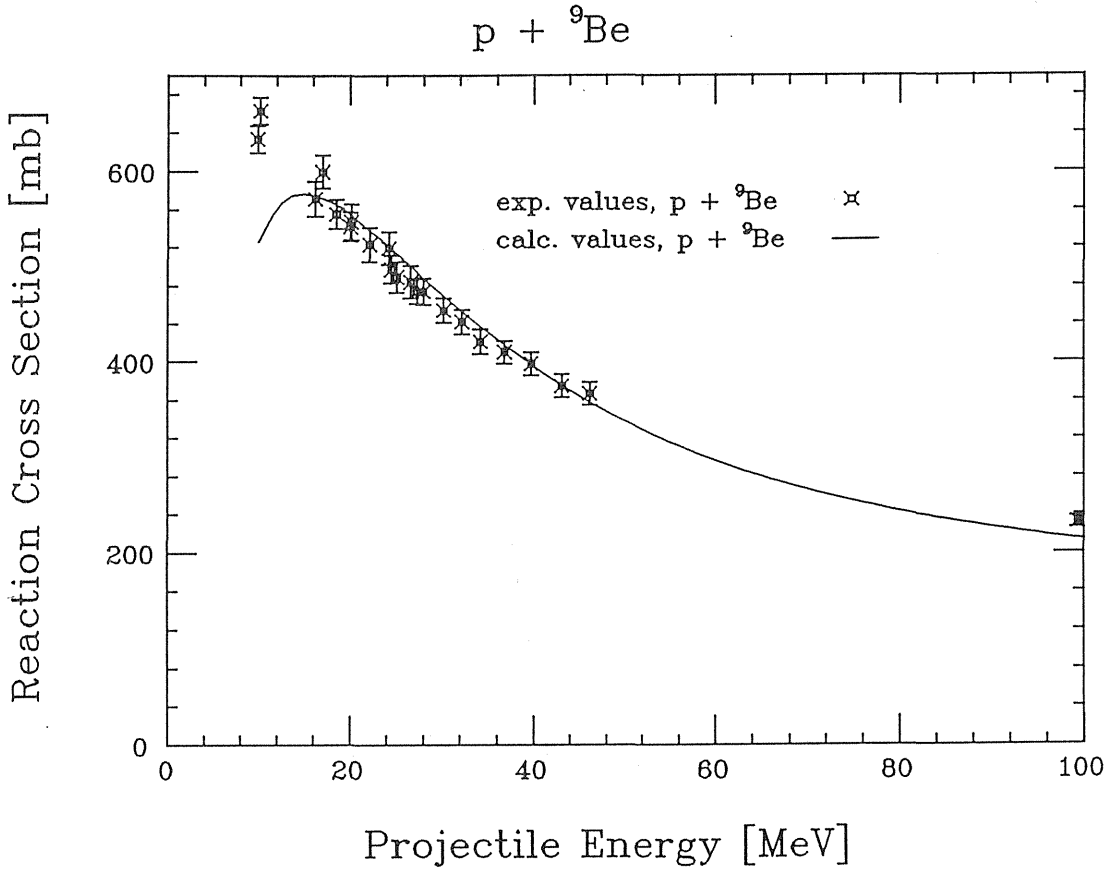

Figure 14b The same calculations as in **Figure 14a**, but only the low energy region is shown.

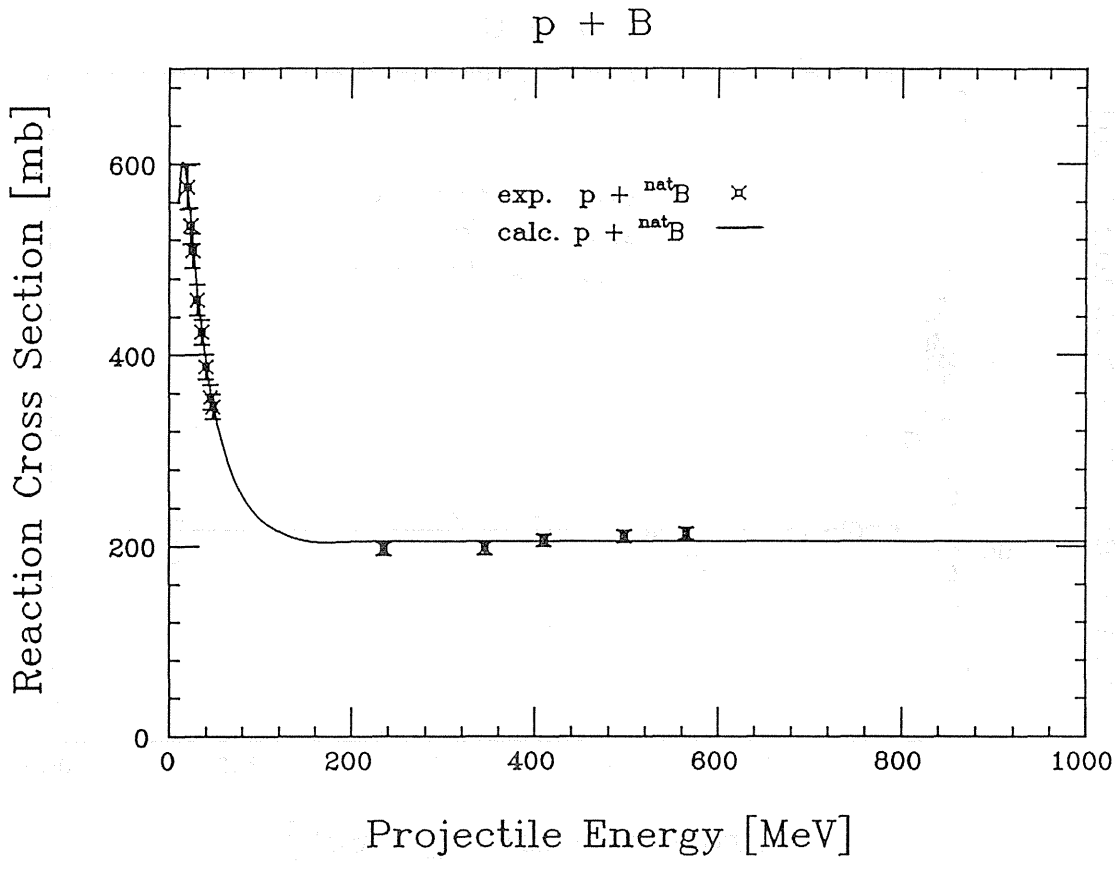

Figure 15a Calculated σ_{reac}, together with experimental data [29], for the interactions of protons with ^{nat}B.

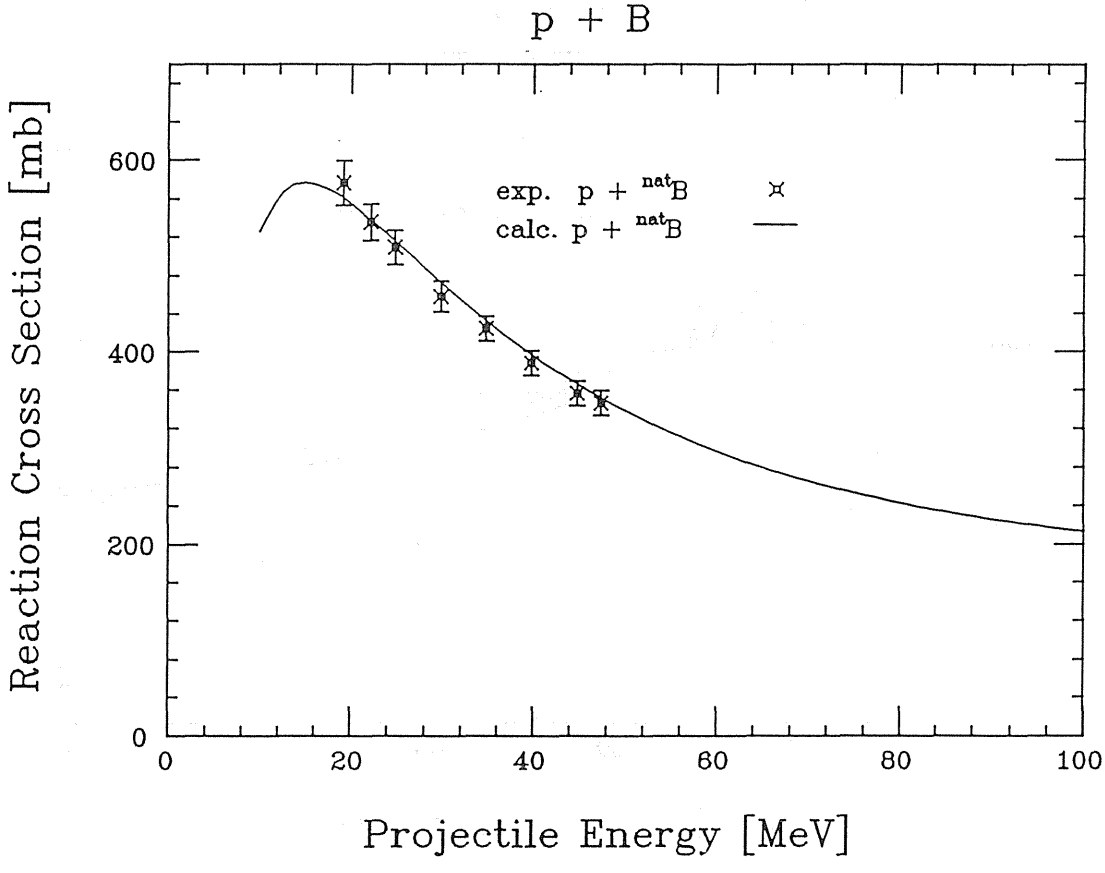

Figure 15b The same calculations as in **Figure 15a**, but only the low energy region is shown.

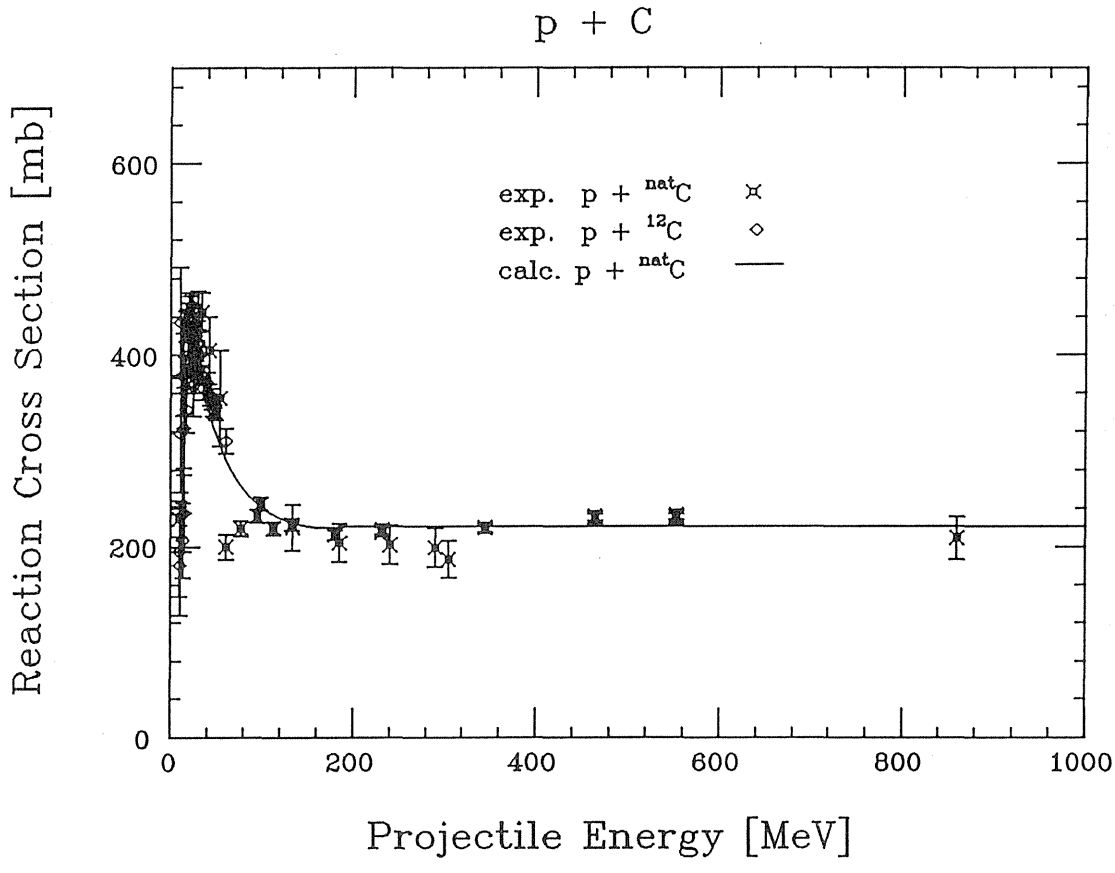

Figure 16a Calculated σ_{reac}, together with experimental data [29], for the interactions of protons with C.

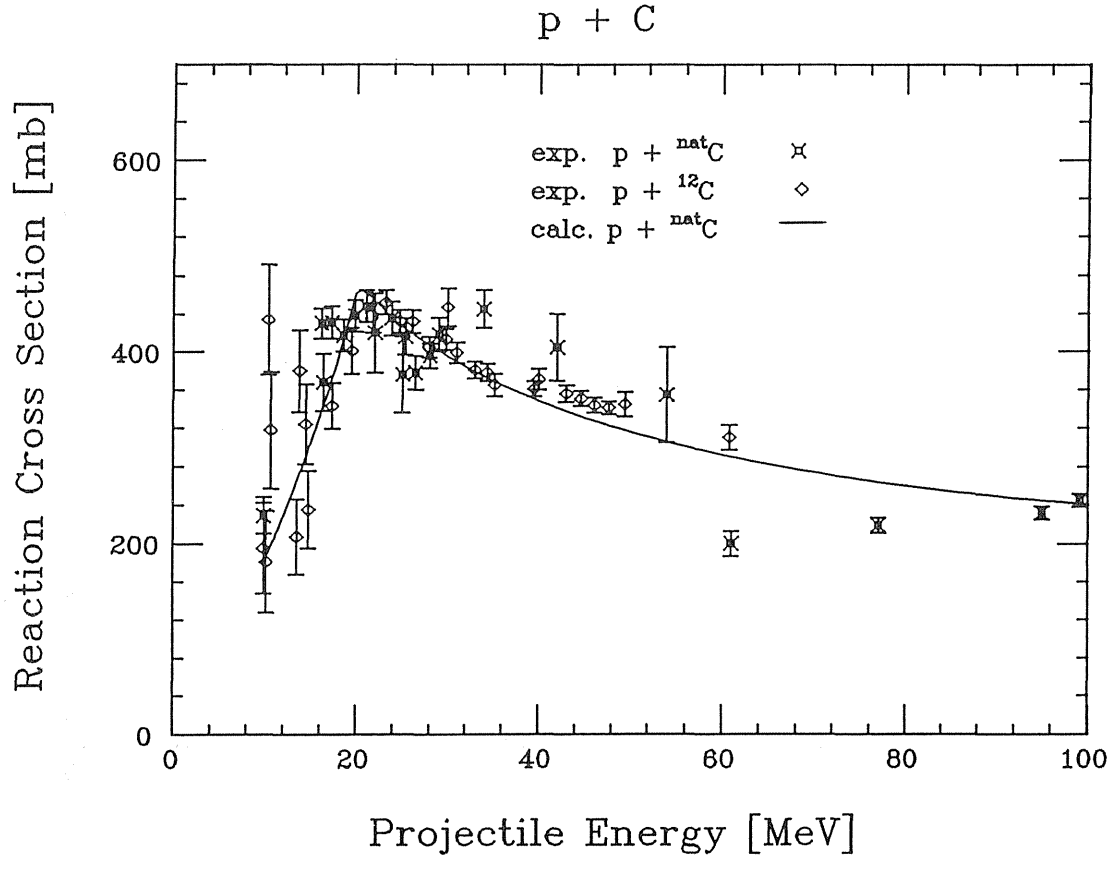

Figure 16b The same calculations as in **Figure 16a**, but only the low energy region is shown.

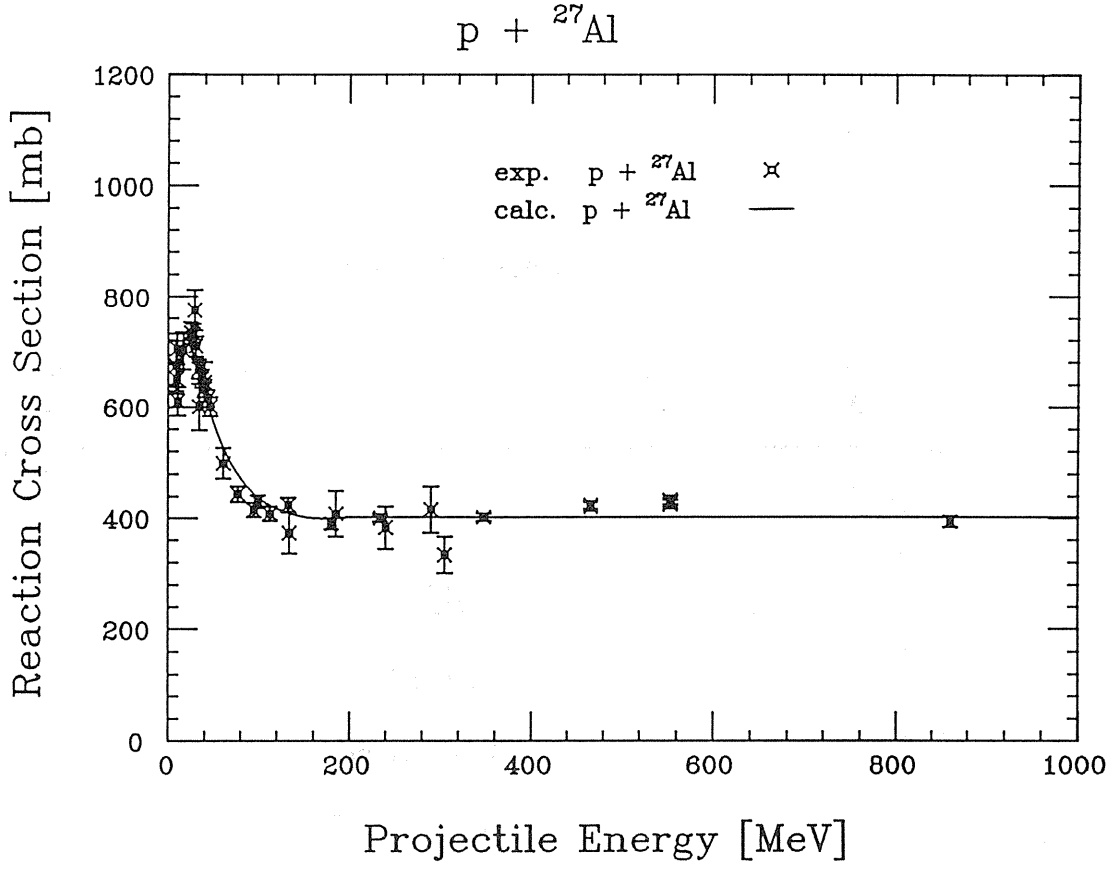

Figure 17a Calculated σ_{reac}, together with experimental data [29], for the interactions of protons with ^{27}Al.

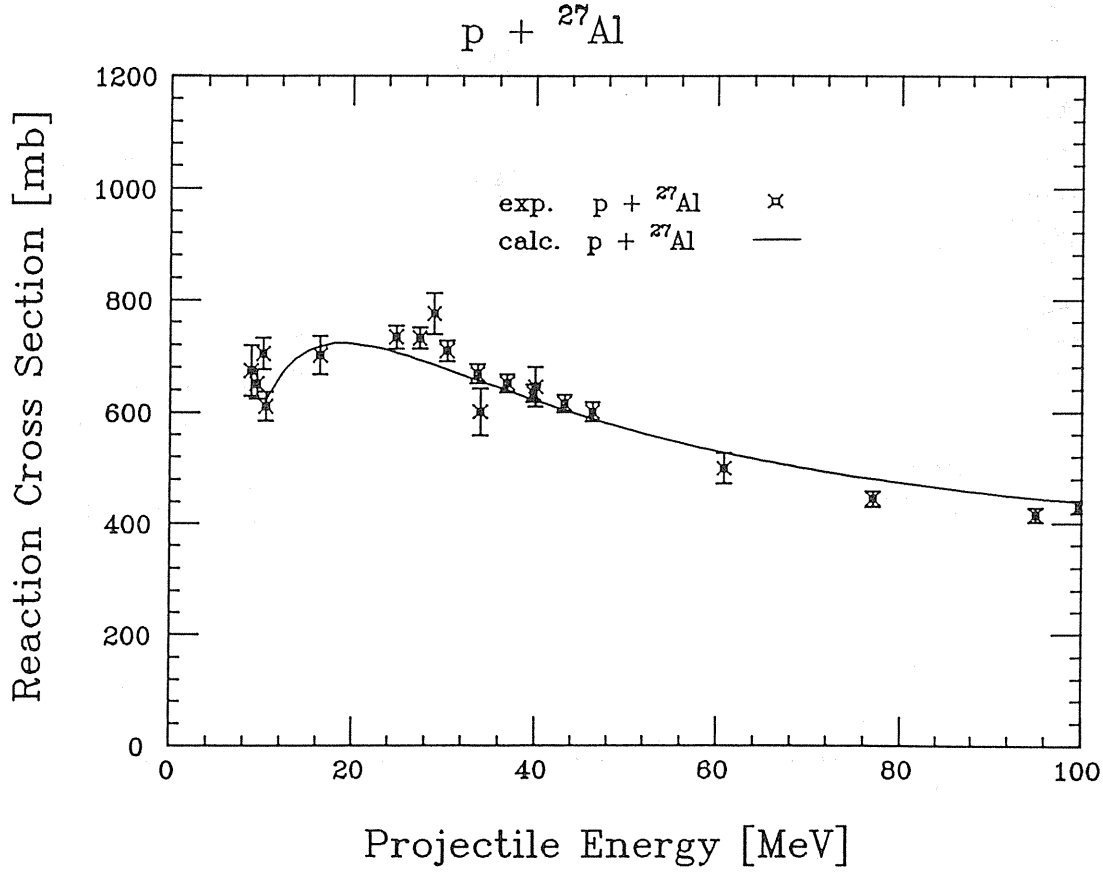

Figure 17b The same calculations as in **Figure 17a**, but only the low energy region is shown.

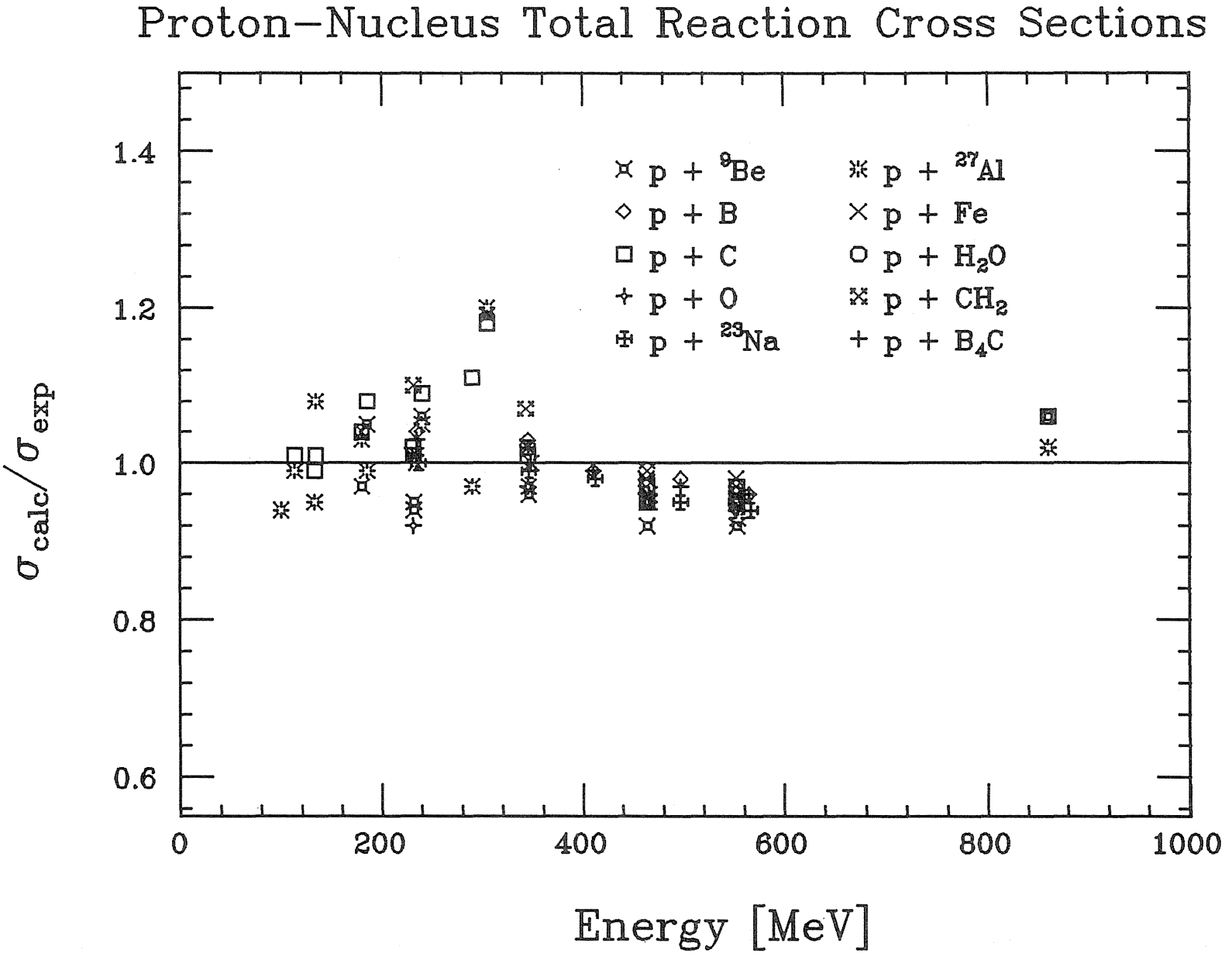

Figure 18 σ(calc)/σ(exp) for all reactions with incident energies ≥ 100 MeV, i.e. for the reactions tabulated in **Table XXV.**

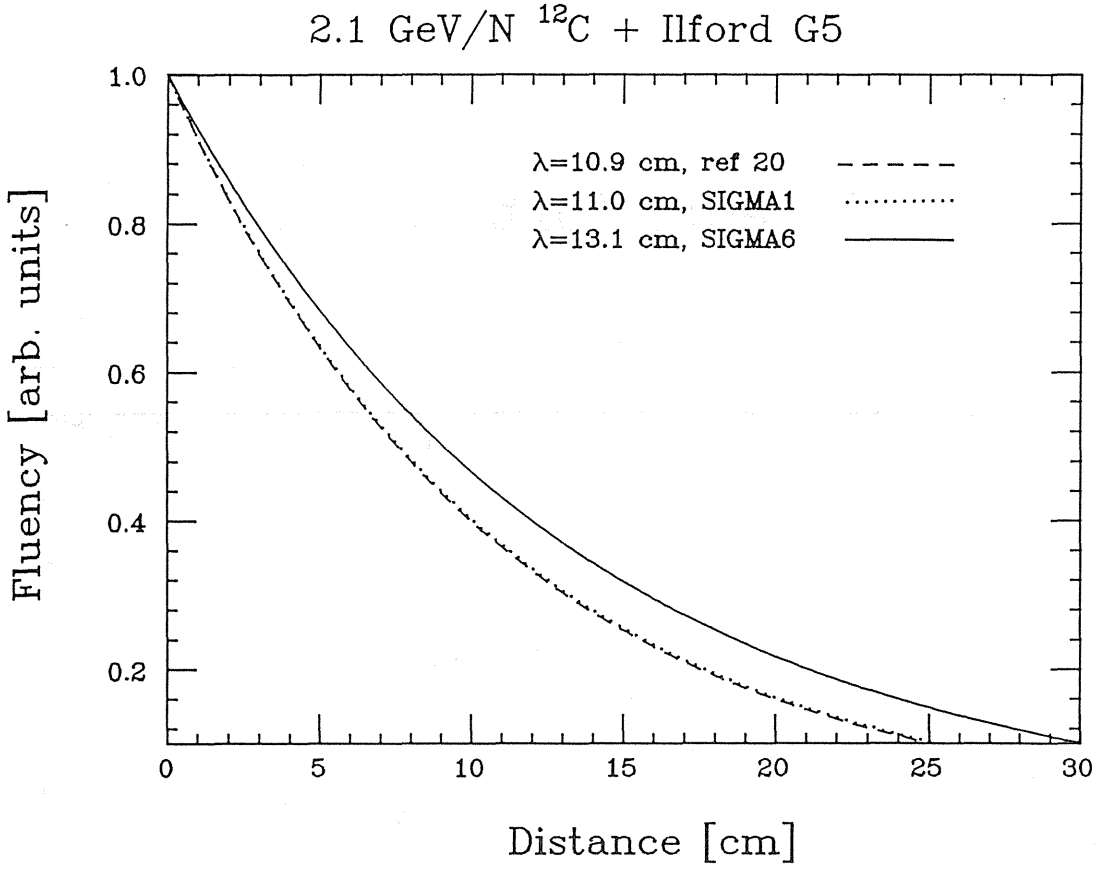

Figure 19a Fluency Distributions for 2.1 GeV/N ^{12}C in Ilford G5 emulsion [20].

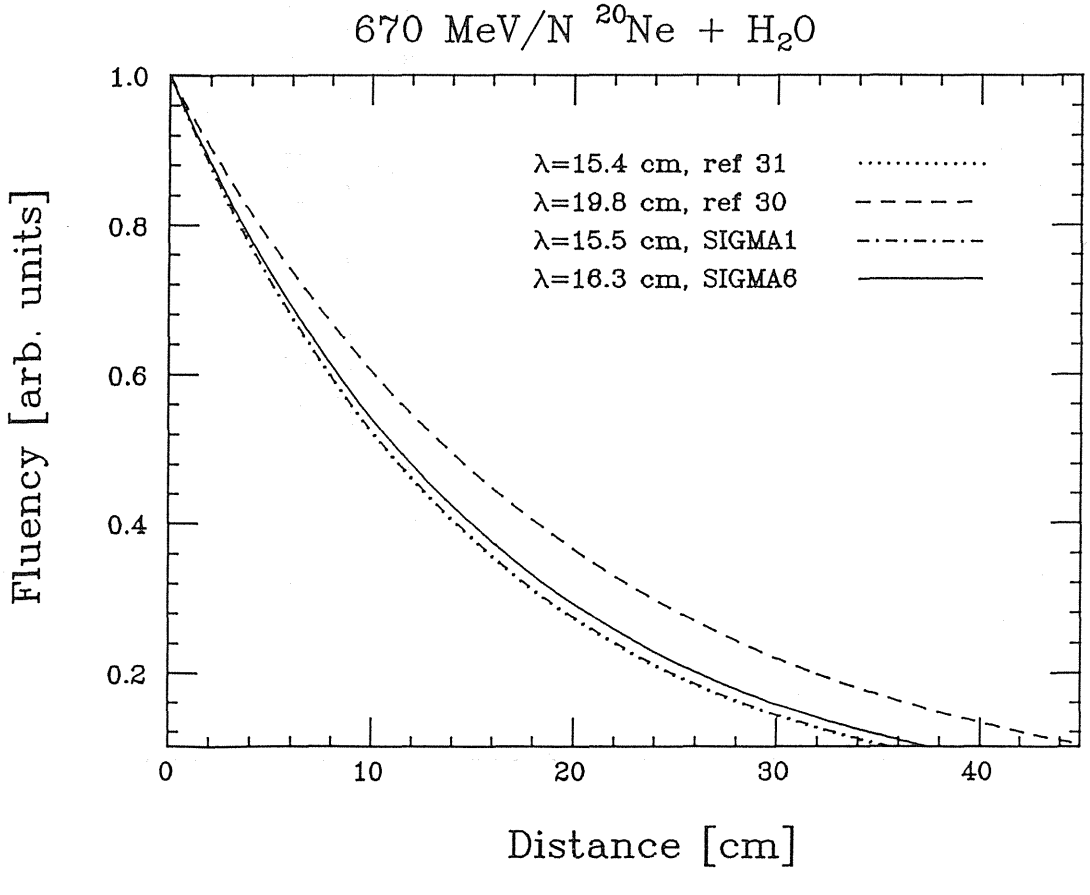

Figure 19b Fluency Distributions for 670 MeV/N ^{20}Ne water [30,31].

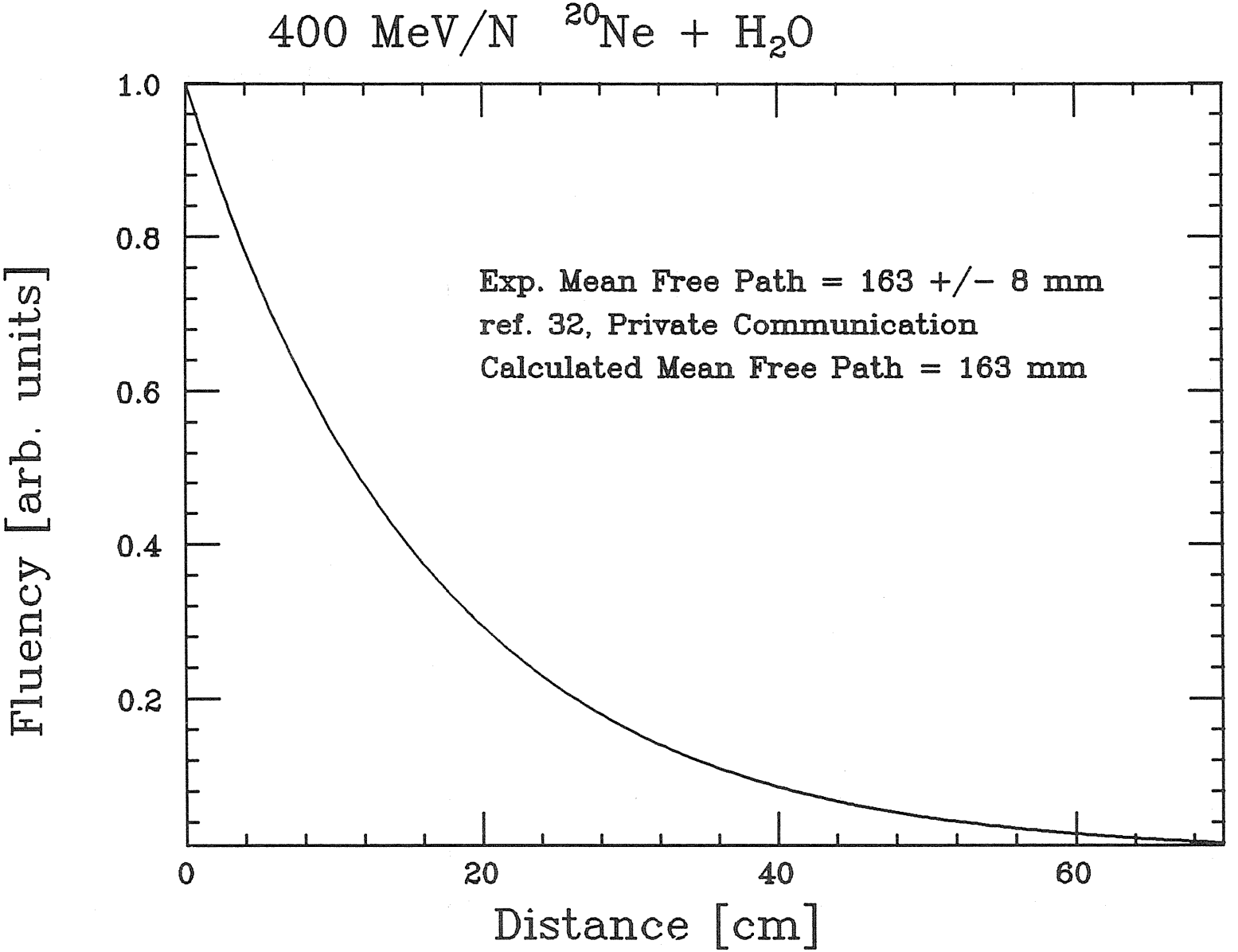

Figure 20 Fluency Distributions for 400 MeV/N ^{20}Ne in water[32].

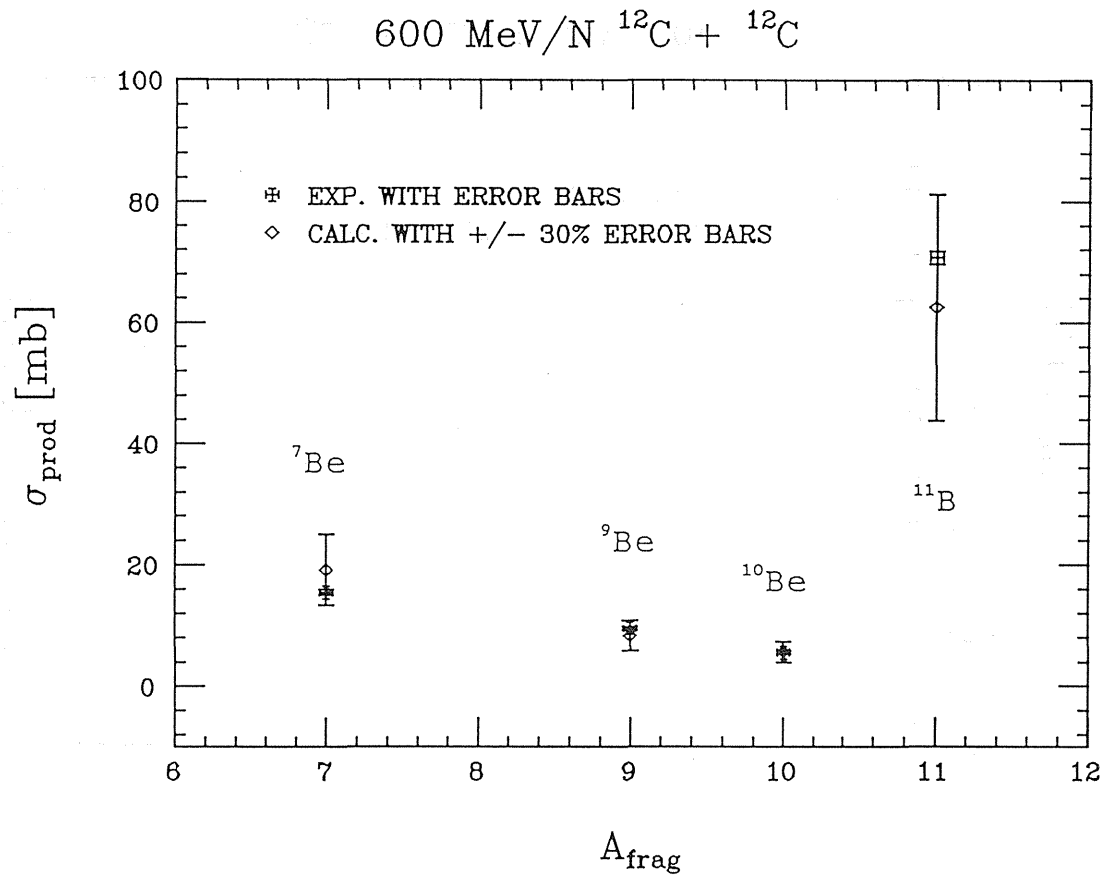

Figure 21

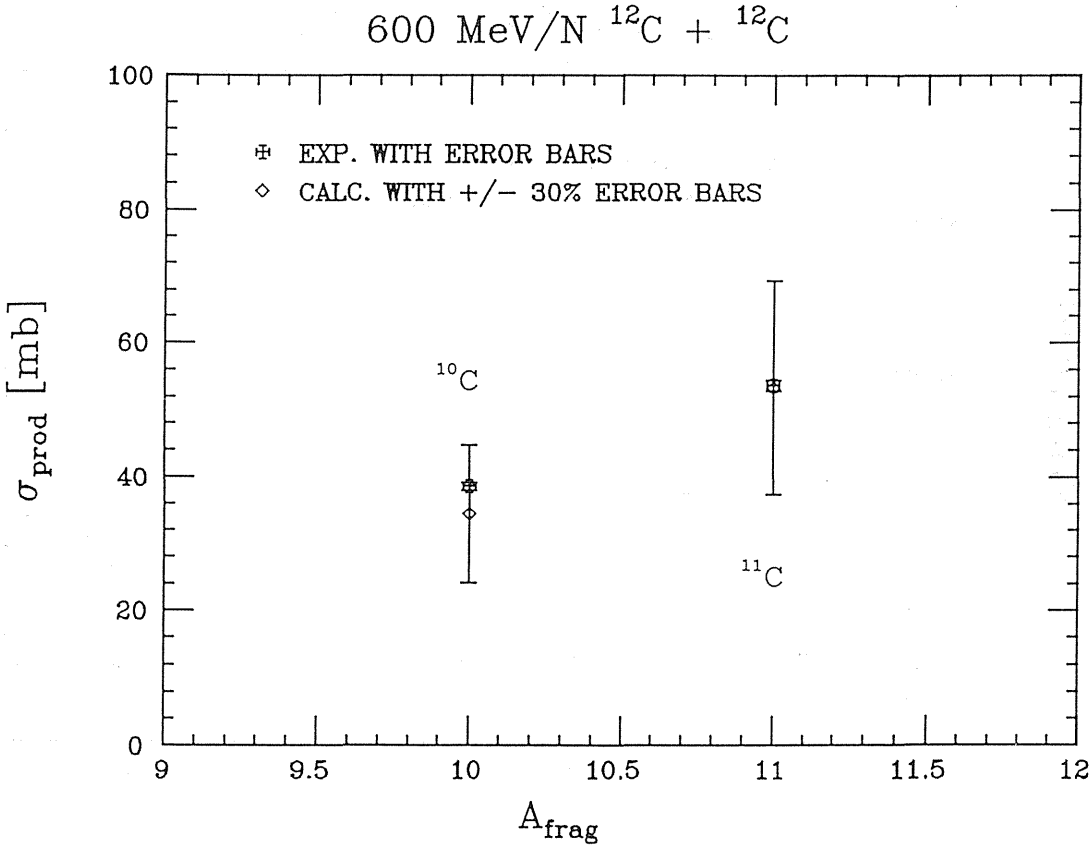

Figure 22

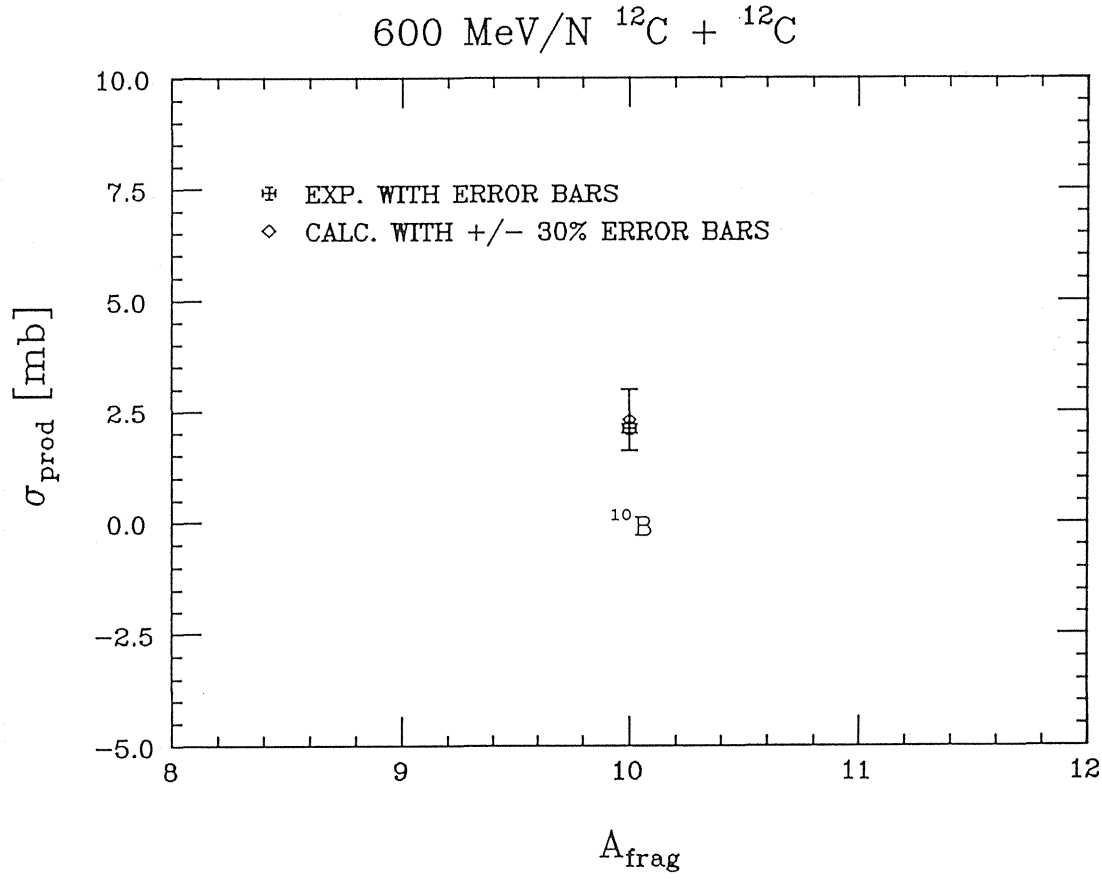

Figure 23

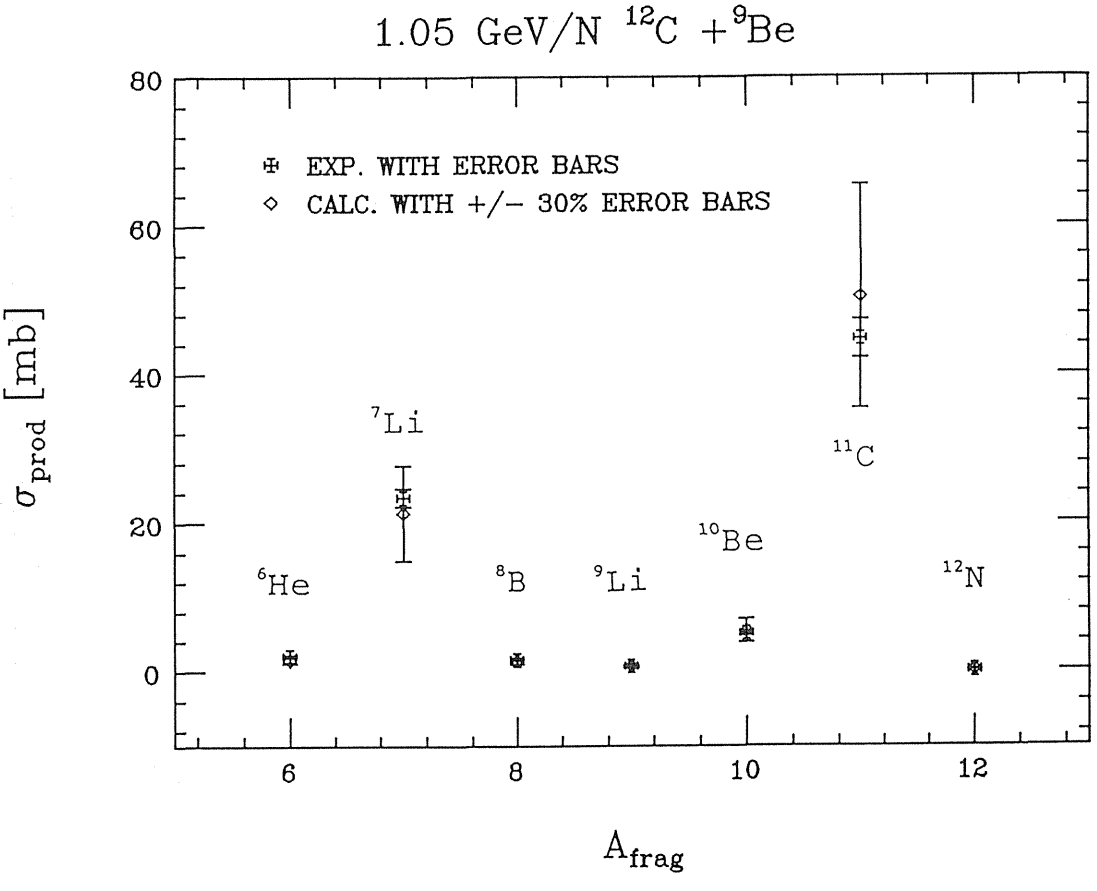

Figure 24

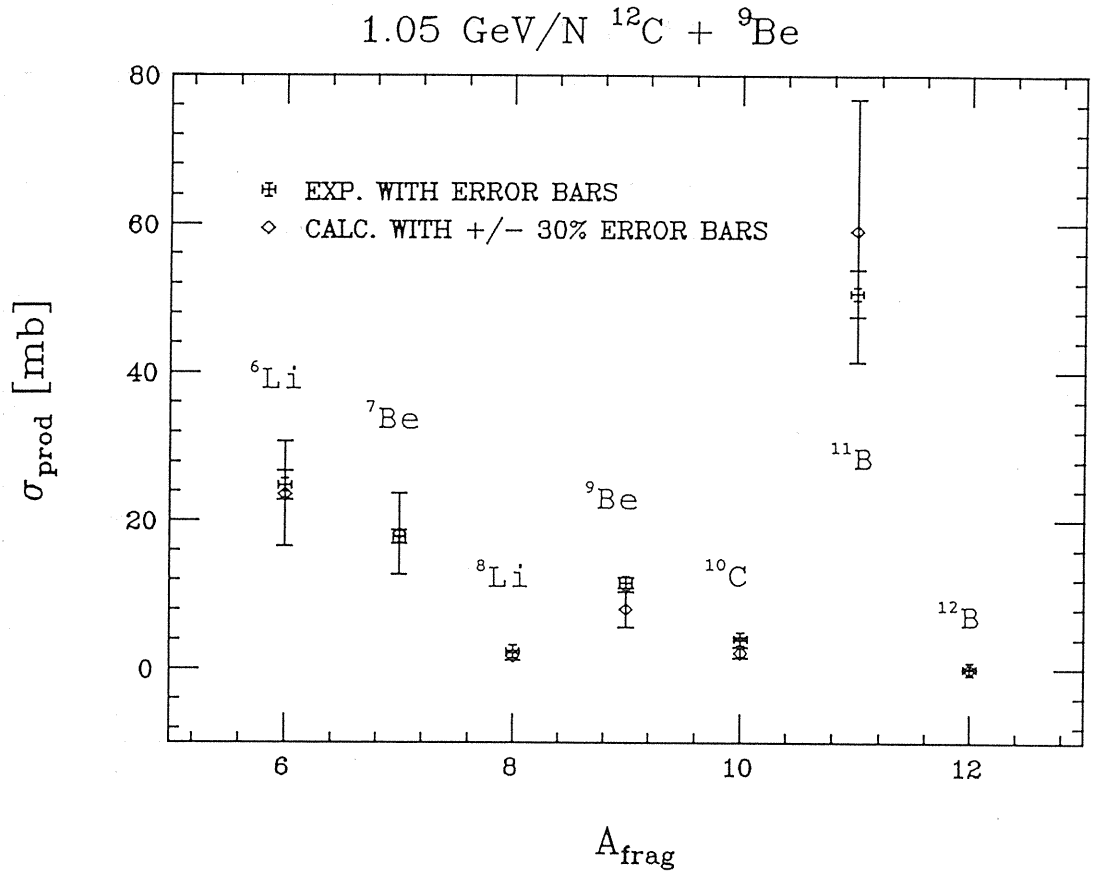

Figure 25

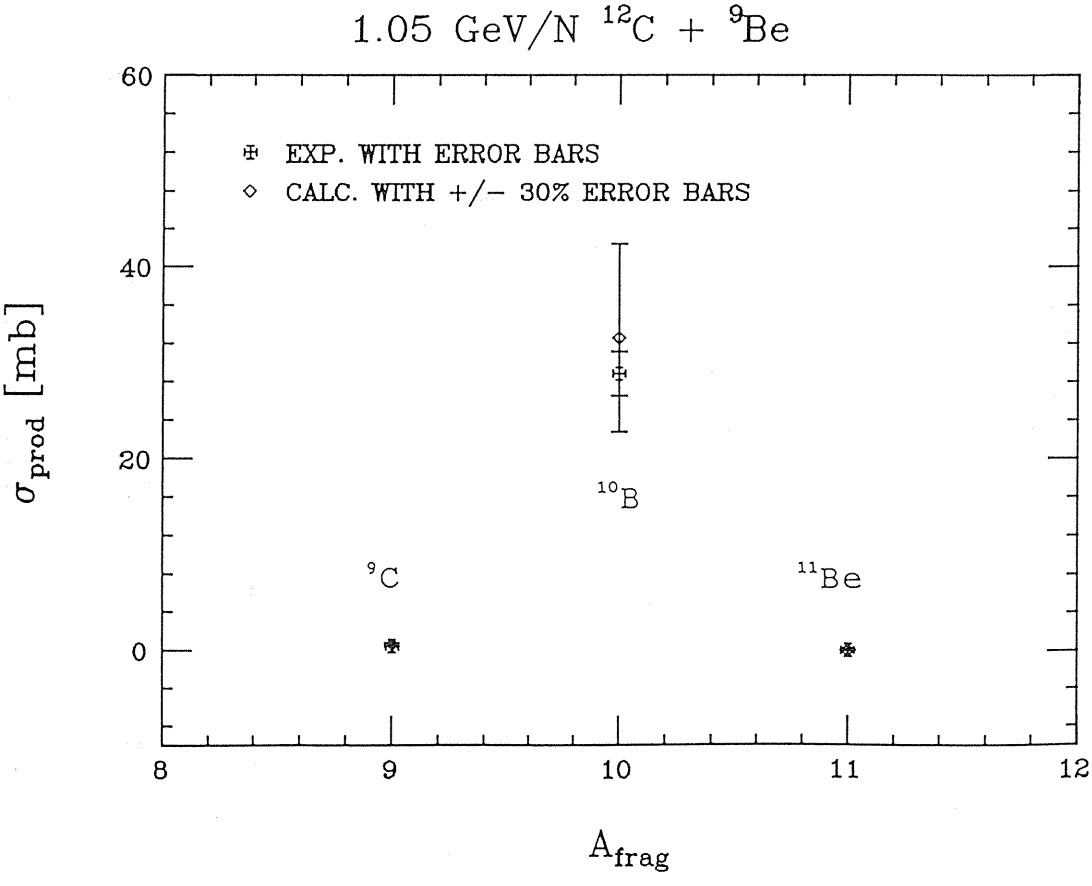

Figure 26

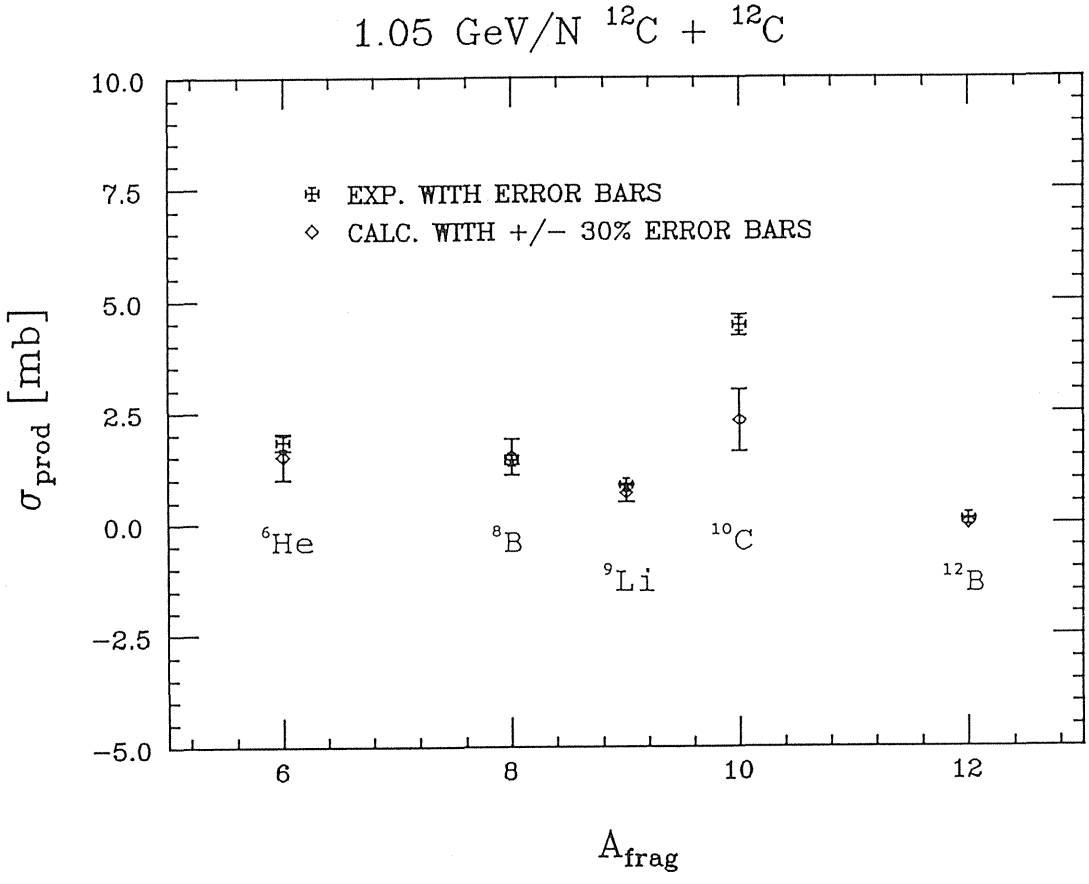

Figure 27

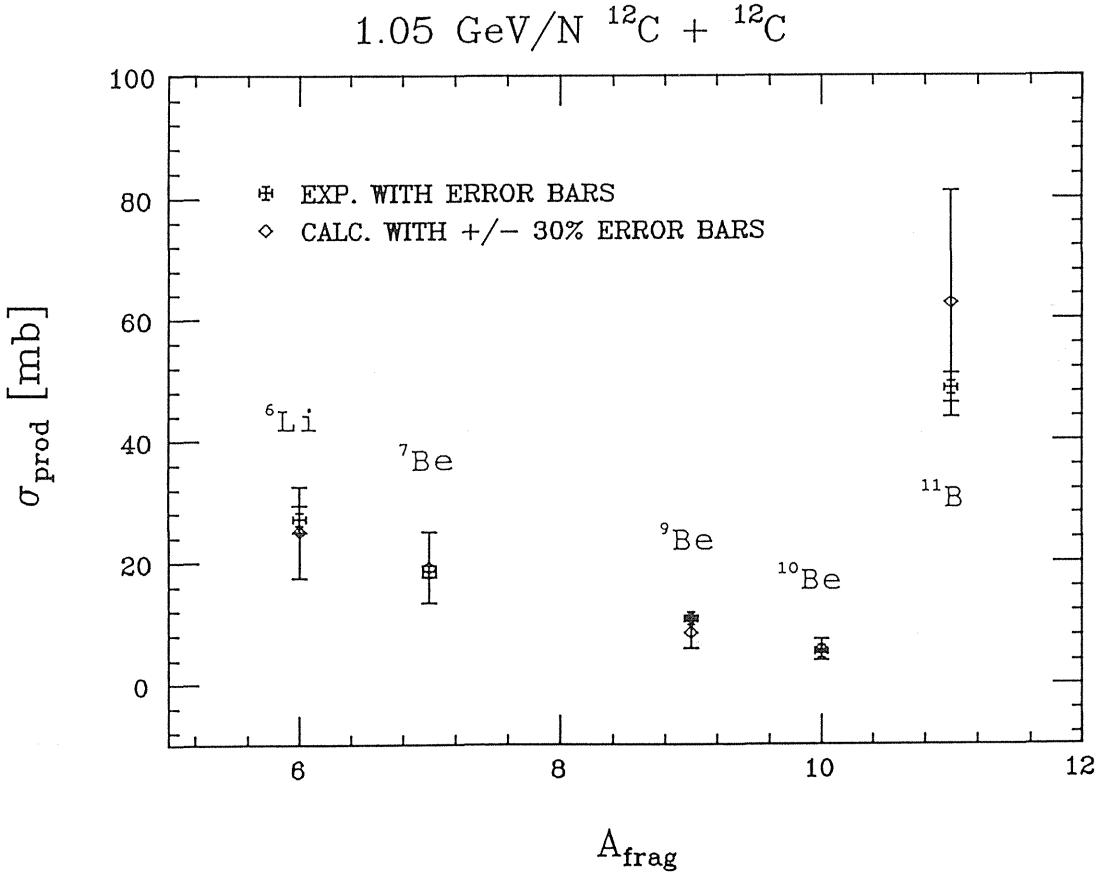

Figure 28

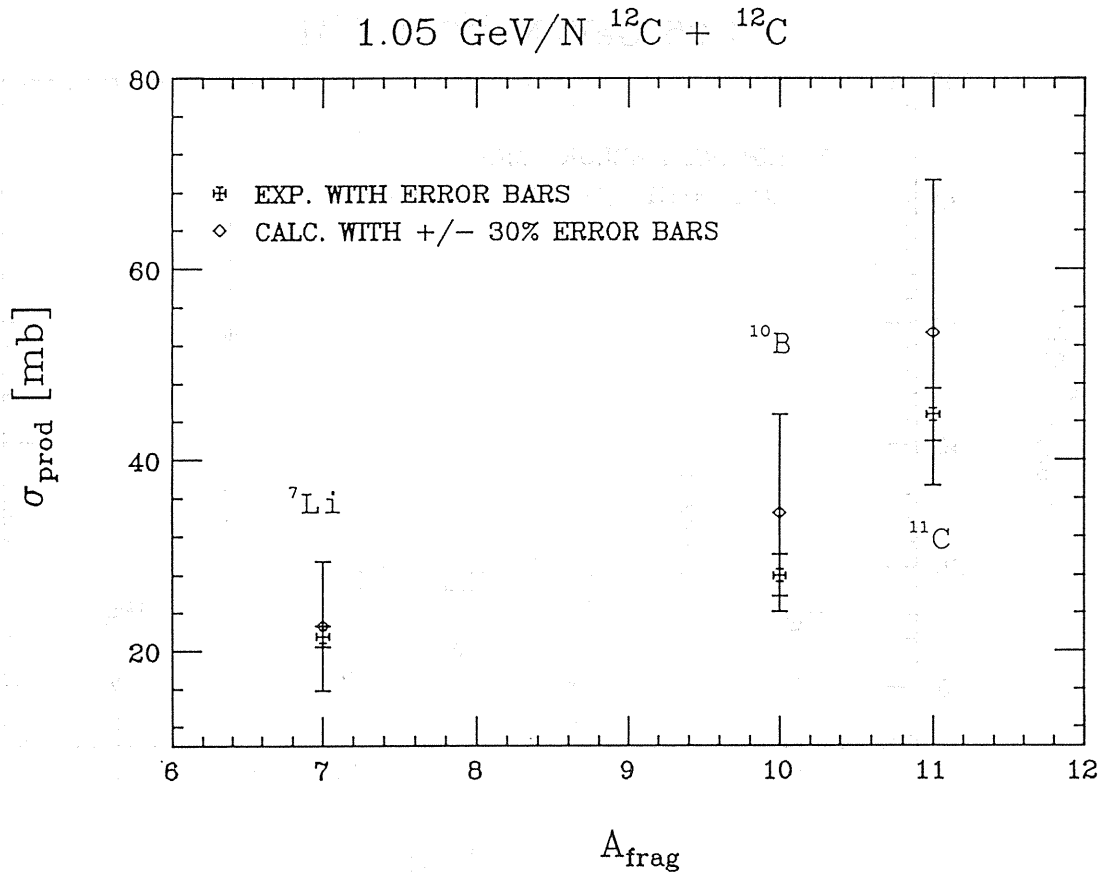

Figure 29

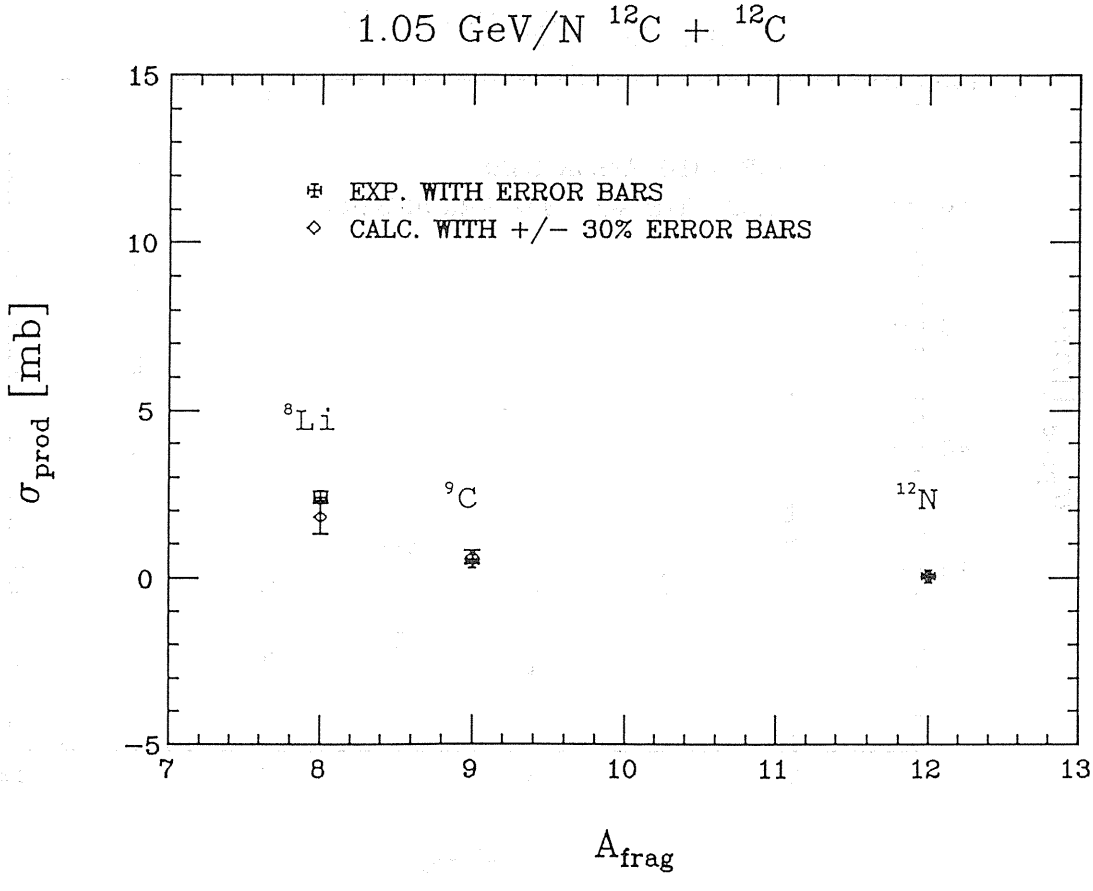

Figure 30

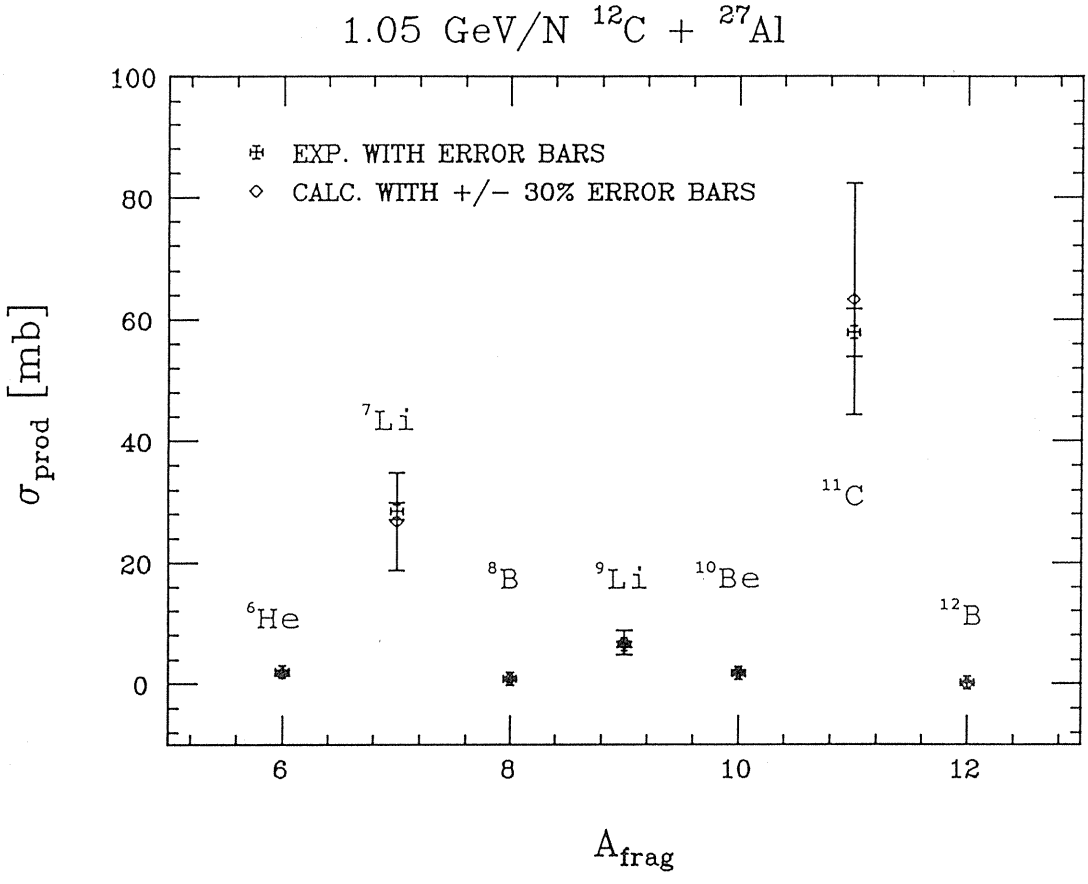

Figure 31

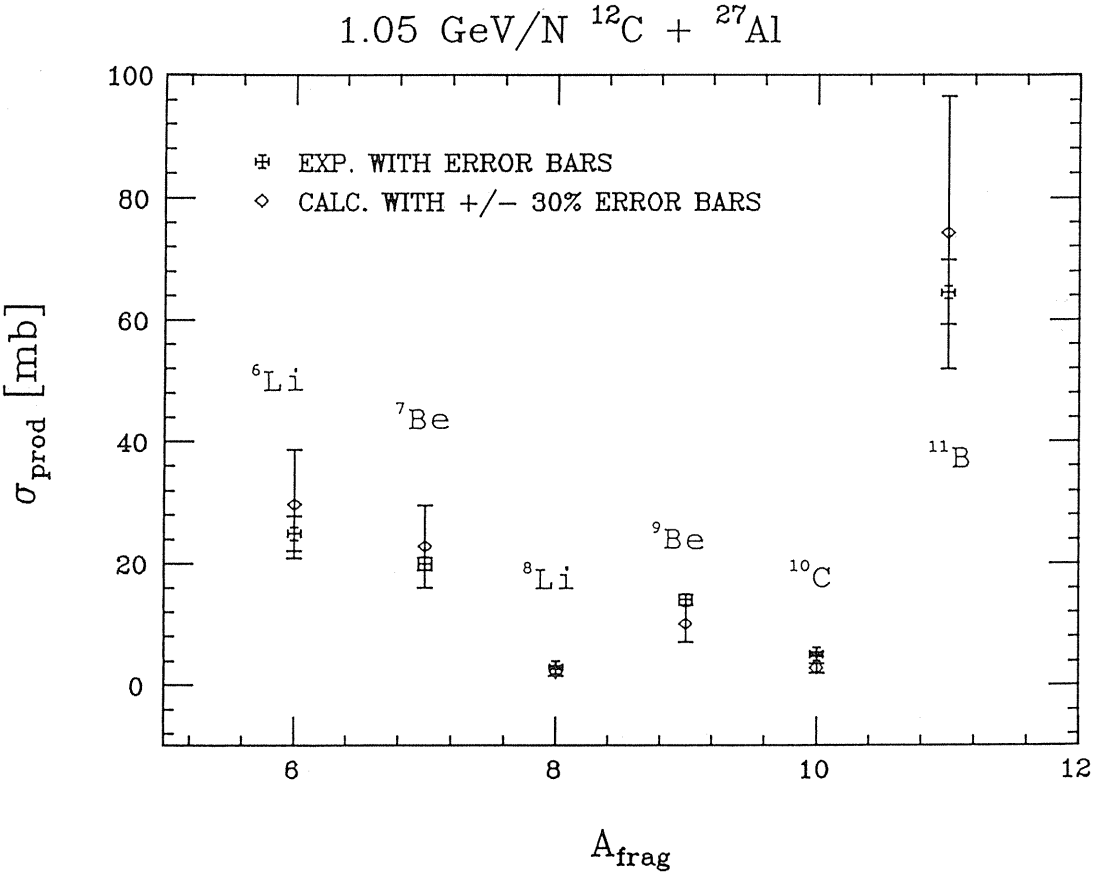

Figure 32

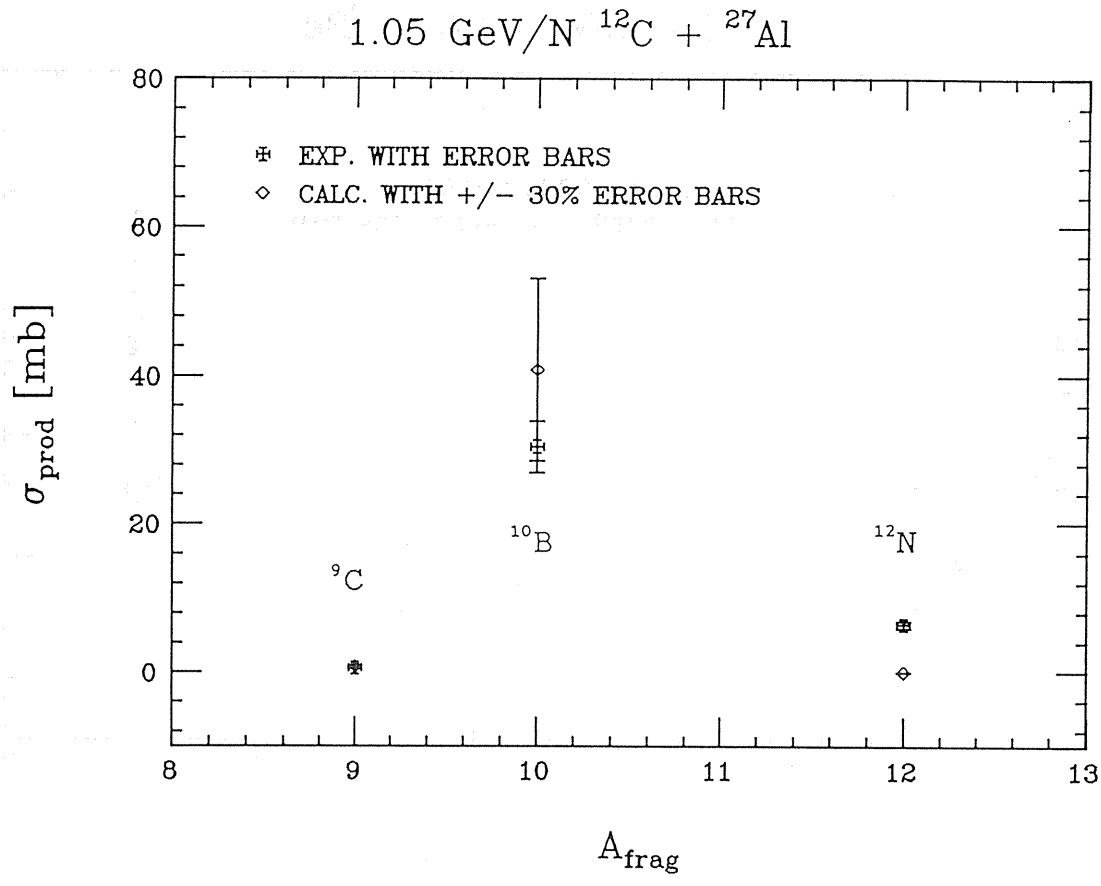

Figure 33

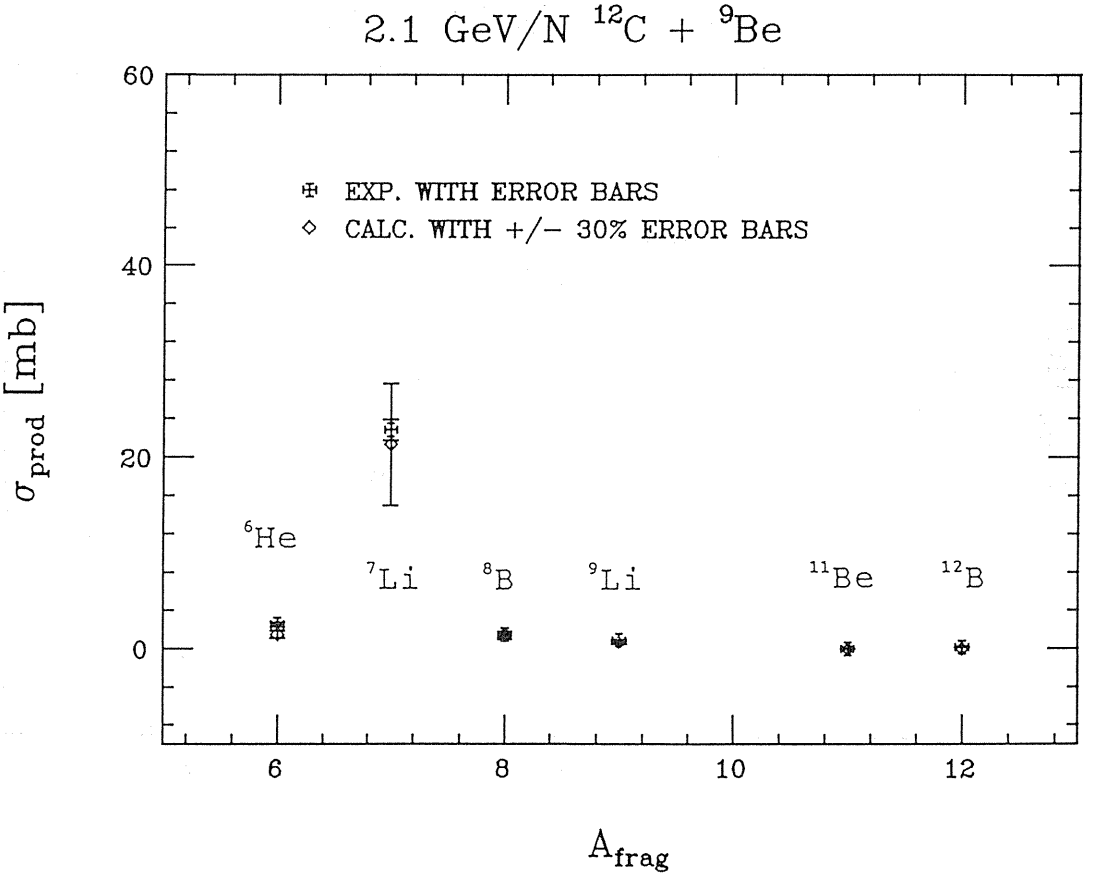

Figure 34

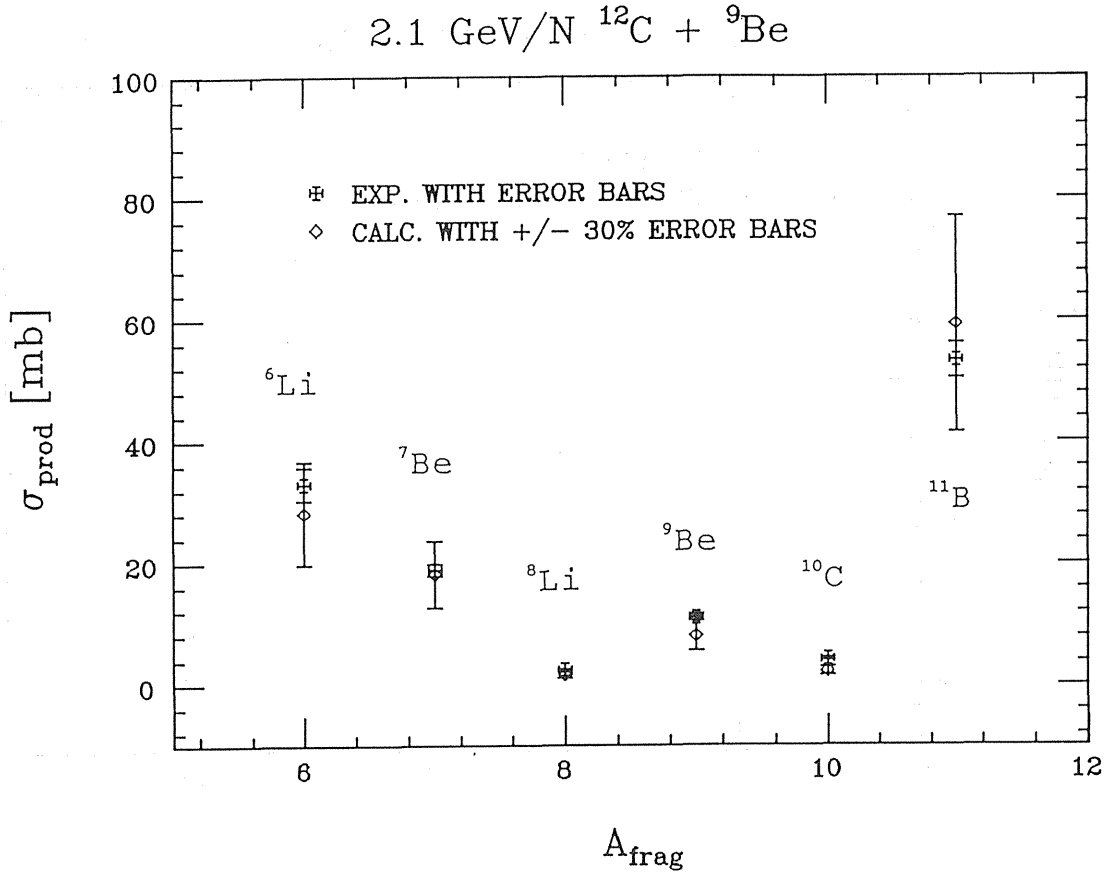

Figure 35

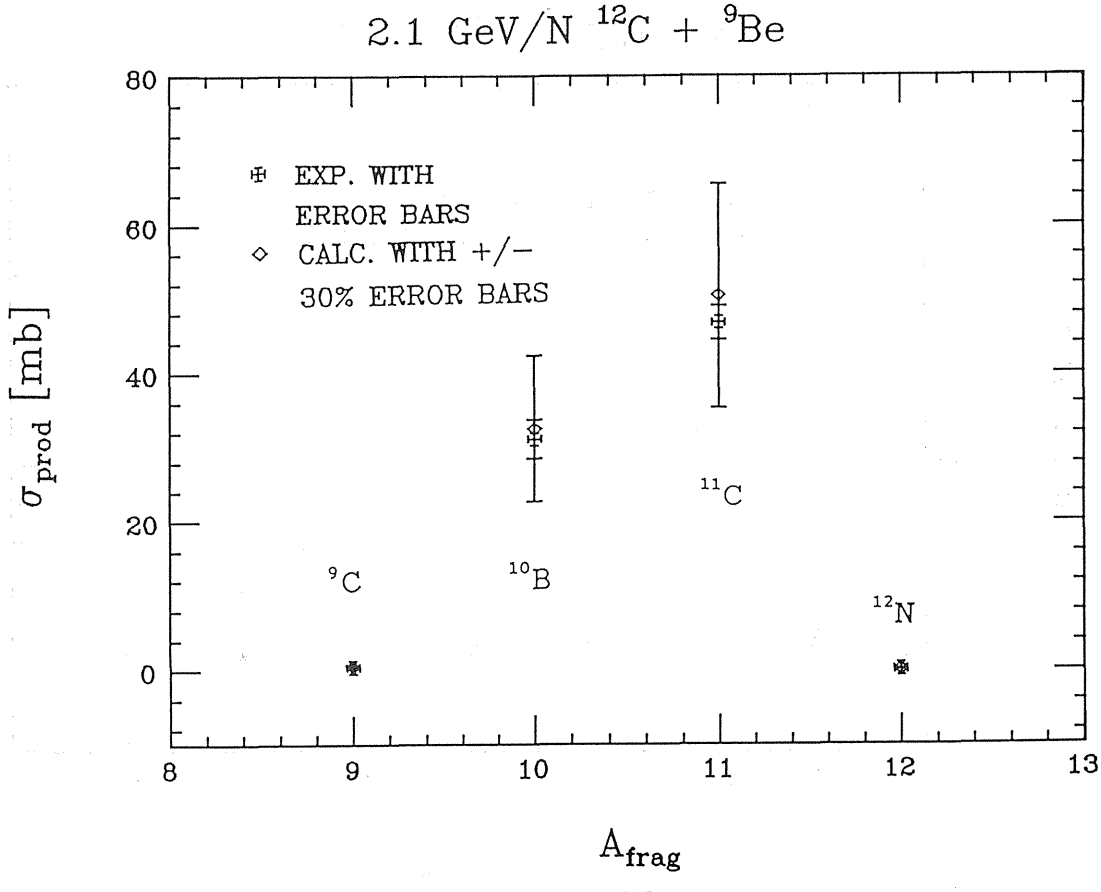

Figure 36

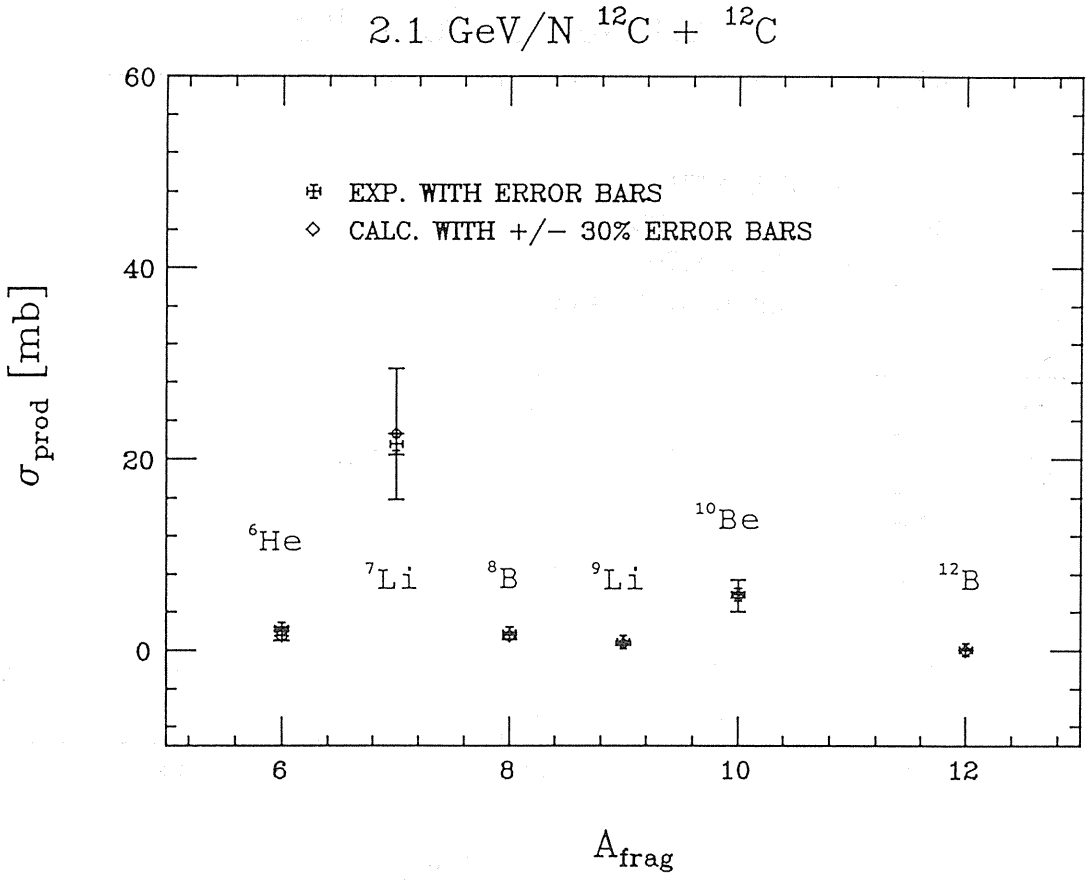

Figure 37

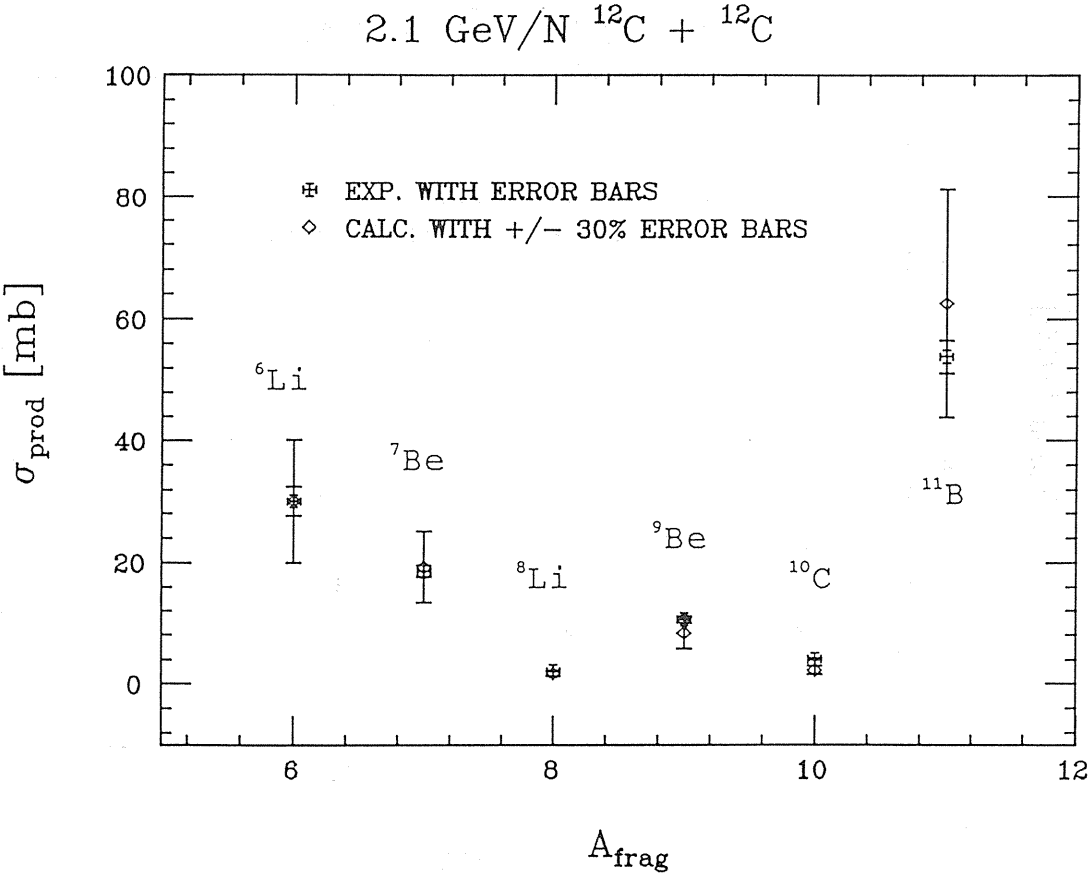

Figure 38

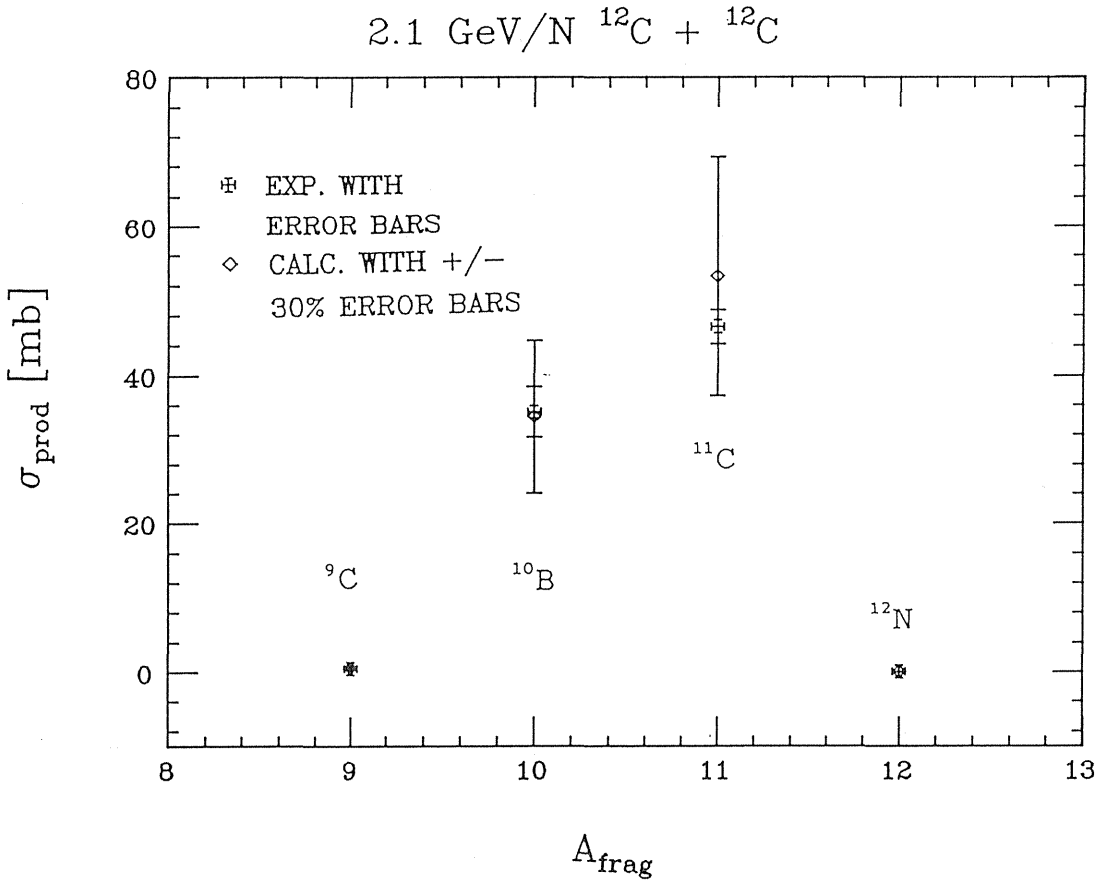

Figure 39

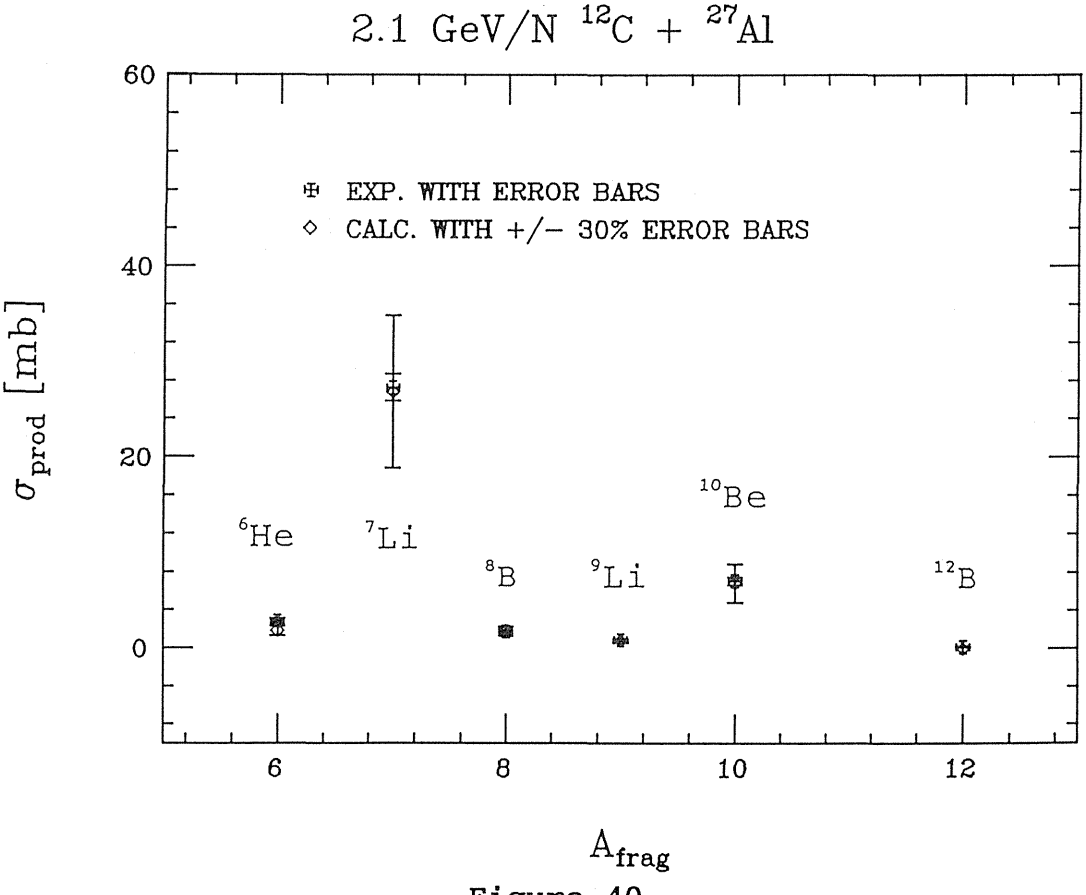

Figure 40

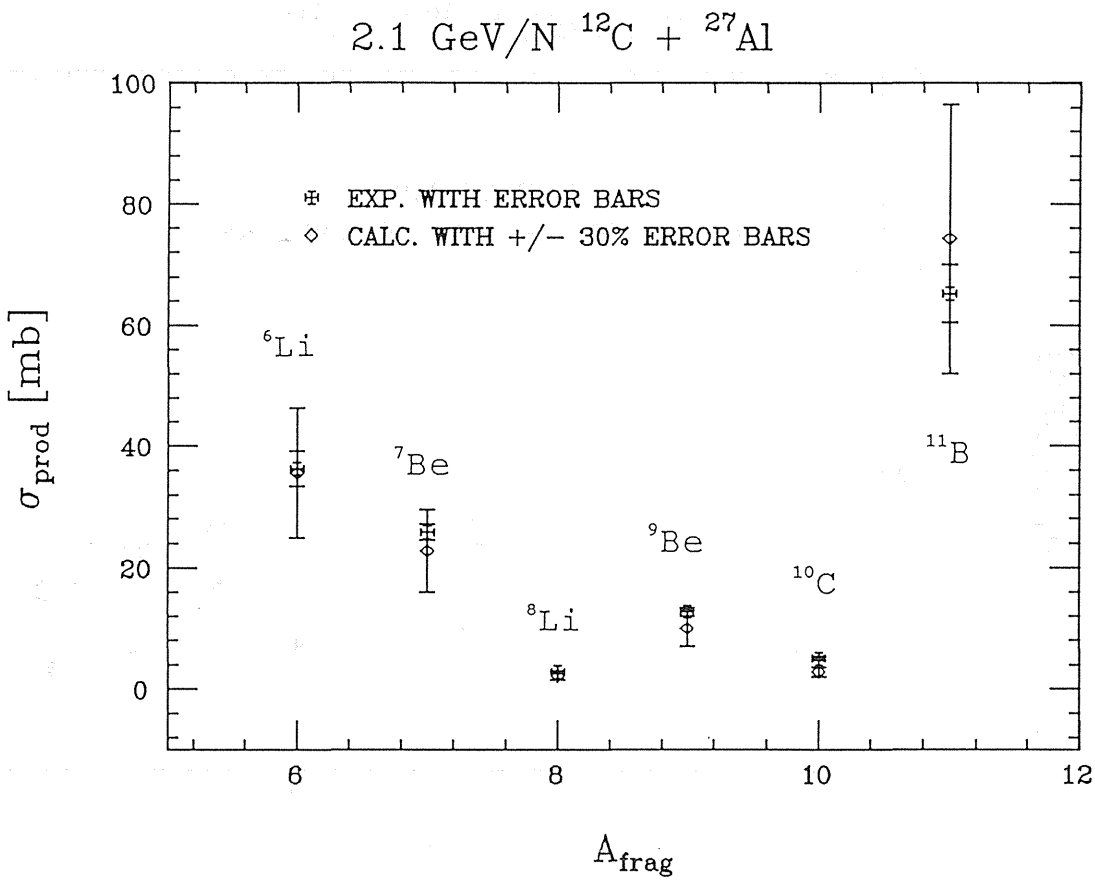

Figure 41

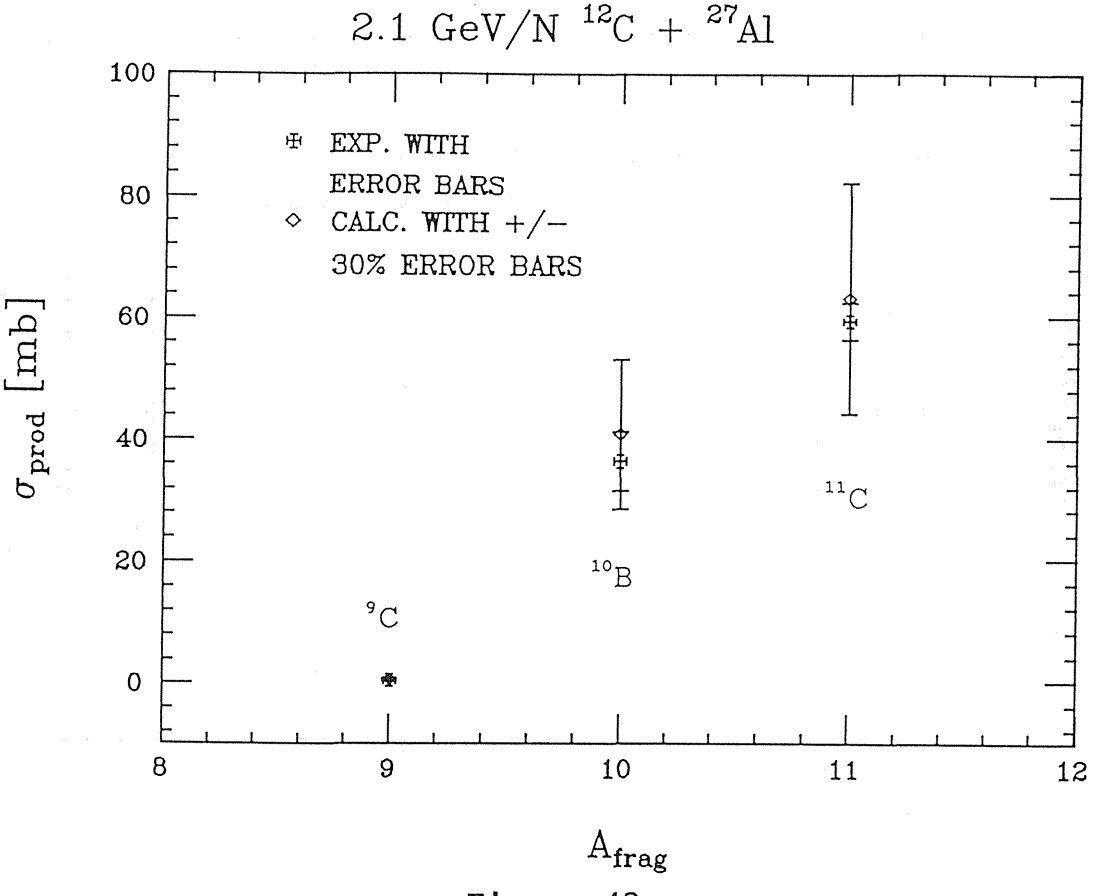

Figure 42

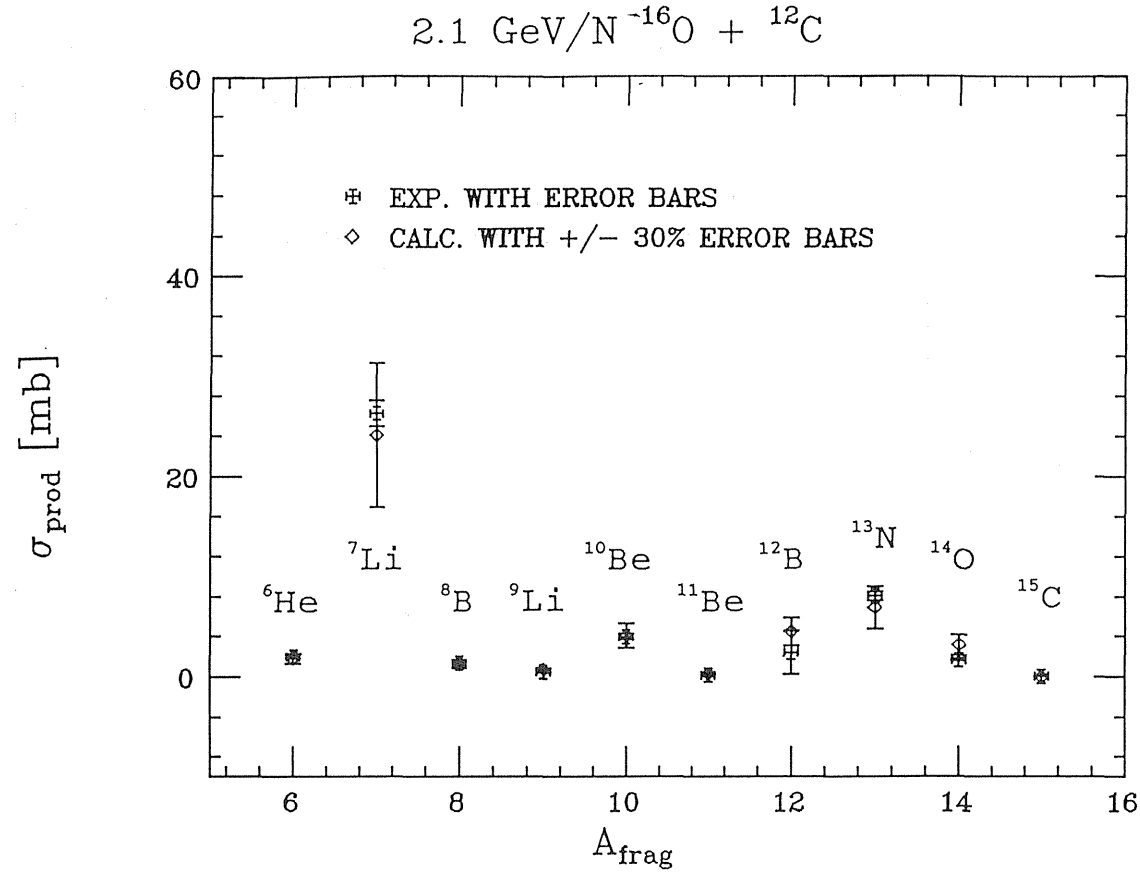

Figure 43

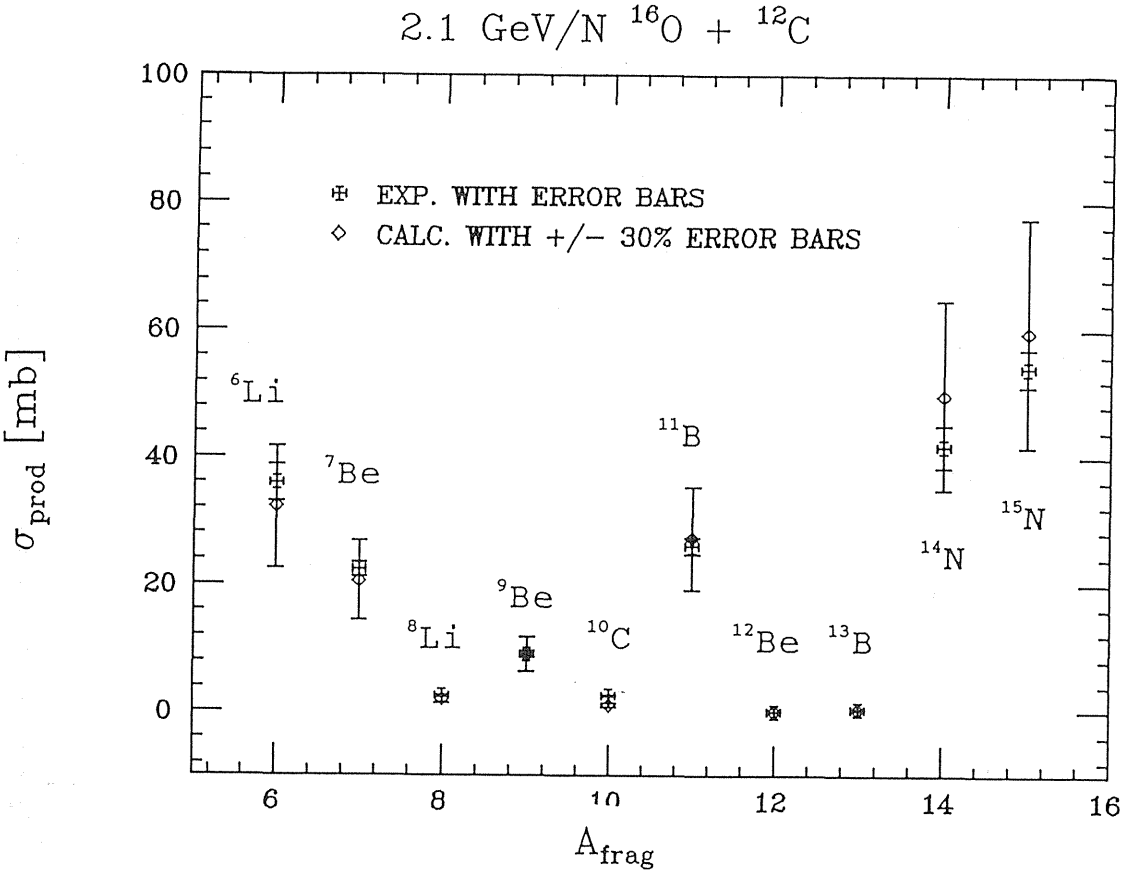

Figure 44

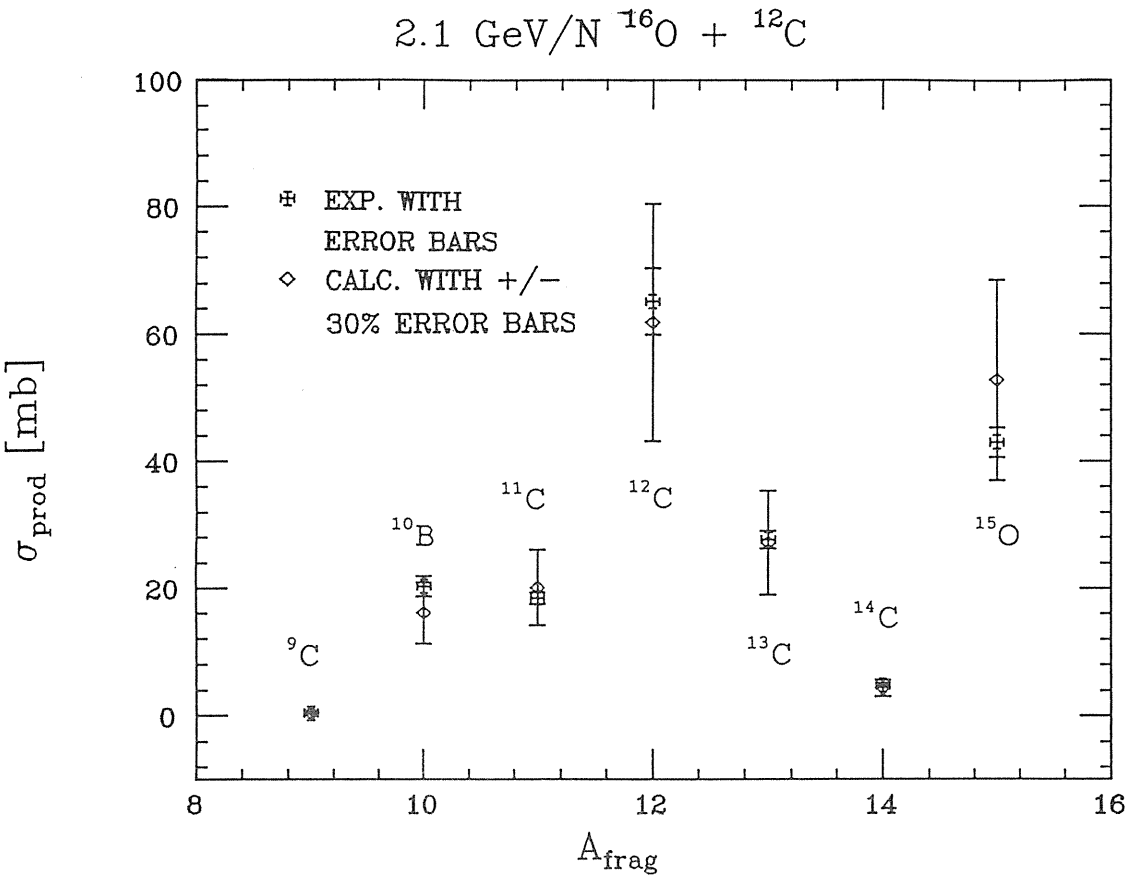

Figure 45

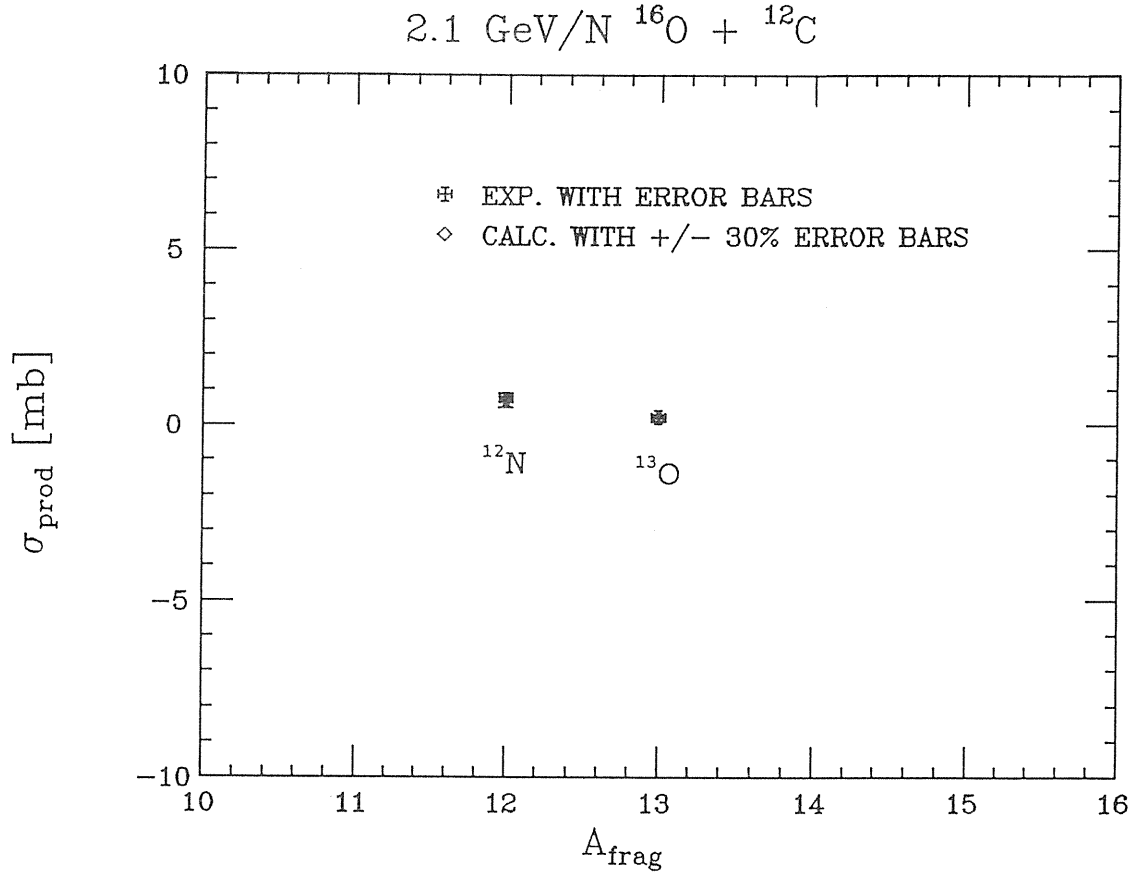

Figure 46